Controlling the Assembly of Proteins and Cells on SiO_2 Surfaces

by

Jiehyun Seong

Bachelor of Science, Chemical Engineering (1996)
Seoul National University

Master of Science, Chemical Engineering (1998)
Seoul National University

Submitted to the Department of Chemical Engineering
in partial fulfillment of the requirements for the degree of

Doctor of Philosophy in Chemical Engineering

at the
MASSACHUSETTS INSTITUTE OF TECHNOLOGY
February 2004

Signature of Author_____
Department of Chemical Engineering
December 12, 2003

Certified by_____
Paul E. Laibinis
Associate Professor of Chemical Engineering, Rice University
Thesis Advisor

Certified by_____
Robert Langer
Germeshausen Professor of Chemical and Biomedical Engineering
Thesis Co-Advisor

Accepted
by_____
Daniel Blankschtein
Professor of Chemical Engineering
Chairman, Committee for Graduate Students

Controlling the Assembly of Proteins and Cells on SiO_2 Surfaces

by

Jiehyun Seong

Submitted to the Department of Chemical Engineering on December 12, 2003,
in partial fulfillment of the requirements for the degree of
Doctor of Philosophy of Chemical Engineering

Abstract

A variety of devices -- biochips, implants, and membrane filters among them -- are challenged in their operation by having to contact biological solutions.. An ever-present problem for such devices is "biofouling," resulting from the nonspecific adsorption of proteins, cells, and other agents onto their surfaces. The ability to produce surfaces with specifically immobilized biological species that can avoid the nonspecific adsorption of other species has been essential for constructing solid-state devices that interface to biological systems.

An effective strategy for achieving "bioinertness" for surfaces is their modification by poly(ethylene glycol)s (PEGs), which provides protein and cell repelling properties. This thesis centers on the development of ultrathin films of PEG on SiO_2 surfaces that 1) can resist the nonspecific adsorption of proteins and cells (*"bioinert surfaces"*) and 2) can provide surface sites for the specific immobilization of biomolecules (*"bioactive surfaces"*). Effective methods to achieve these goals were accomplished by incorporating multivalent surface anchoring groups into one polymer chain or by forming densely-packed monolayers of PEG on surfaces.

In one approach, bioinert surfaces were prepared by a multivalent attachment of a PEG-grafted polymer backbone to a surface. Two systems were examined: 1) graft copolymers of poly(acrylic acid) expressing PEG-containing side chains, and 2) a random copolymer composed of an "anchor part" (trimethoxysilane) and a "functional part" (PEG). In the first system, PEG-containing films were formed by an electrostatic interaction between the PAA backbone and the underlying amine-modified surface. In the second system, the formation of multiple covalent bonds between the anchor moiety and the surface was responsible for generating PEG films. The formation of covalent bonds and the direct coupling of PEG to native surfaces are advantages of this system. The use of these bioinert surfaces for the direct patterning of proteins and cells was also addressed. Capillary force lithography (CFL) technique was applied to form patterned PEG microstructures. PEG microstructures localized proteins and cells onto the exposed surfaces not only by the inert nature of PEG but also by acting as a physical barrier. The number of cells in a given PEG barrier could be manipulated by varying the feature size of patterns.

Biofunctional surfaces were prepared from PEG-containing self-assembled monolayers (SAMs). Specifically, an acetate-capped tri(ethylene glycol) (EG_3)-terminated alkyltrichlorosilane formed SAMs (EG_3OAc SAM) that were subsequently reduced to hydroxyl-capped EG_3 (EG_3OH SAM) films produced a non-biofouling surface which

simultaneously allows subsequent immobilization of proteins. The attachment of protein A to this surface produced a high density array of this agent for the attachment of antibodies as needed for sensing and other applications. Mixed SAMs of "reactive EG_3" (EG_3OH) and methoxy-capped, "inert EG_3" (EG_3OMe) controlled the surface reactivity and thus the amount of immobilized protein A on the surface. The binding activity of the resulting protein A surface towards immunoglobulin G (IgG) depended on the surface density of protein A and was systematically varied. On the surfaces with high protein A density, IgG binding was hindered presumably as a result of spatial restrictions caused by the dense packing of the protein A molecules. On surfaces with low protein A densities, IgG binding activity was also low instead being limited by the number of available binding sites. Maximal IgG loading was achieved at intermediate protein A immobilization levels. The mixed SAM platform composed of inert and reactive EG-based functional groups offers key attributes for the controlled construction of biosensing and diagnostic components.

Thesis Advisors:

Paul E. Laibinis, Associate Professor of Chemical Engineering, Rice University
Robert Langer, Germeshausen Professor of Chemical and Biomedical Engineering, MIT

To my mother and father, Haesook Lee and Siyong Sung,

and my sisters, Jungeun and Hongjin,

and Sangyong,

and the family

Acknowledgments

I am fortunate to have a number of great people around me during my stay at MIT. In particular, I would like to thank the following people.

• Professor Paul E. Laibinis for having me in his group and his constant support. His prompt responses to emails and phone discussions and his frequent visits to MIT made our interactions nearly the same whether he was around or away.
• Professor Bob Langer for accepting me as a co-advised student. I joined his group in 2001, and just by being a "Langer Lab" member, I learned a lot.

• Professors Linda G. Griffith and Michael F. Rubner for being on my thesis committee and for giving constructive feedback and suggestions. I also thank professor Rubner for helping me prepare for quals in my first year and for his care to PPST students when he was a director of PPST.

• Professors Daniel Blankschtein and Gregory C. Rutledge for making decisions in support of the interst of students and being on my side.

• Dr. Ron Rieder for giving me a chance to work with him for more than four years. His project introduced to me the interesting field of biosensors. I also appreciate his generous help by providing my references when needed.

• Manish, Hyun-Goo, Tim, Harpreet, and Andre, and former PEL group members for their friendship and helpful discussions, and for proofreading my writings. Special thanks to Hyun-Goo and Manish, for filling my last year in 66-425 with lots of fun and enjoyable memories. In the PAA-*g*-(PEG-*r*-PPG) work, Hyun-Goo has been an excellent collaborator and Geoff provided his polymers. My EG_3 SAM work would have been much difficult without the solid groundwork and preliminary studies of Seok-Won. I thank them for making my thesis work interesting and fruitful.
• Current and former Langer Lab people. Many thanks to Ali, Omid, and Hyungshin for their friendship. Kahp Yang for introducing to me the interesting area of capillary force lithography. Thanh-Nga for her help in XPS and AFM experiments. More special thanks to Sangyong for being incredibly supportive in both emotional and practical ways.
• Professor Kookheon Char at Seoul National University for his continued mentorship.

• Hyuntae, Sangkyun, Yun Sung, and Jeeyoung, and many others for hanging out together and lending their ears when needed, especially in my early years at MIT.

• My parents, Haesook Lee and Siyong Sung, and my lovely sisters Jungeun and Hongjin for their endless belief in me, which kept me motivated when nothing else worked. I look forward to entering my next phase of growth with SYJ in my long journey of life.

Table of Contents

List of Figures

List of Schemes

List of Tables

Chapter 1. Introduction

1.1. Motivation and Thesis Outline

The construction of solid-state devices that interface fabricated systems with biological components requires methods for assembling biological species on the device surface in controlled ways. Examples include biosensors,[1-7] bioreactors,[8] chip-based diagnostic assays,[9,10] separation devices such as membrane filters and affinity chromatography,[11-15] substrates for solid-phase peptide synthesis, and biomaterials used for implants and tissue engineering.[16-18]

One common problem that limits the successful operation of such devices is "biofouling." Biofouling is a term used to describe the irreversible, nonspecific adsorption and accumulation of biological species, such as proteins, bacteria, and cells on solid surfaces[19] (Figure 1.1). For solid-state systems that incorporate such species as receptors or other active elements, the structural integrity of these immobilized biological species is often greatly affected by their local interactions with an underlying surface. Thus, the effects that cause non-specific adsorption can alter the activity and binding abilities of the biological species on the surfaces through conformational or orientational changes effected by the surface, ultimately leading to the loss of biological function. Hence, the performance of such devices can be improved by promoting specific molecular interactions and simultaneously suppressing nonspecific adsorption events. For example, the activity of an immobilized antibody or an immobilized enzyme reaches its optimum when its active sites are oriented away from the surface and thus becomes available to its targets. Because the biofouling phenomenon, or nonspecific adsorption, is such an important issue, the development of

methods to prepare non-biofouling surfaces continues to be an area of aggressive research activity.

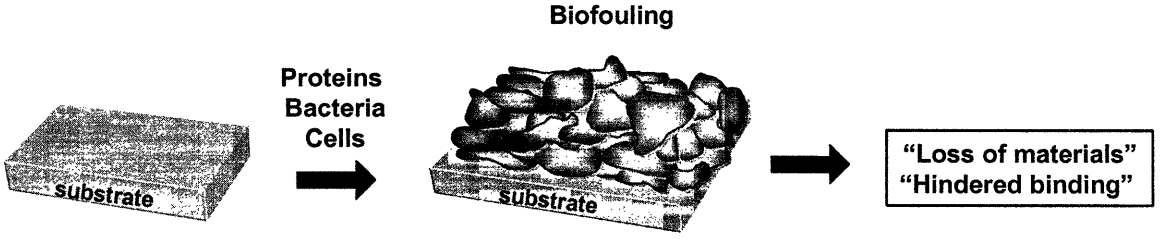

Figure 1.1. Conceptual drawing depicting a biofouling process.

An effective strategy for preventing biofouling is the modification of surfaces with poly(ethylene glycol)s (PEGs), as ways to incorporate its protein- and cell-repelling properties.[20] Many reports have studied on the surface functionalization of gold substrates with thiolated PEG derivatives, partly because of the strong affinity between a gold surface and thiol functionality, the weak interaction between PEG and gold, and the ease of characterizing derivatized surfaces. However, despite its practical importance in devices and in biology laboratories and despite the superior robustness of siloxane linkages to gold-thiol bonds, the functionalization of silicon surfaces needs to be studied more.

This thesis centers on controlling the assembly of proteins and cells on silicon dioxide-based surfaces by ultrathin films of PEG. In particular, this thesis discusses surface functionalization of SiO_2-based substrates so that the SiO_2-containing substrates 1) can resist the nonspecific adsorption of proteins and cells ("*bioinert*" surfaces) and 2) can provide specific sites for the immobilization of biomolecules ("*bioactive*" surfaces) to a surface while retaining the required biological inertness. One critical factor in efficient PEG coating is the

ability to increase the surface coverage of PEG. Surface coverage can be increased either by incorporating "multivalent" surface anchoring groups into one polymer chain or by forming "densely-packed monolayers" of PEG. The former strategy has an advantage over the use of PEG-derivatives with a "monovalent" anchoring group in that the surface density of PEG can be controlled by varying the grafting ratio of PEG. Thus, this method may lead to greater protein resistance of the surfaces, which is the motivation of the work in Chapters 2[21] and 3[22]. On the other hand, the latter strategy provides densely-packed, homogeneous, and oriented monolayers with a more readily defined film structure. Using the latter approach, two or more adsorbates can be adsorbed together to form mixed films of controlled compositions and constituencies. The composition of the film can be controlled by systematic variations in the composition of the adsorbates in solution, which is the basis of Chapters 5[23] and 6, and was used for enhancing the bioactivity of an immobilized receptor.

Chapters 2 and 3 describe the construction of non-biofouling SiO_2 surfaces from PEG-containing polymers that have been specifically designed to incorporate multivalent surface anchoring sites. These polymers form thin films on the SiO_2 surfaces by straightforward solution phase adsorption processes. Chapter 4 discusses an application using the non-biofouling coating strategy to pattern the deposition of proteins and cells. Chapters 5 details the preparation of bioactive surfaces comprising "densely-packed" self-assembled monolayers (SAMs) that terminate with PEG groups present as short oligomers. Notably, as few as two or three ethylene glycol (EG) groups are sufficient, when densely packed, to produce nonfouling surfaces. The organization present in these SAMs produces a difference in molecular design strategy from that using long PEG sequence for the films formed by polymer adsorption. Chapter 6 discusses the optimization of the bioactivity of surface-

immobilized proteins through the use of mixed SAMs comprising one PEG component with an inert (-OCH_3) terminus and another with a terminating reactive (-OH) functional groups. The rest of Chapter 1 provides short background on the substrates used in this thesis and the general non-biofouling properties of PEG.

1.2. Silicon-based Surfaces

This thesis focuses on the tailoring of silicon dioxide surfaces for the controlled assembly of biological species. Silicon dioxide surfaces include silicon with its native oxide (Si/SiO_2), glass and quartz (SiO_2), and poly(dimethylsiloxane) (PDMS) with oxidized surface ($_{ox}$PDMS). Silicon is one of the most widely used materials in the manufacture of various types of biomedical microdevices. Examples include silicon-based biosensors,[24-26] microfabricated devices for electrophoretic separation[27] and cell sorting[28]. When exposed to air or moisture, the outermost surface of silicon gradually oxidizes and grows a thin layer of native oxide (SiO_2). Polished silicon wafers offer themselves as a valuable substrate for the study of surface phenomena on silicon, in that they are easy to handle, provide smooth surfaces over a large area and, more importantly, can be conveniently analyzed by a useful surface characterization technique called ellipsometry. Needless to say, glass and quartz, made of silicon dioxide (SiO_2), are commonly used materials in laboratories. Oxidized silicon (SiO_2) materials contain surface silanol (Si-OH) groups. Silanol groups are ionizable in water with an isoelectric point (pI) of 2-3. Thus, the surfaces exposing SiO_2 are charged in aqueous systems. These charged surfaces facilitate nonspecific adsorption of proteins.

PDMS is a silicon elastomer that is extensively used in the fabrication of microfluidic device.[29,30] Its high gas permeability[31] and the ensuing potential for the supply of oxygen is well-suited to the cell culture in microdevices. As a transparent material, PDMS allows direct

observations of its inside under an optical microscope. The low cost of PDMS is also a plus. The biocompatibility of PDMS has been demonstrated by the success in patterned cell culture, speading, and growth on microstructured PDMS devices or in a microfluidic network.[32-34] Although native PDMS surfaces are neutral without surface charges and have a low surface energy, they can readily incur protein adsorption by hydrophobic interaction.

1.3. Poly(ethylene glycol) (PEG)

Poly(ethylene glycol) (PEG) is well-known for its protein- and cell-repellent properties, for reasons that remain not yet clearly understood. The particularly useful property of PEG is its ability to exclude interactions with other polymers or biological components in aqueous solution. Its inertness is due to its strongly hydrophilic nature resulting from hydrogen bond interactions. As a result, the functionalization of the surfaces with PEG species has been the most popular strategy for preventing protein adsorption and cell adhesion at interaces.

1.3.1. Bioinertness of PEG-Grafted Surfaces

Several explanations have been suggested for low protein adsorption characteristics of PEG on surfaces. The non-ionic and hydrophilic nature of PEG is said to account for the invisibility of PEG in biological systems.[35] In other words, the PEG molecule does not contain any functional groups that would provide sites for interactions with proteins, such as through hydrophobic or ionic contacts. The level of hydration is reported to be roughly two to three water molecules for each ethylene glycol (EG) unit and may similarly explain the passive nature of PEG in not being recognized by proteins.[36] The rapid mobility of the PEG chains in an aqueous solution is reported to prevent protein adsorption as well, by being less available to proteins.[37] The low interfacial energy at the PEG/water interface was also found

to be responsible for weakening the driving force towards protein adsorption.[38] For example, PEG molecules are reported to occupy a space in water that provide very little perturbation to the native structure of water.[39] The large excluded volume of PEG in aqueous solution is also responsible for the bioinertness of PEG in water.[37]

For systems exposing PEG brushes made of long polymer chains at high surface densities, "steric repulsion" theory has accounted for the protein resistance of PEG to a good extent. This theory associates the protein resistance of a PEG brush with its conformational free energy. Two elements contribute to steric repulsion: an elastic element and an osmotic element.[40] The elastic, or volume restriction, element describes the loss of conformational entropy. This entropy loss results from the reduced volume available for each polymer segment, upon the approaching of two surfaces. The osmotic, or mixing, element results from the increase in the polymer concentration on the compressed surfaces. Conformational entropy of PEG chains is reduced when a protein (or other large molecule) compresses or interpenetrates the PEG segments, leading to an increase in the osmotic repulsive term. The protein resistance of a PEG grafted surface has been viewed as resulting from the greater contribution of the steric repulsion effect than the collection of other attractive effects.[41] The steric repulsion approach was extended by Halperin.[42] He analyzed the steric repulsion in terms of two adsorption mechanisms for small and large proteins, and obtained scaling relationships for the free energy. For PEG systems in the "non-brush" regime, simulations based on single-chain mean-field (SCMF) theory have been employed to find the condition where a protein minimally adsorbs.[43-46] The main idea of this approach was that all the intramolecular and surface interactions are exactly considered and the intermolecular interactions are approximated with a mean-field theory.

Despite their smaller steric repulsion barrier, oligo(ethylene glycol) (oEG)-terminated alkanethiol SAMs on gold[47,48] and oEG-terminated trichlorosilane SAMs on SiO_2 surfaces[23,49] exhibit an ability to prevent protein adsorption. The analyses of these systems based on a "steric repulsion" mechanism are inappropriate for explaining the protein resistance of such short chain PEGs, *i.e.*, oEG-terminated SAMs the surfaces are comprised of densely-packed molecules with reduced conformational freedom. In the case of oEG-terminated SAMs, the molecular conformations of EG moieties were found to better explain the protein resistance. FT-IR measurements of methoxy-capped tri(ethylene glycol) (EG_3OMe)-terminated alkanethiol SAMs on gold and silver revealed that EG_3OMe SAMs on gold, in helical and amorphous conformations, repelled proteins successfully while the same adsorbates on silver, in planar all-*trans* structure, was not protein-resistant.[50] Repulsion between fibrinogen and the EG_3OMe SAM on gold and the attractive interaction between fibrinogen and the EG_3OMe SAM on silver was further confirmed from the force measurements by atomic force microscopy (AFM).[51] Another AFM measurements suggested that the EG_3OMe SAMs were negatively charged.[52,53] *Ab initio* molecular modeling of the two oEG conformations, helical and *trans*, tethered to a substrate, and their electrostatic fields showed that the oEG in helical conformation associated with water much more strongly than the oEG in all-*trans* conformation.[54] The interfacial water layer formed adjacent to the helical oEG-coated surface was highly stable. For example, the interphase water layer extended up to 5 nm from the surface, and had a viscosity that was six orders of magnitude higher than that of bulk water.[55] Thus, proteins could not penetrate the solvated oEG layer and reach the substrate. A Monte Carlo simulation also proposed that water molecules can penetrate into the near surface region to render the helical oEG SAM substantially disordered, whereas the oEG SAM in all-*trans* configuration is more resistant

against the penetration of water molecules,[56] which supports the sum frequency generation experiments[57]. Increase in temperature rapidly converted the helical conformation of oEG SAM to all-*trans*.[58] Therefore, studies of oEG on various substrates revealed that increasing the level of hydration inside the PEG layer was be suggested to be the cause of protein resistance, and the degree of solvation of PEG depended on the molecular conformation of grafted PEG.[50,54,55,59,60]

1.3.2. Surface Modification by PEG

Various strategies have been pursued to modify SiO_2-based surfaces (*e.g.*, silicon, glass, silicon dioxide, quartz) with PEG. Linear PEGs have been grafted to surfaces by various coupling methods. For example, glass or quartz surfaces were first derivatized with 3-aminopropyltrialkoxysilanes, followed by a direct coupling to an epoxide-terminated PEG[61] or a tresyl-terminated PEG,[62-64] or by coupling to an unmodified PEG through use of a diisocyanate crosslinker.[65] The photolysis of a phenyl azide-terminated PEG has also been used as an alternative grafting approach.[66] The direct coupling of PEGs with SiO_2-based surfaces has been achieved by the use of trichlorosilane-terminated PEGs,[67,68] trimethoxysilane-terminated PEGs,[36] and by the vacuum deposition of PEGs onto a water plasma-treated surface.[69]

Examples of non-biofouling modification of SiO_2-based surfaces are not limited to the use of linear PEG. Block copolymers, graft copolymers, networks or hydrogels, and PEG-terminated alkyltrichlorosilanes have been used to modify surfaces. PEG-*b*-poly(propylene glycol) (PPG) -*b*-PEG triblock copolymers have been physisorbed through PPG[70] or covalently grafted by γ-irradiation[71] to SiO_2 surfaces that was previously modified hydrophobic. Other examples of PEG-containing block copolymers used to attach PEG by

physical adsorption onto hydrophobized glass through hydrophobic moieties include PEG-*b*-poly(butylenes glycol)-*b*-PEG[72,73] and PEG-b-polystyrene[74]. The electrostatic interaction between various PEG-containing copolymers such as a poly(*n*-acetylethyleneimine)-*b*-PEG-*b*-poly(*n*-acetylethyleneimine) triblock copolymer,[75,76] or a poly(*l*-lysine) (PLL)-g-PEG graft copolymer[77-79] and a SiO_2 surface has also been used to graft PEGs. PEG films on glass have been prepared by the physisorption of poly(methyl methacrylate) (PMMA)-*g*-PEG graft copolymers,[80] or, alternatively, by a radiation-induced graft polymerization of poly(ethylene glycol) methacrylate (PEGMA),[81] to yield PMMA-*g*-PEG polymer films. Techniques based on vacuum environment, such as plasma deposition of tetraglyme,[82-84] polymerization of ethylene oxide under vacuum,[85] and plasma polymerization of ethylene oxide-containing allyl ether[86-88] have been pursued as alternative. PEG brushes polymerized from surfaces by surface-initiated radical polymerization of PEG-modified acrylates have been recently reported.[89,90] As discussed in Section 1.3.1, SAMs of oEG-terminated trichlorosilane also renders the SiO_2-based surfaces protein-resistant.[23,49,68]

1.4. References for Chapter 1

(1) Asanov, A. N.; Wilson, W. W.; Odham, P. B. Regenerable biosensor platform: A total internal reflection fluorescence cell with electrochemical control. *Anal. Chem.* **1998**, *70*, 1156-1163.

(2) Lahiri, J.; Isaacs, L.; Tien, J.; Whitesides, G. M. A strategy for the generation of surfaces presenting ligands for studies of binding based on an active ester as a common reactive intermediate: A surface plasmon resonance study. *Anal. Chem.* **1999**, *71*, 777-790.

(3) Luppa, P. B.; Sokoll, L. J.; Chan, D. W. Immunosensors - principles and applications to clinical chemistry. *Clin. Chim. Acta* **2001**, *314*, 1-26.

(4) Ramsden, J. J. Optical biosensors. *J. Mol. Recognit.* **1997**, *10*, 109-120.

(5) Rogers, K. R. Principles of affinity-based biosensors. *Mol. Biotechnol.* **2000**, *14*, 109-129.

(6) Wink, T.; van Zuilen, S. J.; Bult, A.; van Bennekom, W. P. Self-assembled monolayers for biosensors. *Analyst* **1997**, *122*, R43-R50.

(7) Moussy, F.; Harrison, D. J. Prevention of the rapid degradation of subcutaneously

implanted ag/agcl reference electrodes using polymer-coatings. *Anal. Chem.* **1994**, *66*, 674-679.

(8) Ganapathi-Desai, S.; Butterfield, D. A.; Bhattacharyya, D. Kinetics and active fraction determination of a protease enzyme immobilized on functionalized membranes: Mathematical modeling and experimental results. *Biotechnol. Progr.* **1998**, *14*, 865-873.

(9) McGlennen, R. C. Miniaturization technologies for molecular diagnostics. *Clin. Chem.* **2001**, *47*, 393-402.

(10) Rebeski, D. E.; Winger, E. M.; Shin, Y. K.; Lelenta, M.; Robinson, M. M.; Varecka, R.; Crowther, J. R. Identification of unacceptable background caused by non-specific protein adsorption to the plastic surface of 96-well immunoassay plates using a standardized enzyme-linked immunosorbent assay procedure. *J. Immunol. Methods* **1999**, *226*, 85-92.

(11) Petsch, D.; Anspach, F. B. Endotoxin removal from protein solutions. *J. Biotechnol.* **2000**, *76*, 97-119.

(12) Teng, S. F.; Sproule, K.; Husain, A.; Lowe, C. R. Affinity chromatography on immobilized "biomimetic" ligands synthesis, immobilization and chromatographic assessment of an immunoglobulin g-binding ligand. *J. Chromatogr. B* **2000**, *740*, 1-15.

(13) Novotny, M. V. Capillary biomolecular separations. *J. Chromatogr. B* **1997**, *689*, 55-70.

(14) Novotny, M. V. Microcolumn liquid chromatography in biochemical analysis. In *High resolution separation and analysis of biological macromolecules, pt. A*, **1996**; Vol. 270, pp 101-133.

(15) Xu, B.; Vermeulen, N. P. E. Preparation of wall-coated open-tubular capillary columns for gas chromatography. *J. Chromatogr.* **1988**, *445*, 1-28.

(16) Bizios, R. Osteoblasts - an in-vitro model of bone-implant interactions - mini review. *Biotechnol. Bioeng.* **1994**, *43*, 582-585.

(17) Ducheyne, P.; Qiu, Q. Bioactive ceramics: The effect of surface reactivity on bone formation and bone cell function. *Biomaterials* **1999**, *20*, 2287-2303.

(18) Tang, L. P.; Eaton, J. W. Inflammatory responses to biomaterials. *Am. J. Clin. Pathol.* **1995**, *103*, 466-471.

(19) Malmsten, M., *Ed. Biopolymers at interfaces*; Marcel Dekker: New York, 1998; Vol. 75.

(20) Lee, J. H.; Lee, H. B.; Andrade, J. D. Blood compatibility of polyethylene oxide surfaces. *Prog. Polym. Sci.* **1995**, *20*, 1043-1079.

(21) Seong, J.; Choi, H.-G.; Moeser, G. D.; Laibinis, P. E. Preparation of protein- and cell-resistant surfaces on silicon dioxide surfaces by polyether-grafted poly(acrylic acid) thin films. *Polym. Preprint.* **2003**, *44*, 189-190.

(22) Jon, S.; Seong, J.; Khademhosseini, A.; Tran, T.-N. T.; Laibinis, P. E.; Langer, R. Construction of nonbiofouling surfaces by polymeric self-assembled monolayers. *Langmuir* **2003**, *19*, 9989-9993.

(23) Seong, J.; Lee, S.-W.; Laibinis, P. E. Formation, characterization, protein resistance, and reactivity of $Cl_3Si(CH_2)_{11}(OCH_2CH_2)_3OH$ self-assembled monolayers. *Mat. Res. Soc. Sym. Proc.* **2002**, *724*, 63-68.

(24) Goosen, J. F. L. Design considerations for silicon sensors for use in catheters and guide wires. *Smart. Mater. Struct.* **2002**, *11*, 804-812.

(25) McConnel, H. M.; Owicki, J. C.; Parce, J. W.; Miller, D. L.; Baxter, G. T.; Wada, H. G.; Pitchford, S. The cytosensor microphysiometer: Biological applications of silicon technology. *Science* **1992**, *257*, 1906-1912.

(26) Parce, J. W.; Owicki, J. C.; Kercso, K. M.; Sigal, G. B.; Wada, H. G.; Muir, V. C.; Bousse, L. J.; Ross, K. L.; Sikic, B. I.; McConnell, H. M. Detection of cell-affecting agents with a silicon biosensor. *Science* **1989**, *246*, 243-247.

(27) Manz, A.; Harrison, D. J.; Verpoorte, E. M.; Fettinger, J. C.; Paulus, A.; Ludi, H.; Widmer, H. M. Planar chips technology for miniaturization and integration of separation techniques into monitoring systems. *J. Chromatogr.* **1992**, *593*.

(28) Fu, A. Y.; Spence, C.; Scherer, A.; Arnold, F. H.; Quake, S. R. A microfabricated fluorescence-activated cell sorter. *Nat. Biotechnol.* **1999**, *17*, 1109-1111.

(29) Anderson, J. R.; Chiu, D. T.; Jackman, R. J.; Cherniavskaya, O.; McDonald, J. C.; Wu, H. K.; Whitesides, S. H.; Whitesides, G. M. Fabrication of topologically complex three-dimensional microfluidic systems in pdms by rapid prototyping. *Anal. Chem.* **2000**, *72*, 3158-3164.

(30) Chiu, D. T.; Jeon, N. L.; Huang, S.; Kane, R. S.; Wargo, C. J.; Choi, I. S.; Ingber, D. E.; Whitesides, G. M. Patterned deposition of cells and proteins onto surfaces by using three-dimensional microfluidic systems. *P. Natl. Acad. Sci.* **2000**, *97*, 2408-2413.

(31) Charati, S. G.; Stern, S. A. Diffusion of gases in silicone polymers: Molecular dynamics simulations. *Macromolecules* **1998**, *31*, 5529-5535.

(32) Borenstein, J. T.; Terai, H.; King, K. R.; Weinberg, E. J.; Kaazempur-Mofrad, M. R.; Vacanti, J. P. Microfabrication technology for vascularized tissue engineering. *Biomed. Microdevices* **2002**, *4*, 167-175.

(33) Bhatia, S. N.; Balis, U. J.; Yarmush, M. L.; Toner, M. Microfabrication of hepatocyte/fibroblast co-cultures: Role of homotypic cell interactions. *Biotechnol. Progr.* **1998**, *14*, 378-387.

(34) Folch, A.; Toner, M. Microengineering of cellular interactions. *Annu. Rev. Biomed. Eng.* **2000**, *02*, 227-256.

(35) Harris, J. M., *Ed. Poly(ethylene glycol) chemistry : Biotechnical and biomedical applications*; Plenum Press, 1992.

(36) Yang, Z. H.; Galloway, J. A.; Yu, H. U. Protein interactions with poly(ethylene glycol) self-assembled monolayers on glass substrates: Diffusion and adsorption. *Langmuir* **1999**, *15*, 8405-8411.

(37) Nagaoka, S.; Mori, Y.; Takiuchi, H.; Yokoata, K.; Tanzawa, H.; Nishiumi, S. Interaction between blood components and hydrogels with poly(oxyethylene) chains. In *Polymers as biomaterials*; Shalaby, S. W.;Hoffman, A. S.;Ratner, B. D.;Horbett, T. A., *Eds.*; Plenum Press: New York, **1985**, pp 361-374.

(38) Norde, W. Adsorption of proteins from solution at the solid-liquid interface. *Adv.*

Colloid Interf. Sci. **1986**, *25*, 267-340.

(39) Kjellander, R.; Florin, E. Water-structure and changes in thermal-stability of the system poly(ethylene oxide)-water. *J. Chem. Soc., Farad. T.* **1981**, *77*.

(40) Alexander, S. Polymer adsorption on small spheres - scaling approach. *J. Phys. (Paris)* **1977**, *38*, 977-981.

(41) Jeon, S. I.; Lee, J. H.; Andrade, J. D.; de Gennes, P. G. Protein-surface interactions in the presence of polyethylene oxide. 1. Simplified theory. *J. Coll. Interf. Sci.* **1991**, *142*, 149-158.

(42) Halperin, A. Polymer brushes that resist adsorption of model proteins: Design parameters. *Langmuir* **1999**, *15*, 2525-2533.

(43) Papisov, M. I. Theoretical considerations of res-avoiding liposomes: Molecular mechanics and chemistry of liposome interactions. *Adv. Drug Deliv. Rev.* **1998**, *32*, 119-138.

(44) Szleifer, I. Protein adsorption on tethered polymer layers: Effect of polymer chain architecture and composition. *Physica A* **1997**, *244*, 370-388.

(45) Szleifer, I. Protein adsorption on surfaces with grafted polymers: A theoretical approach. *Biophys. J.* **1997**, *72*, 595-612.

(46) Fang, F.; Szleifer, I. Kinetics and thermodynamics of protein adsorption: A generalized molecular theoretical approach. *Biophys. J.* **2001**, *80*, 2568-2589.

(47) Prime, K. L.; Whitesides, G. M. Self-assembled organic monolayers - model systems for studying adsorption of proteins at surfaces. *Science* **1991**, *252*, 1164-1167.

(48) Prime, K. L.; Whitesides, G. M. Adsorption of proteins onto surfaces containing end-attached oligo(ethylene oxide) - a model system using self-assembled monolayers. *J. Am. Chem. Soc.* **1993**, *115*, 10714-10721.

(49) Lee, S.-W.; Laibinis, P. E. Protein-resistant coatings for glass and metal oxide surfaces derived from oligo(ethylene glycol)-terminated alkyltrichlorosilanes. *Biomaterials* **1998**, *19*, 1669-1675.

(50) Harder, P.; Grunze, M.; Dahint, R.; Whitesides, G. M.; Laibinis, P. E. Molecular conformation in oligo(ethylene glycol)-terminated self-assembled monolayers on gold and silver surfaces determines their ability to resist protein adsorption. *J. Phys. Chem. B* **1998**, *102*, 426-436.

(51) Feldman, K.; Haehner, G.; Spencer, N. D.; Harder, P.; Grunze, M. Probing resistance to protein adsorption of oligo(ethylene glycol)-terminated self-assembled monolayers by scanning force microscopy. *J. Am. Chem. Soc.* **1999**, *121*, 10134-10141.

(52) Dicke, C.; Haehner, G. Interaction between a hydrophobic probe and tri(ethylene glycol)-containing self-assembled monolayers on gold studied with force spectroscopy in aqueous electrolyte solution. *J. Phys. Chem. B* **2002**, *106*, 4450-4456.

(53) Dicke, C.; Haehner, G. pH-dependent force spectroscopy of tri(ethylene glycol)- and methyl-terminated self-assembled monolayers adsorbed on gold. *J. Am. Chem. Soc.* **2002**, *124*, 12619-12625.

(54) Wang, R. L. C.; Kreuzer, H. J.; Grunze, M. Molecular conformation and solvation of

oligo(ethylene glycol)- terminated self-assembled monolayers and their resistance to protein adsorption. *J. Phys. Chem. B* **1997**, *101*, 9767-9773.

(55) Kim, H. I.; Kushmerick, J. G.; Houston, J. E.; Bunker, B. C. Viscous "interface" water adjacent to oligo(ethylene glycol)-termianted self-assembled monolayers. *Langmuir* **2003**, *19*, 9271-9275.

(56) Pertsin, A. J.; Grunze, M. Computer simulation of water near the surface of oligo(ethylene glycol)-terminated alkanethiol self-assembled monolayers. *Langmuir* **2000**, *16*, 8829-8841.

(57) Zolk, M.; Eisert, F.; Pipper, J.; Herrwerth, S.; Eck, W.; Buck, M.; Grunze, M. Solvation of oligo(ethylene glycol)-terminated self-assembled monolayers studied by vibrational sum frequency spectroscopy. *Langmuir* **2000**, *16*, 5849-5852.

(58) Valiokas, R.; Östblom, M.; Svedhem, S.; Svensson, S. C. T.; Liedberg, B. Temperature-driven phase transitions in oligo(ethylene glycol)-terminated self-assembled monolayers. *J. Phys. Chem. B* **2000**, *104*, 7565-7569.

(59) Wang, R. L. C.; Kreuzer, H. J.; Grunze, M. The interaction of oligo(ethylene oxide) with water: A quantum mechanical study. *Phys. Chem. Chem. Phys.* **2000**, *2*, 3613-3622.

(60) Zwahlen, M.; Herrwerth, S.; Eck, W.; Grunze, M.; Hähner, G. Conformational order in oligo(ethylene glycol)-terminated self-assembled monolayers on gold determined by soft x-ray absorption. *Langmuir* **2003**, *19*, 9305-9310.

(61) Emoto, K.; Harris, J. M.; van Alstine, J. M. Grafting poly(ethylene glycol) epoxide to amino-derivatized quartz: Effect of temperature and ph on grafting density. *Anal. Chem.* **1996**, *68*, 3751-3757.

(62) Sofia, S. J.; Merrill, E. W. Grafting of PEO to polymer surfaces using electron beam irradiation. *J. Biomed. Mater. Res.* **1998**, *40*, 153-163.

(63) Stark, M. B.; Holmberg, K. Covalent immobilization of lipase in organic-solvents. *Biotechnol. Bioeng.* **1989**, *34*, 942-950.

(64) Irvine, D. J.; Mayes, A. M.; Satija, S. K.; Barker, J. G.; Sofia-Allgor, S. J.; Griffith, L. G. Comparison of tethered star and linear poly(ethylene oxide) for control of biomaterials surface properties. *J. Biomed. Mater. Res.* **1998**, *40*, 498-509.

(65) Jenney, C. R.; Anderson, J. M. Effects of surface-coupled polyethylene oxide on human macrophage adhesion and foreign body giant cell formation in vitro. *J. Biomed. Mater. Res.* **1999**, *44*, 206-216.

(66) Tseng, Y.-C.; Park, K. Synthesis of photoreactive poly(ethylene glycol) and its application to the prevention of surface-induced platelet activation. *J. Biomed. Mater. Res.* **1992**, *26*, 373-391.

(67) Zhang, M.; Desai, T. A.; Ferrari, M. Proteins and cells on peg immobilized silicon surfaces. *Biomaterials* **1998**, *19*, 953-960.

(68) Jo, S.; Park, K. Surface modification using silanated poly(ethylene glycol)s. *Biomaterials* **2000**, *21*, 605-616.

(69) Alcantar, N. A.; Aydil, E. S.; Israelachvili, J. N. Polyethylene glycol-coated

biocompatible surfaces. *J. Biomed. Mater. Res.* **2000**, *51*, 343-351.

(70) Kamath, K. R.; Danilich, M. J.; Marchant, R. E.; Park, K. Platelet interactions with plasma-polymerized ethylene oxide and *n*-vinyl-2-pyrrolidone films and linear poly(ethylene oxide) layer. *J. Biomater. Sci., Polym. Ed.* **1996**, *7*, 977-988.

(71) Amiji, M.; Park, K. Surface modification by radiation-induced grafting of PEO/PPO/PEO triblock copolymers. *J. Coll. Interf. Sci.* **1993**, *155*, 251-255.

(72) Gingell, D.; Owens, N. Inhibition of platelet spreading from plasma onto glass by an adsorbed layer of a novel fluorescent-labeled poly(ethylene oxide)/poly(butylene oxide) block copolymer - characteristics of the exclusion zone probed by means of polystyrene beads and macromolecules. *J. Biomed. Mater. Res.* **1994**, *28*, 491-503.

(73) Gingell, D.; Owens, N. F.; Hodge, P.; Nicholas, C. V.; Odell, R. Adsorption of a novel fluorescent derivative of a poly(ethylene oxide)/poly(butylene oxide) block copolymer on octadecyl glass studied by total internal-reflection fluorescence and interferometry. *J. Biomed. Mater. Res.* **1994**, *28*, 505-513.

(74) Grainger, D. W.; Nojiri, C.; Okano, T.; Kim, S. W. *In vitro* and *ex vivo* platelet interactions with hydrophilic hydrophobic poly(ethylene oxide)-polystyrene multiblock copolymers. *J. Biomed. Mater. Res.* **1989**, *23*, 979-1005.

(75) Maechling-Strasser, C.; Dejardin, P.; Galin, J. C.; Schmitt, A. Preadsorption of polymers on glass and silica to reduce fibrinogen adsorption. *J. Biomed. Mater. Res.* **1989**, *23*, 1385-1393.

(76) Maechling-Strasser, C.; Dejardin, P.; Galin, J. C.; Schmitt, A.; Housse-Ferrari, V.; Sebille, B.; Mulvihill, J. N.; Cazenave, J. P. Synthesis and adsorption of a poly(*n*-acetylethylenimine)-polyethylene oxide-poly(*n*-acetylethylenimine) triblock-copolymer at a silica/solution interface. Influence of its preadsorption on platelet adhesion and fibrinogen adsorption. *J. Biomed. Mater. Res.* **1989**, *23*, 1395-1410.

(77) Michel, R.; Reviakine, I.; Sutherland, D.; Fokas, C.; Csucs, G.; Danuser, G.; Spencer, N. D.; Textor, M. A novel approach to produce biologically relevant chemical patterns at the nanometer scale: Selective molecular assembly patterning combined with colloidal lithography. *Langmuir* **2002**, *18*, 8580-8586.

(78) Michel, R.; Lussi, J. W.; Csucs, G.; Reviakine, I.; Danuser, G.; Ketterer, B.; Hubbell, J. A.; Textor, M.; Spencer, N. D. Selective molecular assembly patterning: A new approach to micro- and nanochemical patterning of surfaces for biological applications. *Langmuir* **2002**, *18*, 3281-3287.

(79) Csucs, G.; Michel, R.; Lussi, J. W.; Textor, M.; Danuser, G. Microcontact printing of novel co-polymers in combination with proteins for cell-biological applications. *Biomaterials* **2003**, *24*, 1713-1720.

(80) Irvine, D. J.; Mayes, A. M.; Griffith, L. G. Nanoscale clustering of rgd peptides at surfaces using comb polymers. 1. Synthesis and characterization of comb thin films. *Biomacromolecules* **2001**, *2*, 85-94.

(81) Sun, Y. H.; Gombotz, W. R.; Hoffman, A. S. Synthesis and characterization of non-fouling polymer surfaces: I. Radiation grafting of hydroxyethyl methacrylate and

polyethylene glycol methacrylate onto silastic film. *J. Bioact. Compat. Polym.* **1986**, *1*, 316-334.

(82) Shen, M.; Wagner, M. S.; Castner, D. G.; Ratner, B. D.; Horbett, T. A. Multivariate surface analysis of plasma-deposited tetraglyme for reduction of protein adsorption and monocyte adhesion. *Langmuir* **2003**, *19*, 1692-1699.

(83) Shen, M.; Pan, Y. V.; Wagner, M. S.; Hauch, K. D.; Castner, D. G.; Ratner, B. D.; Horbett, T. A. Inhibition of monocyte adhesion and fibrinogen adsorption on glow discharge plasma deposited tetraethylene glycol dimethyl ether. *J. Biomater. Sci., Polym. Ed.* **2001**, *12*, 961-978.

(84) Lopez, G. P.; Ratner, B. D.; Tidwell, C. D.; Haycox, C. L.; Rapoza, R. J.; Horbett, T. A. Glow discharge plasma deposition of tetraethylene glycol dimethyl ether for fouling-resistant biomaterial surfaces. *J. Biomed. Mater. Res.* **1992**, *26*, 415-439.

(85) Popat, K. C.; Johnson, R. W.; Desai, T. A. Characterization of vapor deposited poly(ethylene glycol) films on silicon surfaces for surface modification of microfluidic systems. *J. Vac. Sci. Technol., B* **2003**, *21*, 645-654.

(86) Pan, Y. V.; McDevitt, T. C.; Kim, T. K.; Leach-Scampavia, D.; Stayton, P. S.; Denton, D. D.; Ratner, B. D. Micro-scale cell patterning on nonfouling plasma polymerized tetraglyme coatings by protein microcontact printing. *Plasmas Polym.* **2002**, *7*, 171-183.

(87) Wu, Y. J.; Timmons, R. B.; Jen, J. S.; Molock, F. E. Non-fouling surfaces produced by gas phase pulsed plasma polymerization of an ultra low molecular weight ethylene oxide containing monomer. *Colloids Surf., B* **2000**, *18*, 235-248.

(88) Beyer, D.; Knoll, W.; Ringsdorf, H.; Wang, J. H.; Timmons, R. B.; Sluka, P. Reduced protein adsorption on plastics via direct plasma deposition of triethylene glycol monoallyl ether. *J. Biomed. Mater. Res.* **1997**, *36*, 181-189.

(89) Andruzzi, L.; Senaratne, W.; Hexemer, A.; Ober, C. K.; Kramer, E. J. PEG-based biostable surfaces by controlled radical polymerization. *Polym. Mat. Sci. Eng.* **2003**, *88*, 604-605.

(90) Senaratne, W.; Andruzzi, L.; Sheets, E. D.; Holowka, D.; Ilic, B.; Hexemer, A.; Baird, B.; Kramer, E. J.; Ober, C. K. Exploring the potential of surface grown PEG-polymer brushes for biotechnology applications. *Polym. Mat. Sci. Eng.* **2003**, *88*, 337-338.

Chapter 2. Preparation of Non-Biofouling Surfaces by Polyanionic Graft Copolymers of Poly(ethylene glycol).

2.1. Introduction

Nonspecific accumulation of biological components onto device surfaces causes adverse biological events in the device performance. For example, the nonspecific adsorption of proteins and cells directly affects the sensitivity, specificity, and reproducibility of chip-based bioassays. Thus, creating protein- and cell-resistant surfaces has been one of the main challenges in the development of biosensors,[1-4] chip-based bioassays,[5,6] and bioreactors[7,8].

The protein- and cell-repelling property of PEG[9] has motivated researchers to create PEG-coated surfaces for imparting non-biofouling properties to surfaces. A generic approach to functionalizing silicon dioxide surfaces (*e.g.*, glasses, quartz, silicon wafers, and PDMS with a thin oxide layer generated by an O_2 plasma treatment) with PEG is to tether PEG moieties whose chain ends are modified to have strong attraction with the underlying substrates. One example is the derivatization of the surfaces by amine-terminated silanes and the subsequent grafting of end-functionalized (*e.g.*, epoxy-terminated) PEG to the amine-terminated surfaces.[10-12] Another attempt is direct silanization of surfaces using silanated PEG derivatives such as mono-trichlorosilyl PEG[13,14] and mono-trialkoxysilyl PEG[15,16]. While these approaches are versatile, they may not result in efficient PEG coatings. First, they rely on end-immobilization of PEG derivatives which have only one reactive end group per polymer chain. Second, when the adsorbate to be grafted deviates from a long hydrocarbon chain, it is difficult to form a densely packed layer using a trichlorosilane or a trialkoxysilane group. This difficulty can be attributed to the fact that the interactions

between the hydrocarbon chains gather the chains to self assemble to form a closely packed monolayer.[17]

Considering the above limitations of monovalent PEG, one alternative strategy for creating an effective PEG coating with high surface density is to incorporate multiple surface anchoring groups in one polymer chain. Graft copolymers where PEG side chains are grafted onto a polymer backbone may offer a straightforward approach to the design of such multivalent polymers. The objective of the work discussed in this chapter and the following chapter is to devise efficient methods for anchoring PEG chains on SiO_2 surfaces by using graft copolymers of PEG.

Previous attempts at applying graft copolymers of poly(L-lysine)-*g*-poly(ethylene glycol) (PLL-*g*-PEG) to biofouling resistant coating have demonstrated their versatile applicability.[18-20] In the PLL-*g*-PEG approach, PEG chains are attached to negatively charged surfaces via electrostatic interaction between the cationic backbone of PLL and the surface. This system provides an effective strategy for modifying metal oxides and other negatively charged surfaces; however, it requires multistep preparation from expensive reactants.

This chapter focuses on the generation of non-biofouling surfaces by anionic graft copolymers having a poly(acrylic acid) (PAA) backbone and PEG-containing side chains. The polyanionic main chain, PAA, serves as an 'anchor part' for attaching to positively charged surfaces through electrostatic interactions between PAA and the underlying surfaces. The polymer used as side chains was Jeffamine XTJ-234, a polyoxyalkyleneamine produced by Huntsman Co. It is a random copolymer of ethylene glycol (EG) and propylene glycol (PG) containing 86 mol % of EG units (PEG-*r*-PPG). It contains one primary amine group and one methoxy group attached to each terminus of the polyether chain. As a member of

Jeffamine® brand family, XTJ-234 is mainly employed as an epoxy curing agent. However, the reactive amine group at one chain end can be explored in other reactions. The other end is terminated with a methoxy group. This inert chain end may be used in preventing the polymer from forming networks between the reactants. A class of graft copolymers that includes a PAA backbone and incorporates different grafting ratios of a linear polyether chain was prepared. For simplicity, this graft copolymer will be denoted as PAA-x%*g*-(PEG-*r*-PPG), where x% of the carboxylic acid group reacted with Jeffamine XTJ-234. Si/SiO_2 and PDMS surfaces were used as substrates. Si/SiO_2 wafers were used as a model SiO_2 surface because they are easy to handle and characterize by various surface characterization methods. Films were formed and tested on PDMS slabs as well because PDMS surfaces are widely used in microfluidic devices and bioreactors.

2.2. Experimental Section

2.2.1. Materials

Jeffamine XTJ-234 (H_2N-(PEG-*r*-PPG)-OCH_3; EG/PG = 6.1/1 and M_w *ca.* 3,000 as provided by Huntsman) was obtained from Huntsman Co. (Houston, TX). Lysozyme (EC 2326204), fibrinogen (EC 2325986), hexokinase (EC 2326115), and insulin (EC 2342912) were from Sigma. N-(6-Aminohexyl)aminopropyltrimethoxysilane ($H_2N(CH_2)_6NH(CH_2)_3Si(OCH_3)_3$; AHPTS) was obtained from Gelest, Inc. (Morrisville, PA). Sodium hydroxide was purchased from Mallinckrodt. Deutrated dimethyl sulfoxide (DMSO-d^6) was from Cambridge Isotope Laboratories (Cambridge, MA). Poly(acrylic acid) (PAA; 50 wt% aqueous solution, M_w 5,000), and other materials were obtained from Aldrich (Milwaukee, WI) unless specified otherwise. All chemicals were used as received.

Poly(dimethylsiloxane) (PDMS) elastomeric substrates were made by casting the mixture of 10:1 prepolymer and the curing agent in a two-component silicon elastomer kit (Sylgard 184; Dow Corning) onto a glass petri dish and then annealing the cast mixture at 70 °C for 2 h. Typical thickness of the PDMS slab was 2 mm.

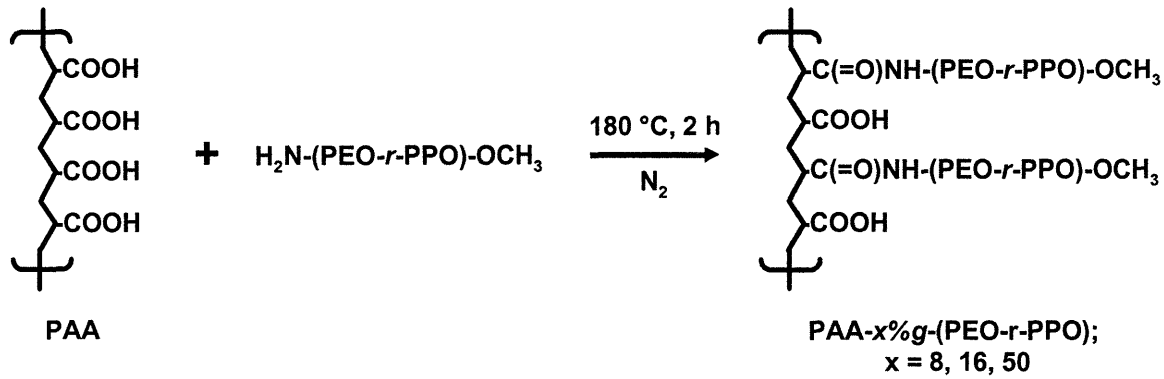

Scheme 2.1. Synthesis of PAA-x%g-(PEG-r-PPG) polymer. A grafting percentage x% means that x% of the carboxylic acid groups on the PAA backbone were coupled with H_2N-(PEG-*r*-PPG)-OCH_3 to form amide bonds.

A one-step synthetic procedure to form the PAA-g-(PEG-r-PPG) graft copolymers via a simple amidation reaction at 180 °C has been described elsewhere.[21] By this procedure, a series of related graft copolymers with 8%, 16%, and 50% of the backbone PAA chains grafted with Jeffamine XTJ-234 were prepared (Scheme 2.1). The products were obtained as highly viscous liquid and were stored at room temperature as 33 wt% aqueous solutions. ^{1}H-NMR spectra of the polymers were obtained using a Bruker instrument (Avance DPX 400). To obtain ^{1}H-NMR spectra, a small portion of the aqueous solutions of each graft copolymer was dialyzed and lyophilized to remove water and dissolved in DMSO-d^6 at a concentration of *ca.* 1 wt%. Reaction yields after 2 h reaction were 95% for 8%, 16% graft copolymers and

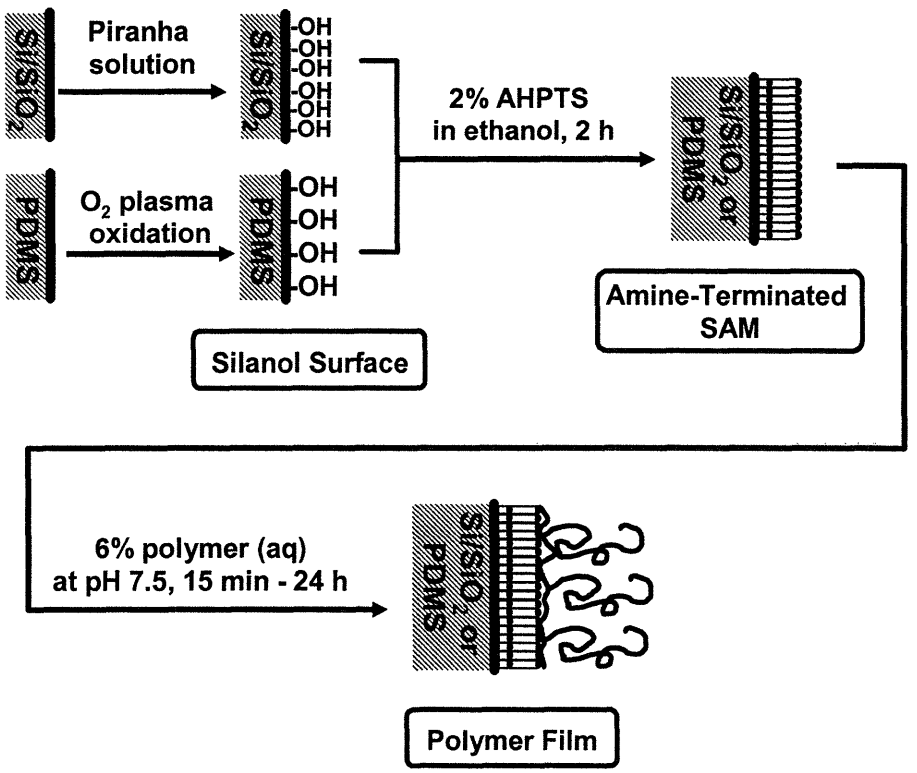

Scheme 2.2. Schematic diagram of the modification procedure for producing PAA-*g*-(PEG-*r*-PPG) films on Si/SiO_2 wafers and PDMS surfaces.

83% for 50% graft copolymers, as calculated from the optical density (O.D.) at 570 nm after Ninhydrin reaction using reactant H_2N-(PEG-*r*-PPG)-OCH_3 as a reference. Details of Ninhydrin test are described elsewhere.[22] These graft polymers will be denoted by PAA-x%g-(PEG-r-PPG) with x = 8, 16, and 50, respectively. Grafting of PEG-r-PPG was further confirmed by IR and ^{1}H-NMR spectra.

2.2.2. Formation of Graft Copolymer Films on Si/SiO_2 and PDMS Surfaces

Scheme 2.2 illustrates the sample fabrication procedure to create PAA-*g*-(PEG-*r*-PPG) layers on Si/SiO_2 and PDMS surfaces.

Preparation of amino-containing self-assembled monolayers (SAMs). Si/SiO_2 wafers were cleaned by immersion in 'piranha' solution (v/v 7/3 mixture of *conc.* H_2SO_4 and 30 %

H_2O_2 (*aq*)) for 30 min at 80 °C. (CAUTION: 'Piranha' solution reacts violently with many organic materials and should be handled with care.) The substrates were then rinsed immediately with deionized water, and dried in a stream of N_2. AHPTS was dissolved in dry ethanol to a concentration of 2 %. After measuring bare ellipsometric optical constants on the substrates, they were immediately transferred to an AHPTS solution. After 2 h of contact, the samples were rinsed with ethanol, sonicated in ethanol for 15 min, and dried in a stream of N_2.

PDMS substrates were first oxidized in an oxygen plasma cleaner/sterilizer (PDC-32G, Harrick Scientific) for 30 s at 0.15 Torr O_2 pressure, and then immersed into a solution of AHPTS in dry ethanol (2%) for 2-24 h. The PDMS substrates were then removed from solution, rinsed with ethanol, sonicated in ethanol for 15 min, and dried under the stream of N_2.

Adsorption of polymers onto AHPTS SAMs. The Si/SiO_2 wafers and PDMS substrates containing an AHPTS SAM were immersed into 7 % aqueous solutions of PAA-*g*-(PEG-*r*-PPG) at pH 7.4 for 0.5 h (Si/SiO_2 wafers) or for 24 h (PDMS), followed by rinsing with distilled water and drying under N_2.

2.2.3. Protein Adsorption on Polymer Modified Surfaces.

The examined proteins were each dissolved at a concentration of 0.25 mg/mL in 10 mM phosphate buffer saline (PBS) solution (pH = 7.4). The PBS solution was prepared by dissolving a Phosphate Buffered Saline Tablet (Sigma) in 200 mL of deionized water to obtain a solution that contained 10 mM sodium phosphate buffer, 2.7 mM KCl, and 137 mM NaCl. Substrates were immersed in the protein solution for 24 h, and were washed sequentially with PBS solution and water to remove non-adsorbed proteins and salts in the PBS solution. The samples were then blown dry in a stream of N_2.

2.2.4. Bacterial growth and adhesion.

The bacterial adhesion on the polymer films was assessed *in vitro* by culturing *E. coli* (DPD 2417) on the films. All the polymer-modified Si/SiO_2 wafers were attached to the bottom of the fermentor, autoclaved for 20 min at 125 °C and 28 psi, and cooled down to room temperature. The medium was autoclaved separately and 500 ml was poured into the fermentor in a laminar flow hood. After stabilizing the fermentor to the temperature of 37 °C and aeration of 2 VVM with agitation speed of 150 rpm, the seed culture of *E. coli* was inoculated and cultivated for 11 h. The substrates were then removed from the fermentor and gently rinsed with water, and dried.

The polymer-modified PDMS sheets were attached to petri dishes and autoclaved with the same conditions. After cooling down to room temperature, separately autoclaved medium was poured into the dish and the seed culture of *E. coli* was inoculated. The cells were incubated at 37°C for 20 h. The substrates were then removed from of the dishes, rinsed with water, and dried.

2.2.5. Characterization

Fourier Transform - Infrared Spectroscopy (FT-IR). To monitor the grafting of NH_2-(PEG-*r*-PPG)-OCH_3 onto PAA backbone, FT-IR/ATR spectra of a series of PAA-*g*-(PEG-*r*-PPG) were taken. A small volume of each polymer solution was placed onto a polyethylene (PE) card (Thermo Spectra-Tech). After drying the solvent in 60 °C overnight, the IR spectrum of each polymer on PE card was recorded at the spectral resolution of 1 cm^{-1} on absorption mode on a Digilab FTS 175 spectrometer (Bio-Rad) with a narrow-band MCT detector.

Ellipsometry. The thicknesses of the monolayer films and of adsorbed protein layers on

Si/SiO_2 were measured with a Gaertner L116A ellipsometer (Gaertner Scientific Corporation, IL) at a 70° angle of incidence. A refractive index of 1.46 was used for all films, and a three-phase model was used to calculate thicknesses. Reported are average values of at least five measurements.

Contact angle measurements. A Ramé-Hart goniometer (Mountain Lakes, NJ) equipped with video camera and monitor was used to measure contact angles in both the advancing and receding modes (~1 μL/s) on drops of ~3 μL in volume. Reported values represent averages of at least three independent measurements.

X-ray photoelectron spectroscopy (XPS). To determine the surface composition of the substrates at various stages, XPS measurements were performed on a Surface Science Instrument Model X-100 using a monochromatic Al Kα X-ray source and a concentric hemispherical analyzer. The take-off angle for the detector was 35° from the surface plane. Spectra were fit with 100 % Gaussian peaks and a linear baseline. For C(1s) spectra, binding energy data were referenced to the hydrocarbon peak set to 285.0 eV.

Optical Microscopy (OM). To probe the bacterial adhesion of the substrates, adherent *E. coli* cells were imaged with a HFX-DX optical/fluorescence microscope (Nikon, Japan) and a computer-aided picture capturing system (IP-spectrum software).

2.3. Results and Discussion

2.3.1. Formation and Characterization of Polymer Films.

Preparation and characterization of polymers

A series of graft copolymers of PAA-x%g-(PEG-r-PPG) (x = 8, 16, 50) was prepared by heating the stoichiometric mixtures at 180 °C for 2 h under nitrogen. While pure PEG

degraded at 180 °C even with continuous bubbling of nitrogen and could not be grafted onto PAA, use of a PEG-r-PPG random copolymer allowed the reaction to proceed without degradation.

Because the product polymers were used without separation, it was essential to examine the reaction yields and the effect of unreacted polymers on the adsorption behavior of polymers. The latter will be discussed later in this chapter. Ninhydrin reaction[22] was used to obtain reaction yields by comparing the amount of amine in the reaction products arising from unreacted NH_2-(PEG-*r*-PPG)-OCH_3 with the amount of pure amine from NH_2-(PEG-*r*-PPG)-OCH_3 as a reference. Reaction yields after 2 h reaction were 95% for 8% and 16% graft copolymers, and 83% for 50% graft copolymers. Assuming that all the reacted NH_2-(PEG-*r*-PPG)-OCH_3 was grafted onto a PAA backbone, the actual grafting ratios of PAA-*x%g*-(PEG-*r*-PPG) where x = 8, 16, and 50 could be estimated to be 8%, 15%, and 41%, respectively. For simplicity, the nominal grafting ratios of 8%, 16%, and 50%, instead of actual ratios of 8%, 15%, and 41%, will be used throughout this thesis.

The increase in the amount of side chains in the graft copolymers was concurrent with the increase in x, as was evidenced from FT-IR and ^{1}H-NMR studies. The PEG-*r*-PPG chains are grafted onto a PAA backbone via amide linkage formation. Thus, the increase in the grafted side chains increases the relative intensities of C=O stretch peaks from the amide at 1673 cm^{-1} compared to those from carboxylic acid at 1732 cm^{-1} in FT-IR spectrum. Figure 2.1 is the graphical representation of this trend. While the majority of the C=O stretch peak of PAA-*8%g*-(PEG-*r*-PPG) comes from carboxylic acid in PAA backbone (Figure 2.1a), the peak from amide linkage becomes dominant in PAA-*50%g*- (PEG-*r*-PPG) (Figure 2.1c). Because carboxylic acid and amide are prone to rapid proton exchange, quantitative analysis of each group by NMR is difficult. However, the growth of amide peak intensity in the

polymer with increasing grafting ratio can be also qualitatively confirmed from ^{1}H-NMR analysis. In ^{1}H-NMR, PAA has a peak at $\delta \sim 12.4$ (br, 1H, COO*H*). Grafting of PEG-*r*-PPG chains onto a PAA backbone generates a peak at $\delta = 7 \sim 8$ (br, 1H, CON*H*) and decreases the relative peak intensity at $\delta \sim 12.4$. ^{1}H-NMR studies of the graft copolymers using DMSO-d^6 as a solvent revealed that 8% graft copolymer did not have a detectable amide peak while it had the biggest carboxylic acid peak intensity among the three copolymers studied. The peak intensity of $\delta \sim 7.6$ (br) relative to that of $\delta \sim 12.4$ (br) was 0.13 for a 16% graft copolymer. The 50% graft copolymer had the most distinct amide peak among the three graft copolymers but did not have a detectable carboxylic acid peak. These NMR and IR results qualitatively show that polymers with a higher grafting ratio contain more PEG-*r*-PPG side chains.

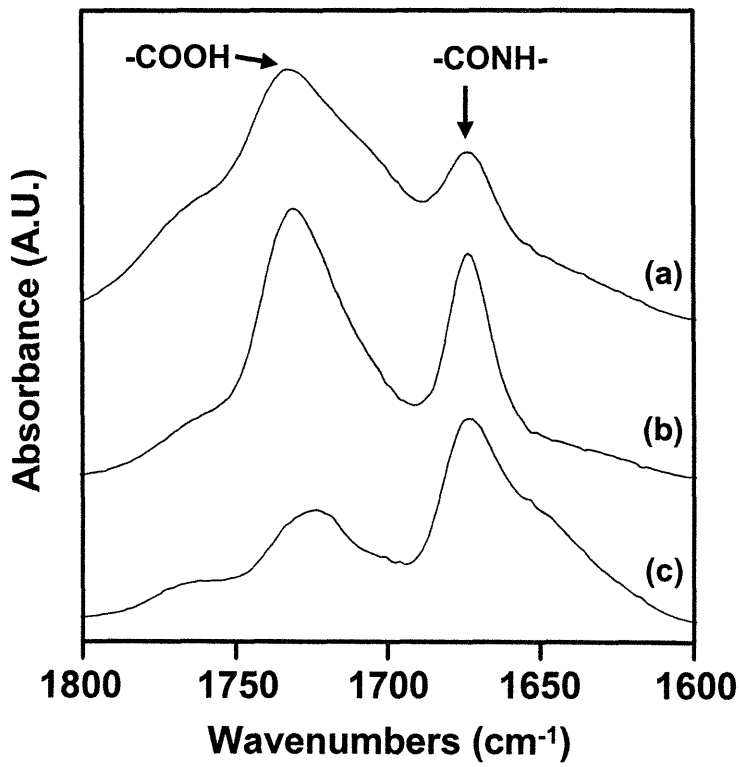

Figure 2.1. FT-IR spectra of PAA-*x*%*g*-(PEG-*r*-PPG) over the C=O stretching region: (a) $x = 8$, (b) $x = 16$, and (c) $x = 50$.

Formation of the PEG-containing polymer films.

The hydroxyl groups present on the Si/SiO_2 wafers and $_{ox}$PDMS slabs were first functionalized with N-(6-aminohexyl)aminopropyltrimethoxysilane (AHPTS) to generate surface amine groups used for adsorption. Thsse positively charged amino surfaces facilitated electrostatic binding with the negatively charged -C(=O)O- groups on the PAA chains to non-covalently hold the PAA-g-(PEG-r-PPG) polymers on the surface. PAA-g-(PEG-r-PPG) films were then prepared by immersing the AHPTS-surfaces in aqueous solutions of PAA-*g*-(PEG-*r*-PPG) at pH 7.5.

PEG-r-PPG films on Si/SiO₂. Dipping the cleaned Si/SiO_2 wafers into 2% AHPTS/ethanol solution for 2 h yielded an amine-containing layer of 12 Å in ellipsometric thickness and with water contact angles of 59° and 30°, advancing (θ_a) and receding (θ_r), respectively. The resulting amine-containing substrates were immersed in the polymer solutions to form PEG-*r*-PPG layers.

Table 2.1. Surface characterization of polymer films of Si/SiO_2/AHPTS/PAA-x%g-(PEG-r-PPG)[a,c]

X	Ellipsometric Thickness (Å)	Water contact angle[b]	
		θ_a	θ_r
8%	10	52°	32°
16%	11	46°	26°
50%	16	38°	20°

[a]x% denotes the percentage of the carboxylic acid groups on PAA that were reacted with NH_2-(PEG-*r*-PPG) chains.

[b]θ_a: advancing angle and θ_r: receding angle.

[c]The surface properties of the underlying AHPTS SAM are as follows: (ellipsometric thickness) 12 Å, (θ_a) 59°, (θ_r) 30°.

Thickness and the contact angles are often the simplest techniques for assessing the surface properties. Table 2.1 summarizes the ellipsometric thicknesses and water contact angles of Si/SiO_2 surfaces after grafting with PAA-*x%g*-(PEG-*r*-PPG). The thicknesses of the polymers were obtained by taking the difference of the thickness of the Si/SiO_2/AHPTS/PAA-*g*-(PEG-*r*-PPG) film and that of AHPTS SAM, *i.e.*, Si/SiO_2/AHPTS. Ellipsometric thickness of AHPTS SAM was 12 ± 1 Å. As expected, ellipsometric thicknesses of the polymer films increased with increasing grafting density of the PEG-*r*-PPG, with 8-12 Å at the lowest for 8% graft polymers and 13-20 Å at the highest for 50% graft polymers. Despite the accompanying increase of PPG moieties on the resulting surface, the surfaces became more hydrophilic with growing PEG-*r*-PPG contents, as evidenced by the decrease in water contact angle with increasing grafting density. In summary, the results in Table 2.1 suggest that the films formed from the polymers with higher grafting of PEG-*r*-PPG side chains are more hydrophilic and contain more polymers.

For PDMS, ellipsometry is not applicable and we used XPS as an alternative for ellipsometry for thickness measurement. To check the feasibility of the use of XPS for thickness calculation of PDMS-based samples, the thickness of the polymer films on Si/SiO_2 wafers determined by XPS was compared with the thickness by ellipsometry (Figure 2.2). The thickness of the films can be estimated based on the attenuation of photoelectron intensity from substrate Si(2p) by the following relation

$$I/I_0 = e^{(-\Delta d/\lambda \cos\theta)} \qquad (2.1)$$

where I and I_0 are the Si(2p) photoelectron intensities of the sample and a reference presenting a film of known thickness, respectively, Δd (Å) = $d - d_0$ is the difference between the thickness of the sample (d) and the reference (d_0), λ is the attenuation length of the Si(2p)

photoelectron intensity through an organic layer (Å), and θ is the take-off angle from surface normal, which was 55° in our experiments. Assuming the films are thin and homogeneous, λ in Å can be estimated as follows[23]

$$\lambda\ (\text{Å}) = 9.0 + 0.022\ \text{KE} \qquad (2.2)$$

where KE is the kinetic energy of photoelectrons (eV) found from the binding energy (BE) of the Si(2p) photoelectrons and from the energy of Al K(α) X-rays of 1486.6 eV by the following relation

$$\text{KE} = 1486.6 - \text{BE} \qquad (2.3)$$

I_0 was obtained by measuring the intensity of the Si(2p) photoelectrons of the SAM from $Cl_3Si(CH_2)_{11}CH_3$ SAM on Si/SiO_2 wafers. The thickness of such SAM was found to be 18.4 Å by ellipsometry, and this value was in good agreement with the expected thickness, considering the bond angles and lengths. Thus, incorporating known I_0, d_0, λ, BE and measured I into equations (2.1)-(2.3) yields thickness d. The XPS-determined thickness of polymer films in Figure 2.2 was obtained by subtracting the XPS-determined thickness of the AHPTS SAM (13 ± 2 Å) from that of Si/SiO_2/AHPTS/PAA-*g*-(PEG-*r*-PPG). Although the thickness of the AHPTS SAM calculated by two independent methods (ellipsometry and XPS) was in satisfactory agreement within experimental uncertainty, for polymer films, XPS-determined thicknesses were 2-3 Å shorter than ellipsometric thicknesses. This discrepancy probably comes from the assumption in equations (2.1)-(2.3) that the intensity of Si(2p) photoelectrons is attenuated by a uniform, homogeneous overlayer of hydrocarbons. This is a valid assumption for AHPTS SAMs. However, for an overlayer with multiple components, *e.g.*, AHPTS SAM, PAA, PEG and PPG, this postulation breaks down. When the film on the substrate is not completely flat and smooth, the contribution of the surface

with a thinner overlayer to the overall Si(2p) photoelectron signals is more weighted than that of the surface with a thicker overlayer. Thus, the average thickness of the polymer film determined by XPS can be smaller than the average ellipsometric thickness (Figure 2.2).

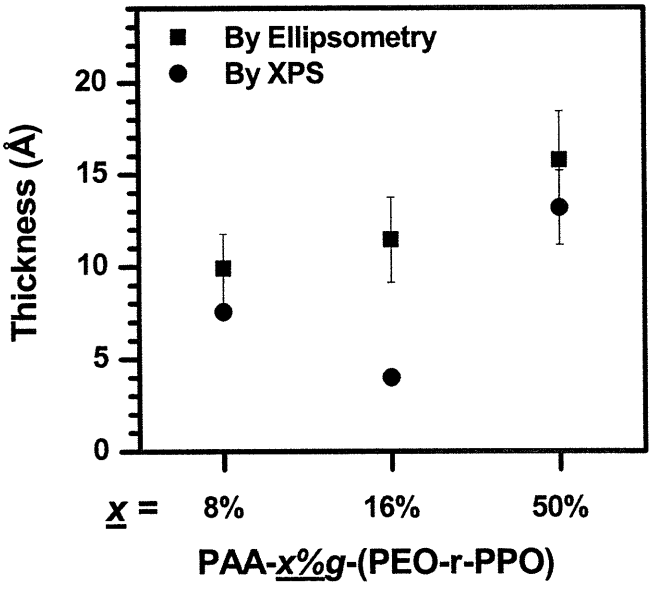

Figure 2.2. Comparison of ellipsometric and XPS-determined thicknesses of polymer films on Si/SiO_2/AHPTS.

The compositional differences between the polymer films with respect to the changes in the PEG-*r*-PPG grafting density are even more evident by XPS analysis. Figure 2.3 presents the high resolution C(1s) XPS spectra of the films of PAA-*x%g*-(PEG-*r*-PPG) on Si/SiO_2/AHPTS. Each spectrum was resolved into three separate binding energy peaks. One example of peak fitting was demonstrated for PAA-*50%g*-(PEG-*r*-PPG) (Figure 2.3d). These three peaks correspond to the following functional groups: peak ***1*** to aliphatic hydrocarbon C-C or C-H, peak ***2*** to C-O and C-N, and peak ***3*** to C(=O)O and C(=O)NH. For each film, carbons associated with C-N arise mainly from AHPTS with a little contribution from PEG-*r*-PPG. Each spectrum in Figure 2.3 was adjusted to have peak ***1*** at 285 eV. As shown in

Figure 2.3, the relative intensities of the peaks vary dramatically with the increasing grafting density of PEG-*r*-PPG. For instance, while the aliphatic carbons (peak *1*) were the majority of carbon atoms in AHPTS SAM, they are less than 50% of the carbons for peak *2* for the polymers with 50% grafting density.

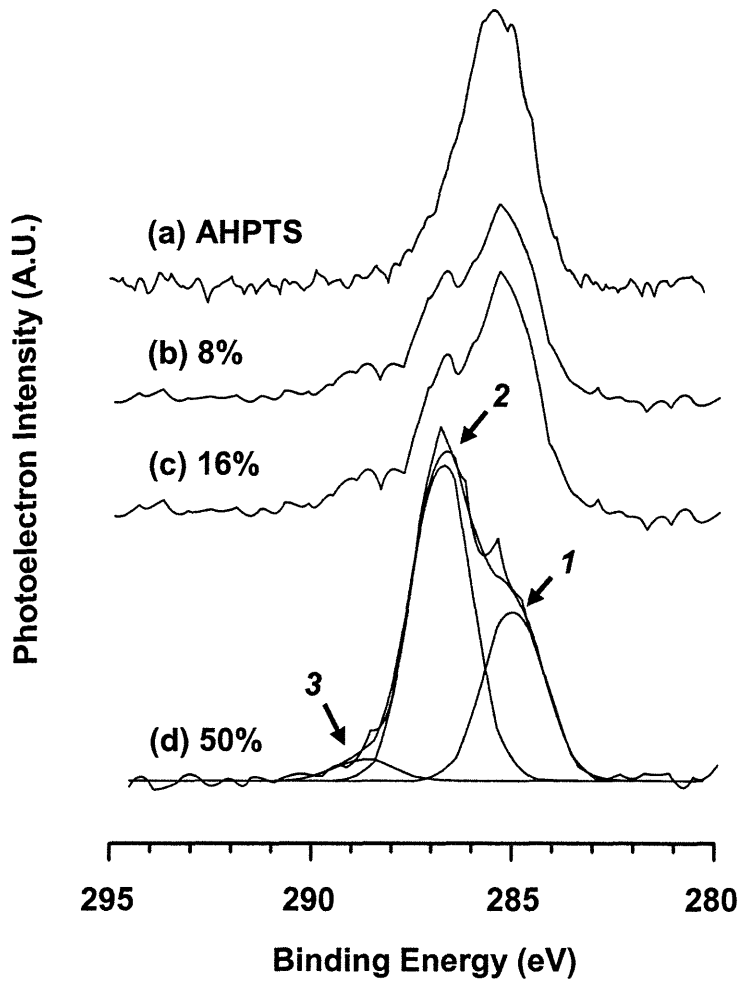

Figure 2.3. High-resolution C(1s) XPS spectra of films of PAA-x%*g*-(PEG-*r*-PPG) on Si/SiO_2/AHPTS at a 55° take-off angle from the surface normal.

Table 2.2 is the tabular representation of this trend. It summarizes the surface composition of the carbons in Si/SiO_2/AHPTS/PAA-*x%g*-(PEG-*r*-PPG), which was determined from the relative intensities of peaks *1*, *2*, and *3* in the C(1s) spectrum of each

film in Figure 2.3. Surfaces with a higher concentration of peak ***2*** suggest that they contain more C-O (ether), *i.e.*, more PEG-*r*-PPG, than those with a lower concentration, judging from the fact that the contribution of C-N (arising mostly from AHPTS) to peak ***2*** is the same for all the polymer surfaces. As listed in Table 2.2, there is a noticeable increase in the ether carbon concentration with increasing grafting density x for the PAA-*x%g*-(PEG-*r*-PPG) modified surfaces.

Table 2.2. High resolution C(1s) XPS composition of Si/SiO_2/AHPTS/PAA-x%*g*-(PEG-*r*-PPG)[a]

x	C(1s) Composition (%)[b]		
	C_1	C_2	C_3
8%	57	34	9
16%	47	46	7
50%	31	64	5
50%[c]	33	60	7

[a]The surface composition of carbons in the underlying AHPTS SAM is as follows: (C_1) 74 %, (C_2) 19 %, (C_3) 7 %. Carbons associated with C_3 come from the oxidation of NH_2 in AHPTS SAM with CO_2 in the air.

[b]C_1 corresponds to aliphatic hydrocarbon CH_2, C_2 to C-O and C-N, and C_3 to C(=O)O and C(=O)NH.

[c]The surface composition of carbons of Si/SiO_2/AHPTS/PAA-50%g-(PEG-r-PPG) after sonicating the surface in a buffer with high salt concentration (3 M NaCl, 200 mM Tris·HCl, pH 7.6, 50 mM $MgCl_2$) for 20 min, followed by immersion in boiling water for 1 h.

As the assembly of carboxylic acid in PAA and amine functionality in AHPTS SAM produces PEG containing polymer film on Si/SiO_2 surfaces through electrostatic interaction, it is important to examine if this non-covalent interaction provides robust grafting of films to

the underlying substrates. This stability question was examined by sonicating the polymer films in a buffer with high salt concentration (3 M NaCl, 200 mM Tris(HCl, pH 7.6, 50 mM $MgCl_2$) for 20 min, followed by immersion in boiling water for 1 h. Samples were subjected to C(1s) XPS analysis before and after these post-treatments. For illustrative purposes, we chose the films with PAA-*50%g*-(PEG-*r*-PPG) because the 50% grafted polymer had the smallest amount of carboxylic acid and thus would have the lowest degree of interaction with amine. The similarity between the C(1s) surface composition of Si/SiO_2/AHPTS/PAA-*50%g*-(PEG-*r*-PPG), before and after these sequential steps, as evidenced in Table 2.2, suggests that the surface structure of the film did not change much after various demanding conditions.

Unreacted NH_2-(PEG-*r*-PPG)-OCH_3 may remain in the polymer since we used the synthesized polymer product without separating it from reactants. This amine-containing polymer is positively charged under our experimental condition. To test the possibility that this unreacted NH_2-(PEG-*r*-PPG)-OCH_3 (no PAA) might be adsorbed onto the negatively charged unmodified Si/SiO_2 by an electrostatic interaction or onto the AHPTS SAM by hydrogen bonding with amine, we compared C(1s) spectra of the unmodified Si/SiO_2 and Si/SiO_2/AHPTS SAM before and after treating these surfaces with NH_2-(PEG-*r*-PPG)-OCH_3. The NH_2-(PEG-*r*-PPG)-OCH_3-treated surfaces were prepared by immersing the bare Si/SiO_2 and Si/SiO_2/AHPTS into a 7% aqueous solution of NH_2-(PEG-*r*-PPG)-OCH_3 at pH 7.5 for 30 min, followed by rinsing with deionized water and drying under N_2 stream. No appreciable changes in the C(1s) spectra were observed after the treatment for both bare Si/SiO_2 and Si/SiO_2/AHPTS (data not shown). The fact that the reactant NH_2-(PEG-*r*-PPG)-OCH_3 did not adsorb onto either surface implies 1) that grafting to a PAA backbone is needed for efficient immobilization of PEG and 2) that the polymers adsorbed onto the AHPTS SAM are mainly grafted copolymers, despite the possible presence of remaining reactants.

PEG-r-PPG films on PDMS. We demonstrated that PEG-containing polymers could be immobilized onto Si/SiO_2 wafer surfaces by derivatization of the substrate with amine functionality and then through the interaction between the PAA backbone and underlying amine surface. The same strategy could be applied to prepare the films on elastomers such as PDMS. AHPTS SAM and the films of PAA-*g*-(PEG-*r*-PPG) were formed employing the same procedure that was used on Si/SiO_2 wafers, except that PDMS slabs were cleaned by an O_2 plasma oxidation to expose silanols on the surface before forming AHPTS SAM.

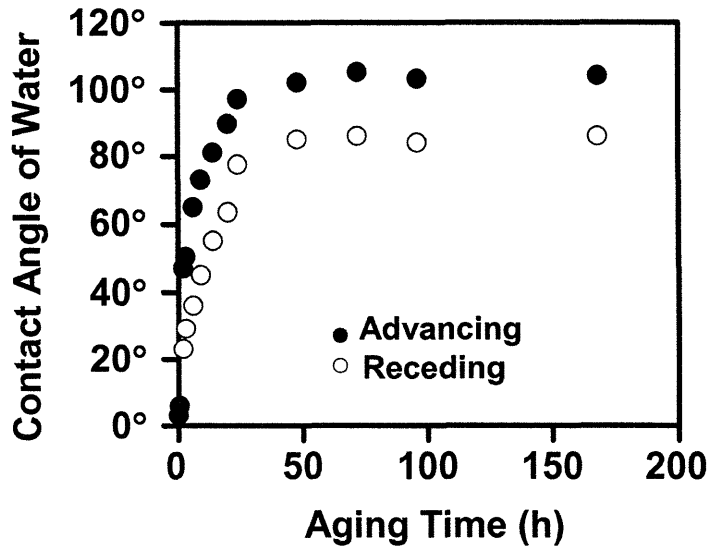

Figure 2.4. Surface reorganization of $_{ox}$PDMS as a function of aging time.

The unmodified PDMS surface was hydrophobic, with advancing water contact angles of 113°. Exposure to O_2 plasma for 1 min rendered the PDMS surface fully hydrophilic with water contact angles close to 0°. The water contact angle remained zero for 1 h. However, in the ambient laboratory environment, it gradually increased and finally reached equilibrium value of 105° after 48 h of exposure (Figure 2.4). Thus the oxidized PDMS was transferred to the AHPTS solution within 1 h of O_2 plasma treatment.

The AHPTS SAMs had similar characteristics on both the Si/SiO_2 wafers and PDMS in terms of their thicknesses, wettabilities, and surface carbon compositions (

Table 2.3). The resulting amine-containing substrates were immersed into the PAA-*g*-(PEG-*r*-PPG) polymer solutions to form PEG-*r*-PPG layers. The formation of the polymer layers on the amino-modified surface was evident by changes in the surface characteristics (see below).

Table 2.3. Surface characterization of polymer films of PDMS/AHPTS/PAA-x%*g*-(PEG-*r*-PPG)[a,b]

x	XPS-determined Thickness (Å)	Water contact angle		C(1s) Composition (%)		
		θ_a	θ_r	CH_2	C-O/C-N	C(=O)O/C(=O)NH
8%	8	46°	26°	44	52	4
16%	8	37°	22°	39	59	1
50%	14	35°	21°	28	66	6

[a] Unmodified PDMS slabs had advancing and receding water contact angles of 113° and 103°, respectively. After oxidization in an O_2 plasma, the advancing contact angle of water was below 10°.

[b]The surface properties of the underlying AHPTS SAM on PDMS are as follows: XPS-determined thickness = 10 Å, θ_a = 56°, θ_r (H_2O) = 33°, and C(1s) composition of 73% CH_2, 20% C-N, and 7% C(=O)NH. Carbons associated with C(=O)NH come from the CO_2 adsorption onto the amine surface of the AHPTS SAM.

Table 2.3 summarizes the film thicknesses determined by Si(2p) XPS, water contact angles, and surface carbon compositions of $_{ox}$PDMS surfaces analyzed by high resolution C(1s) XPS after grafting with PAA-*x%g*-(PEG-*r*-PPG). Similarly to the results of polymer films on Si/SiO_2 substrates (see Table 2.1), 8% and 16% grafted polymer films were of the same thicknesses of 8 Å, while 50% grafted polymer was 14 Å, the thickest. Considering the

discussion in Table 2.1 and Figure 2.2 that the XPS-determined thicknesses tend to have smaller numbers than ellipsometric thicknesses, PAA-*g*-(PEG-*r*-PPG) polymers are of a similar thickness both on Si/SiO_2 wafers and on $_{ox}$PDMS.

Table 2.3 also reveals a substantial increase in the surface composition of peak ***2*** (C-O and C-N) and a decrease in water contact angle as the PEG-*r*-PPG grafting density x% increases. Thus, polymer films with a higher grafting density contain a higher number of PEG moieties and are more hydrophilic, despite the similar thickness for 8% and 16% grafted films.

2.3.2. Protein Repellency of Films

To evaluate the protein-resistance characteristics of the PAA-*x%g*-(PEG-*r*-PPG) coated surfaces, we immersed the polymer coated- and unmodified-Si/SiO_2 and PDMS surfaces in insulin, lysozyme, hexokinase, and fibrinogen solutions (0.25 mg/mL in PBS, pH 7.4) for 2 h. These model proteins were chosen to provide different molecular weights and similar isoelectric points of pI *ca.* 5.4 with lysozyme as a contrast for a different pI of 11. The degree of nonspecific adsorption onto the films was assessed from the increase in the peak intensities of the high resolution N(1s) XPS upon exposure of various polymer films to different protein solutions (Figure 2.5 and Figure 2.6). An increase in N(1s) peak intensity is proportionate to the amount of nitrogen in protein adsorbed on the surface, and thus, is proportionate to the amount of protein in g/cm^2 adsorbed on the surface. The coating resulted in notable reductions in nonspecific protein adsorption as compared to the unmodified substrates.

Protein adsorption of polymer films on Si/SiO_2. Figure 2.5 shows the degree of nonspecific adsorption of proteins onto polymer films on Si/SiO_2 wafers obtained from the

high resolution N(1s) XPS peak intensities. Data for the unmodified Si/SiO_2 surfaces are included for comparison. As seen in Figure 2.5, the adsorbed amounts of the proteins are much smaller on the polymer-coated Si/SiO_2 wafers than on the unmodified wafers. As expected, the N(1s) intensity increased by insulin adsorption continually diminished with use of polymers with increasing (PEG-*r*-PPG) content. Practically no adsorption of insulin occurred when PAA-*50%g*-(PEG-*r*-PPG) was used (Figure 2.5a). The steady decrease of protein adsorption with increasing (PEG-*r*-PPG) content was also observed in the case of hexokinase, another negatively-charged protein (pI 5.2, M_w 100,000), reaching a maximum

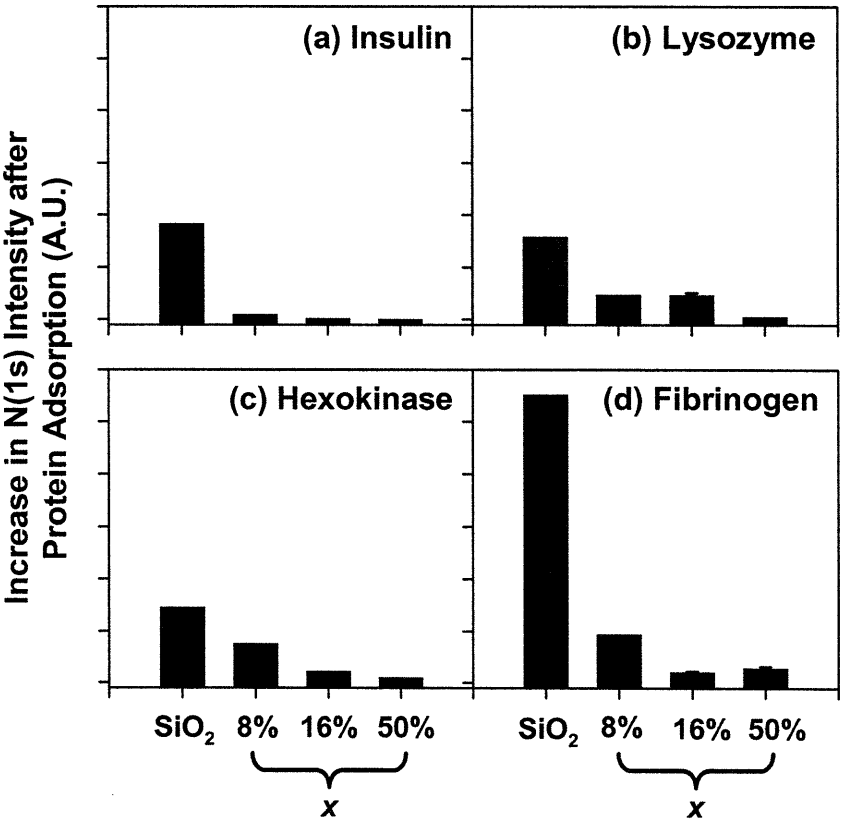

Figure 2.5. Increases in N(1s) XPS intensity upon exposure of PAA-*x%g*-(PEG-*r*-PPG) polymer films on Si/SiO_2 to various protein solutions (0.25 mg/mL in PBS, pH 7.4) for 2 h. of 93% reduction of the unmodified surface when PAA-*50%g*-(PEG-*r*-PPG) was used.

These PAA-*g*-(PEG-*r*-PPG) films reduced the lysozyme (pI 11.1, M_w 14,600) adsorption by

70% with 8% and 16% grafted polymers, and by 96% with 50% grafted polymers. It is of interest to note that increases in N(1s) intensity after lysozyme adsorption onto the 8% and 16% grafted polymer films were close to those after hexokinase adsorption (Figure 2.5b, c), despite the considerable difference in the molecular weights of the two proteins (14,600 *vs* 100,000). The negative charges on the polymer surfaces rising from PAA may attract lysozyme, which is positively charged at pH 7.4, and thus may lower the protein resistance. The tendency for charged surfaces to attract proteins with opposite charges has been reported before.[24-26] In view of that, the noticeable reduction in lysozyme adsorption onto the PAA-*50%g*-(PEG-*r*-PPG) film may have resulted both from the higher PEG moieties and from the smaller number of carboxylate anions on the surface. Fibrinogen, an important protein for blood coagulation,[27,28] is well known for its adhesiveness[29,30]. Its pI and M_w are 5.5 and 340,000, respectively. The conspicuous amount of fibrinogen adsorbed onto the unmodified Si/SiO_2 control shown in Figure 2.5d evidences the stickiness of fibrinogen. The reduction of fibrinogen adsorbed onto the polymer-treated Si/SiO_2 surfaces as compared to untreated Si/SiO_2 surfaces is clearly indicated by the XPS results. For example, the amount of adsorbed fibrinogen was reduced by 83% on PAA-*8%g*-(PEG-*r*-PPG) film, and by 96% and 95% on PAA-*16%g*-(PEG-*r*-PPG) and PAA-*50%g*-(PEG-*r*-PPG) films, respectively.

Protein adsorption of polymer films on PDMS. Similar to the results on Si/SiO_2, modification of PDMS with polymer films reduced the nonspecific adsorption of proteins (Figure 2.6). The dependence of protein resistance on the grafting ratio of (PEG-*r*-PPG) was more evident on PDMS surfaces than on Si/SiO_2 surfaces. For all proteins, the amount of protein adsorbed decreased constantly with the increasing (PEG-*r*-PPG) grafting ratio. On PAA-*50%g*-(PEG-r-PPG), the degree of nonspecific adsorption of insulin, lysozyme, hexokinase, and fibrinogen was 75%, 73%, 84%, and 86%, respectively. The polymer films

on PDMS seemed to have relatively lower protein resistance (e.g. 96% for lysozyme on 50% grafted polymer film, Figure 2.6b) compared to that of Si/SiO_2 wafers (73%, Figure 2.5b). This result is attributed to the large differences in the extent of nonspecific adsorption of protein onto each unmodified substrate. According to the absolute peak intensity, however, the amount of each protein adsorption is similar each other for both substrates.

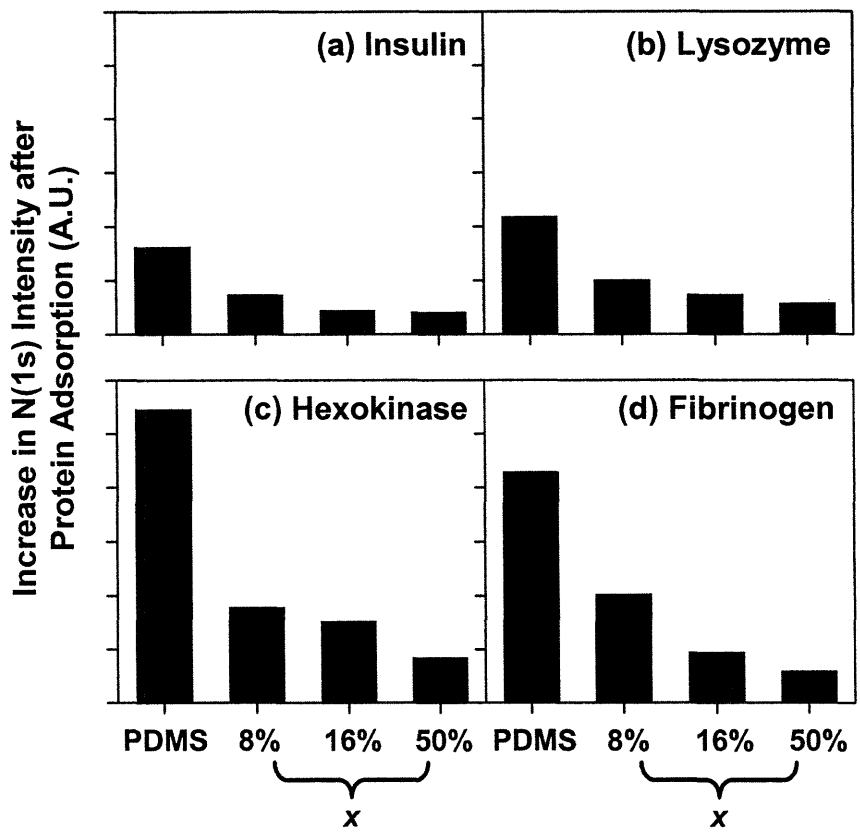

Figure 2.6. Increases in N(1s) XPS intensity upon exposure of PAA-*x*%*g*-(PEG-*r*-PPG) polymer films on Si/SiO_2 to various protein solutions (0.25 mg/mL in PBS, pH 7.4) for 2 h.

2.3.3. Bacterial Growth and Adhesion

To investigate the adhesion of *E. coli* cells on the substrates, PAA-*g*-(PEG-*r*-PPG) films were formed on Si/SiO_2 wafers and PDMS substrates functionalized with AHPTS, and were incubated in a fermentor or petri dishes. The goal of the PAA-*g*-(PEG-*r*-PPG) coating onto

Si/SiO_2 wafers and PDMS substrates is to generate biocompatible surfaces which are capable of preventing and reducing the cell adsorption onto the surface while maintaining cell growth in liquid phase. Thus, cell growth was also inspected for cell adhesion experiments both on Si/SiO_2 wafers and PDMS substrates. After incubation followed by gently rinsing with water and dried, the substrates were imaged directly using optical microscopy (OM).

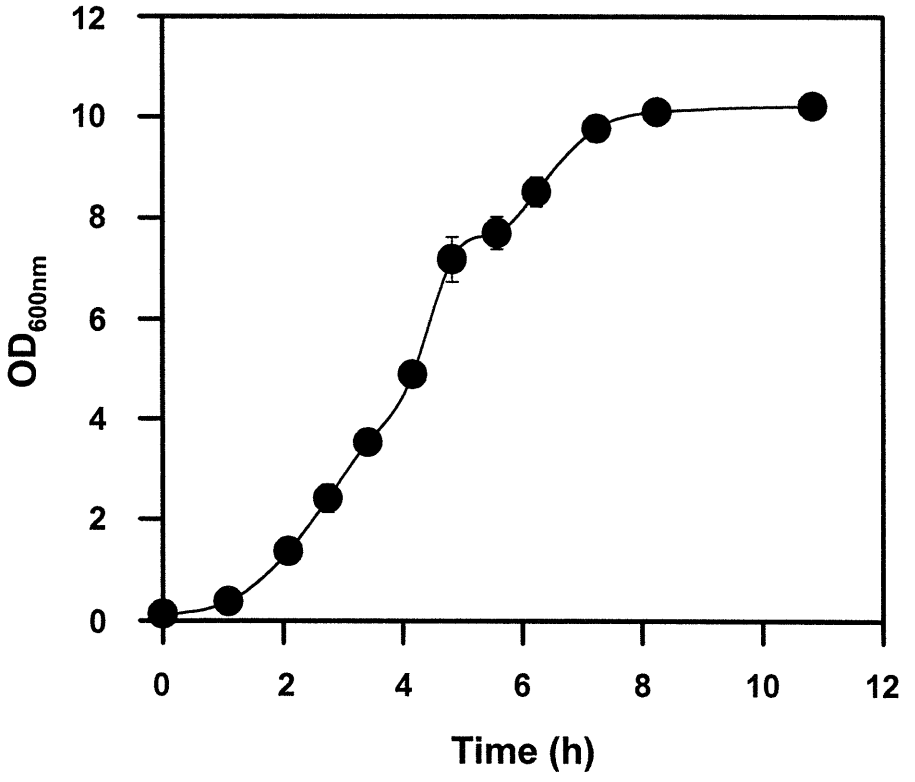

Figure 2.7. Optical density (O.D.) at 600 nm as a function of time. An O.D. value is known to be directly proportional to an *E. coli* concentration in the fermentor and thus is used to monitor the growth of *E. coli* in the fermentation process.

Bacterial adhesion of polymer films on Si/SiO_2. Polymer coated Si/SiO_2 wafers were incubated in the fermentor. After the seed culture of *E. coli* was inoculated, the bacterial cell concentration in the fermentor was monitored by the optical density (O.D.) at 600 nm as a function of time. Figure 2.7 represents the growth of *E. coli* in the fermentation process as

probed by the O.D. at 600 nm. As can be seen from Figure 2.7, the *E. coli* concentration in the fermentor increased exponentially after 1 h lag phase, and then reached stationary phase in 9 h. The final cell density was about OD value 10 measured by spectrometer at 600 nm. From separate experiments, we could also observe during the exponential growth phase the decrease in pH from 7 to 5 as well as the depletion of oxygen. Oxygen level returned to initial value after *E. coli* growth reached the stationary phase. These oxygen depletion and pH decrease indicate the active growth of cells and production of organic acid, respectively. From these results, we can conclude that the cell growth and metabolism are not affected by the PAA-*g*-(PEG-*r*-PPG) coating.

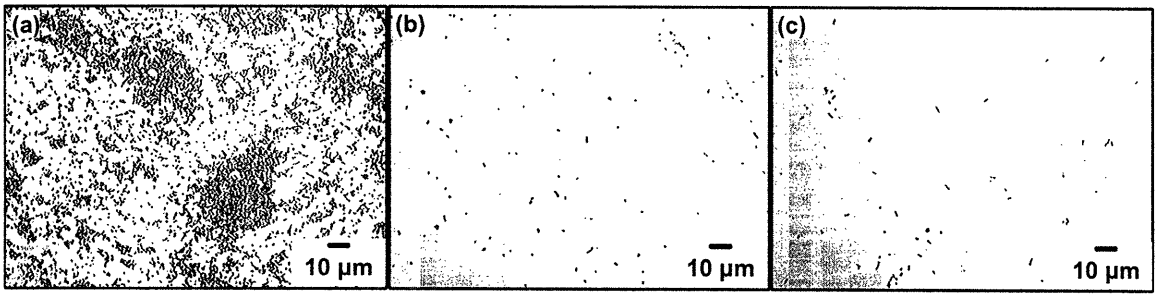

Figure 2.8. Representative images obtained by optical microscopy of *E. coli* adhesion on (a) unmodified Si/SiO_2 wafer, (b) Si/SiO_2 wafer modified with PAA-*16%g*-(PEG-*r*-PPG), and (c) Si/SiO_2 wafer modified with PAA-*50%g*-(PEG-*r*-PPG).

After *E. coli* cells reached the stationary phase, bacterial adhesion on the surfaces was investigated by taking pictures by OM. Figure 2.8 shows the OM images of bacterial cells adhered to Si/SiO_2 wafers modified with polymers. The result of unmodified Si/SiO_2 wafers was included for comparison (Figure 2.8a). Modification of the surface with the polymers greatly reduced bacterial adhesion. For example, the number of bacteria adhered to an unmodified Si/SiO_2 wafer was *ca.* $12.6 \times 10^6/cm^2$, while the bacterial adhesion to PAA-*16%g*-(PEG-*r*-PPG) and PAA-*50%g*-(PEG-*r*-PPG) films were reduced by 96% ($0.48 \times$

$10^6/cm^2$) and 97% ($0.29 \times 10^6/cm^2$), respectively. In addition, whereas *E. coli* cells on unmodified are significantly aggregated (Figure 2.8a), most *E. coli* cells on polymer modified surfaces exist as isolated cells and are uniformly dispersed. These observations clearly demonstrate that modification of Si wafers with PAA-*g*-(PEG-*r*-PPO) suppresses the adhesion of *E. coli*.

Bacterial adhesion of polymer films on PDMS. The polymer coated PDMS surfaces were incubated in petri dishes. Cell growth and pH variation in the petri dish were examined for biocompatibility. At the stationary phase, the O.D. value in the petri dish was 1.25 at 600 nm, which was less than one-eighth of the O.D. value in the fermentor. During the exponential growth phase, the pH decrease in the petri dish (from pH 7 to pH 6) was also smaller than that in the fermentor. These differences could be due to the low oxygen transfer in petri dishes. In fermentor culture, the agitation (150 rpm) was done with aeration (2 vvm) during the entire culture period, which can promote oxygen transfer to the culture broth. On the other hand, cells were grown under the oxygen-limited condition in the petri dish. Although the cell growth and metabolism were less active than in fermentor culture, the cell growth and pH decrease showed similar trend.

Figure 2.9 is the result of *E. coli* adhesion to the polymer films on PDMS. The OM image of adhered *E. coli* cells to unmodified PDMS is included for comparison (Figure 2.9a). In general, *E. coli* cells are less adhesive to the PDMS surface than to the Si/SiO_2 wafers. About 2.4×10^6 *E. coli* cells were adhered to one cm^2 of unmodified PDMS surface, which is approximately one-sixth of the E. coli adhered to the unmodified Si/SiO_2 wafer (Figure 2.8a). Moreover, *E. coli* cells on unmodified PDMS are more uniformly dispersed without aggregation, unlike the behavior of *E. coli* on unmodified Si/SiO_2 wafers. Similar to the

results on Si/SiO_2 wafers, modification of PDMS surface with PAA-*g*-(PEG-*r*-PPG) reduces the bacterial adhesion. Increased incorporation of PEG-*r*-PPG in the PAA backbone yields an increase in bacterial resistance (Figure 2.9b, c, and d). Incorporation of PAA-x%*g*-(PEG-*r*-PPG) (where x = 8, 16, and 50) reduced the bacterial adhesion by 79% ($0.50 \times 10^6/cm^2$), 82% ($0.44 \times 10^6/cm^2$), and 92% ($0.20 \times 10^6/cm^2$), respectively. Table 2.4 is a tabular representation of Figure 2.8 and Figure 2.9, summarizing the amount of adhered *E. coli* to the polymer films on silicon wafers and on PDMS.

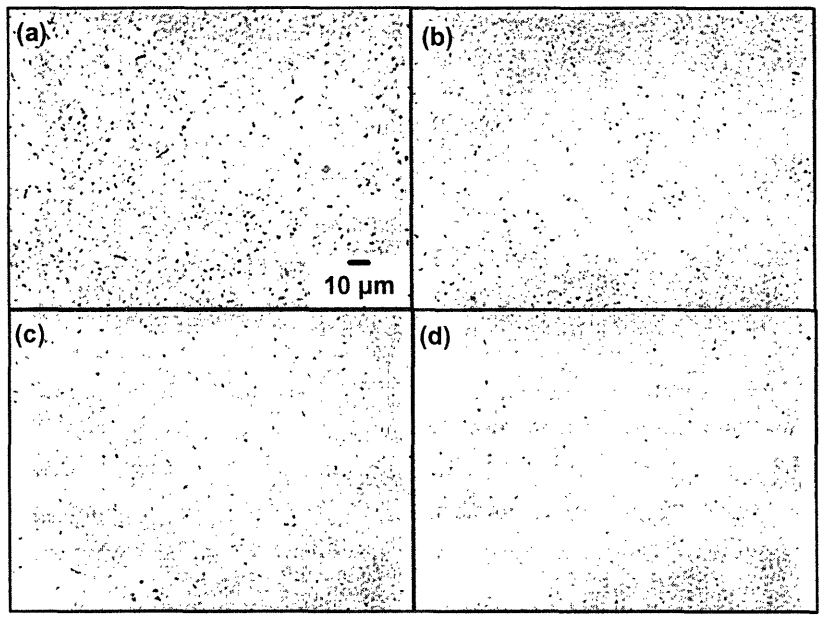

Figure 2.9. Representative images obtained by optical microscopy of *E. coli* adhesion on (a) unmodified PDMS, and on PDMS surfaces modified with (b) PAA-*8%g*-(PEG-*r*-PPG), (c) PAA-*16%g*-(PEG-*r*-PPG) and (d) PAA-*50%g*-(PEG-*r*-PPG).

The seemingly lower resistance of polymer films towards bacterial adhesion is attributed to the lower bacterial adhesion to unmodified PDMS than to unmodified Si/SiO_2 wafers. Si/SiO_2 wafer is well known for its high surface energy. Thus, organic molecules or other contaminants can be spontaneously adsorbed onto the surface to increase the energetic

stability at the interface. On the other hand, PDMS has low surface energy, and the only driving force for the non-specific adsorption is hydrophobic interaction between the adsorbate and PDMS. Thus, native PDMS surfaces show much less cell adhesion than native Si/SiO_2 surfaces. From the reduction of cell adhesion after coating with PAA-g-(PEG-r-PPG) polymer onto both Si/SiO_2 and PDMS surfaces, we can deduce that the modified surfaces have intermediate-surface energy which shows moderate hydrophilic nature and resistance to non-specific adsorption of proteins and cells.

Table 2.4. Amount of E. coli adhered to Si/SiO_2 wafers and PDMS surfaces modified with polymer films. Results of unmodified substrates were included for comparison.

Polymer Films	Number of *E. coli* adhered on the substrates (number of cells/cm^2)	
	on Si/SiO_2 wafer	on PDMS
Native surface	12.6×10^6/cm^2	2.4×10^6/cm^2
PAA-*8%g*-(PEG-*r*-PPG)	n/a	0.50×10^6/cm^2
PAA-*16%g*-(PEG-*r*-PPG)	0.48×10^6/cm^2	0.44×10^6/cm^2
PAA-*50%g*-(PEG-*r*-PPG)	0.29×10^6/cm^2	0.20×10^6/cm^2

2.4. Conclusions

Amidation of PAA with NH_2-(PEG-*r*-PPG)-OCH_3 at 180°C for 2 h provided a straightforward preparation of a graft copolymer with a PAA backbone and PEG-containing side chains. Incorporation of PPG moieties into side chains provided thermal stability. The polymers formed stable ultrathin polymer films containing PEG units. Polymers with higher grafting ratios expose more PEG moieties on the surface and are more effective in resisting nonspecific adsorption of proteins and bacteria.

2.5. References for Chapter 2

(1) Luppa, P. B.; Sokoll, L. J.; Chan, D. W. Immunosensors - principles and applications to clinical chemistry. *Clin. Chim. Acta* **2001**, *314*, 1-26.

(2) Ramsden, J. J. Optical biosensors. *J. Mol. Recognit.* **1997**, *10*, 109-120.

(3) Rogers, K. R. Principles of affinity-based biosensors. *Mol. Biotechnol.* **2000**, *14*, 109-129.

(4) Wink, T.; van Zuilen, S. J.; Bult, A.; van Bennekom, W. P. Self-assembled monolayers for biosensors. *Analyst* **1997**, *122*, R43-R50.

(5) McGlennen, R. C. Miniaturization technologies for molecular diagnostics. *Clin. Chem.* **2001**, *47*, 393-402.

(6) Schneider, B. H.; Dickinson, E. L.; Vach, M. D.; Hoijer, J. V.; Howard, L. V. Optical chip immunoassay for hcg in human whole blood. *Biosens. Bioelectron.* **2000**, *15*, 597-604.

(7) Bouhabila, E. H.; Aïm, R. B.; Buisson, H. Fouling chracterization in membrane bioreactors. *Sep. Purif. Technol.* **2001**, *22-23*, 123-132.

(8) Ognier, S.; Wisniewski, C.; Grasmick, A. Influence of macromolecule adsorption during filtration of a membrane bioreactor mixed liquor suspension. *J. Membr. Sci.* **2002**, *209*, 27-37.

(9) Harris, J. M., *Ed. Poly(ethylene glycol) chemistry: Biotechnical and biomedical applications*; Plenum Press, **1992.**

(10) Emoto, K.; Harris, J. M.; van Alstine, J. M. Grafting poly(ethylene glycol) epoxide to amino-derivatized quartz: Effect of temperature and ph on grafting density. *Anal. Chem.* **1996**, *68*, 3751-3757.

(11) Marlmsten, M.; Emoto, K.; van Alstine, J. M. Effect if chain density on inhibition of protein adsorption by poly(ethylene glycol) based coatings. *J. Colloid Interface Sci.* **1998**, *202*, 507-517.

(12) Sofia, S. J.; Premnath, V.; Merrill, E. W. Poly(ethylene oxide) grafted to silicon surfaces: Grafting density and protein adsorption. *Macromolecules* **1998**, *31*, 5059-5070.

(13) Jo, S.; Park, K. Surface modification using silanated poly(ethylene glycol)s. *Biomaterials* **2000**, *21*, 605-616.

(14) Zhang, M.; Desai, T.; Ferrari, M. Protein and cells on peg immobilized silicon surfaces. *Biomaterials* **1998**, *19*, 953-960.

(15) Papra, A.; Gadegaard, N.; Larsen, N. B. Characterization of ultrathin poly(ethylene glycol) monolayers on silicon substrates. *Langmuir* **2001**, *17*, 1457-1460.

(16) Yang, Z.; Galloway, J. A.; Yu, H. Protein interactions with poly(ethylene glycol) self-assembled monolayers on glass substrates: Diffusion and adsorption. *Langmuir* **1999**, *15*, 8405-8411.

(17) Bunker, B. C.; Carpick, R. W.; Assink, R. A.; Thomas, M. L.; Hankins, M. G.; Voigt, J. A.; Sipola, D.; Boer, M. P. d.; Gulley, G. L. The impact of solution agglomeration on the deposition of self-assembled monolayers. *Langmuir* **2000**, *16*, 7742-7751.

(18) Huang, N.-P.; Michel, R.; Vörös, J.; Textor, M.; Hofer, R.; Rossi, A.; Elbert, D. L.;

Hubbell, J. A.; Spencer, N. D. Poly(l-lysine)-g-poly(ethylene glycol) layers on metal oxide surfaces: Surface-analytical characterization and resistance to serum and fibrinogen adsorption. *Langmuir* **2001**, *17*, 489-498.

(19) Kenausis, G. L.; Vörös, J.; Elbert, D. L.; Huang, N. P.; Hofer, R.; Ruiz-Taylor, L.; Textor, M.; Hubbell, J. A.; Spencer, N. D. Poly(l-lysine)-g-poly(ethylene glycol) layers on metal oxide surfaces: Attachment mechanism and effects of polymer architecture on resistance to protein adsorption. *J. Phys. Chem. B* **2000**, *104*, 3298-3309.

(20) Elbert, D. L.; Hubbell, J. A. Self-assembly and steric stabilization at heterogeneous, biological surfaces using adsorbing block copolymers. *Chem. Biol.* **1998**, *5*, 177-183.

(21) Moeser, G. D.; Roach, K. A.; Green, W. H.; Laibinis, P. E.; Hatton, T. A. Water-based magnetic fluids as extractants for synthetic organic compounds. *Ind. Eng. Chem. Res.* **2002**, *41*, 4739-4749.

(22) Curotto, E.; Aros, F. Quantitative determination of chitosan and the percentage of free amino groups. *Anal. Biochem.* **1993**, *211*, 240-241.

(23) Laibinis, P. E.; Bain, C. D.; Whitesides, G. M. Attenuation of photoelectrons in monolayers of n-alkanethiols adsorbed on copper, silver, and gold. *J. Phys. Chem.* **1991**, *95*, 7017-7021.

(24) Kato, K.; Sano, S.; Ikada, Y. Protein adsorption onto ionic surfaces. *Colloid Surface B.* **1995**, *4*, 221-230.

(25) Ladam, G.; Schaaf, P.; Cuisinier, F. J. C.; Decher, G.; Voegel, J.-C. Protein adsorption onto auto-assembled polyelectrolyte films. *Langmuir* **2001**, *17*, 878-882.

(26) Müller, M.; Rieser, T.; Dubin, P. L.; Lunkwitz, K. Selective interaction between proteins and the outermost surface of polyelectrolyte multilayers: Influence of the polyanion type, ph, and salt. *Macromol. Rap. Commun.* **2001**, *22*, 390-395.

(27) Spraggon, G.; Everse, S. J.; Doolittle, R. F. Crystal structures of fragment d from human fibrinogen and its crosslinked counterpart from fibrin. *Nature* **1997**, *389*, 455-462.

(28) Everse, S. J.; Spraggon, G.; Doolittle, R. F. A three-dimensional consideration of variant human fibrinogens. *Thromb. Haemost.* **1998**, *80*, 1-9.

(29) Feng, L.; Andrade, J. D. Protein adsorption on low temperature isotropic carbon: Iii. Isotherms, competitivity, desorption and exchange of human albumin and fibrinogen. *Biomaterials* **1994**, *15*, 323-333.

(30) Feng, L.; Andrade, J. D. In *Proteins at interfaces II: Fundamentals and applications*; Horbett, T. A., Brash, J. L., *Eds.*; American Chemical Society: Washington DC, 1995; Vol. 602, pp 66-79.

Chapter 3. Construction of Non-Biofouling Surfaces by Covalent Attachment of Surface-Reactive Graft Copolymers of Poly(Ethylene Glycol)

3.1. Introduction

The significance of non-biofouling surfaces has been discussed in previous chapters. As mentioned in Chapter 2, poly(ethylene glycol) (PEG)-grafted copolymers have advantages as protein-resistant and cell-resistant coating materials in that they have multiple interaction sites available for the surfaces. The previous chapter discussed our use of PEG-containing graft copolymers to generate non-biofouling SiO_2 surfaces by multiple linkages with underlying surfaces via electrostatic interaction. Another study reported that non-biofouling surfaces can also be prepared by physical adsorption of PEG-grafted copolymers.[1] Even though these processes have successfully created surfaces that resist biofouling, a more reliable method would be by covalent binding, especially in the field where the surface stability over a long period of time is a critical issue. Applications of polymers with multivalent surface interaction sites to surface functionalization include nano- and micropatterned polymer brushes on silicon dioxide supports using self-assembly of surface-reactive block copolymers.[2] Another example is the robust polymer film formation via multiple thiol-gold linkages.[3] The concept of multiple thiol-gold covalent bond formation in one polymer chain has also been extended to the stable film formation of PEG for non-biofouling coating[4,5] and to the immobilization of biomolecules onto gold substrates[6]. On oxide surfaces, however, no literature is available yet on the concept of multiple "covalent bond formation" for rendering oxide surfaces such as SiO_2 protein- and cell-resistant.

This chapter addresses an efficient approach to constructing non-biofouling surfaces on

silicon dioxide substrates by forming ultrathin polymeric self-assembled monolayers (PSAMs) via multiple covalent linkages. The adsorbate employed in this study is a random copolymer consisting of an "anchor part" (trialkoxysilane) and a "function part" (PEG). The resulting polymer is attached to SiO_2 or other metal oxide surfaces by forming multiple siloxane bonds between the trialkoxysilanes in the "anchor part" and the surface OH groups. Protein resistant and cell repelling properties of the polymer films on various types of SiO_2 surfaces such as Si/SiO_2 wafers, glasses, or oxidized PDMS ($_{ox}$PDMS) surfaces will be discussed. An application of this strategy to non-biofouling coating of microfluidic channel walls will be also addressed.

3.2. Experimental Section

3.2.1. Materials

Poly(ethylene glycol) methyl ether methacrylate (PEGMA; average M_n = *ca.* 475), 3-(trimethoxysilyl)propyl methacrylate (TMSMA), and 2,2'-azobisisobutyronitrile (AIBN) were obtained from Aldrich Chemical Co. (Milwaukee, WI). Insulin (EC 2342912), lysozyme (EC 2326204), fibrinogen (EC 2325986), and fluorescein isothiocyanate-labeled bovine serum albumin (FITC-BSA) were purchased from Sigma. NIH 3T3 fibroblasts, fetal bovine serum, Dulbecco's modified Eagle's medium, and other cell culture supplies were obtained from American Type Culture Collection (ATCC; Manassas, VA). All other materials were purchase from Aldrich (Milwaukee, WI) unless specified otherwise. All chemicals were used as received. Microfluidic channels of poly(dimethylsiloxane) (PDMS) were created by replica molding on a photoresist patterned surface using a two-component silicon elastomer kit (Sylgard 184; Dow Corning). To crosslink the PDMS prepolymer, a

mixture of 10:1 prepolymer and the curing agent was poured on the master and placed at 70 °C for 2 h. The PDMS mold was then peeled from the silicon wafer and then rendered hydrophilic by an O_2 plasma for 1 min prior to use. The oxidized PDMS mold was then bonded to a glass slide, which was previously cleaned using detergent followed by washing with deionized water and methanol several times.

3.2.2. Characterization

Fourier Transform - Infrared (FT-IR) spectra were obtained on a Digilab FTS 175 spectrometer (Bio-Rad, Cambridge, MA) equipped with a narrow band MCT detector at a spectral resolution of 1 cm^{-1}. A small volume of a 0.2 wt% solution of polymer in THF was placed onto a KBr disk (*dia.* 25 mm, Wilmad, Buena, NJ). After drying the solvent, the IR spectrum of the neat polymer on the KBr disk was recorded on absorption mode. Gel permeation chromatography (GPC) was performed using a Hewlett-Packard 1100 series isocratic pump, a Rheodyne model 7125 injector with a 100 μL injection loop, and two PL-Gel mixed-D columns in series (5 μm, 300 × 7.5 mm, Polymer Laboratories, Amherst, MA). $CHCl_3$ (HPLC grade) was used as the eluent at a flow rate of 1.0 mL/min. ^1H NMR (400 MHz) and ^{13}C NMR (100 MHz) spectra were recorded on a Bruker instrument (Avance DPX 400). The thicknesses of the monolayer films were measured with a Gaertner L116A ellipsometer (Gaertner Scientific Corporation, IL) at a 70° angle of incidence. A refractive index of 1.46 was used for all films, and a three-phase model was used to calculate thicknesses. A Ramé-Hart goniometer (Mountain Lakes, NJ) equipped with video camera and monitor was used to measure contact angles in both the advancing and receding modes (*ca.* 1 μL/s) on drops of ~3 μL in volume. Reported values represent averages of at least three independent measurements. XPS spectra were obtained using a Kratos AXIS Ultra

Imaging X-ray Photoelectron Spectrometer with a monochromatized Al K X-ray source and a 160 mm concentric hemispherical energy analyzer for acquisition of spectra and scanned images, lateral resolution down to 20 μm. The spot size was 300 μm × 700 μm. Scanning force micrographs (1.0 × 1.0 μm^2) were performed in tapping mode on a NanoScope III Dimension (Veeco Instruments Inc., Woodbury, NY) in air. The scan rate was 1 Hz and 256 lines were scanned per sample. Some of the images shown were flattened but not further manipulated. Tapping mode tips, NSC15 - 300 kHz, were obtained from MikroMasch (Portland). Data were processed using Nanoscope III 4.31r6 software (Veeco Instruments Inc., Woodbury, NY). Optical and fluorescence images were taken with a confocal optical/fluorescence microscope (Axiovert 200, Zeiss) and a computer-aided image capturing system (IP-spectrum software).

3.2.3. Preparation of Poly(TMSMA-*r*-PEGMA)

Prior to polymerization, neat PEGMA was flowed through the inhibitor removal column (Aldrich Chemical Co.). The synthetic scheme of Poly(TMSMA-*r*-PEGMA) is show in Scheme 3.1. In detail, PEGMA (4.75 g, 10 mmol, 1 equiv), TMSMA (2.5 g, 10 mmol, 1 equiv), and AIBN (16.5 mg, 0.1 mmol, 0.01 equiv) were placed in a vial and dissolved in 10 mL of tetrahydrofuran (THF, anhydrous, inhibitor free, 99.9 %). After the mixture was degassed for 20 min using an Ar gas stream, the vial was sealed with a Teflon-lined screw-cap. The polymerization reaction was performed at 70 °C for 24 h. After evaporation of solvent under vacuum, the polymer was obtained as a colorless, viscous liquid. ^{1}H-NMR (400 MHz, $CDCl_3$): δ = 4.13 (br, 2H, CO_2-C***H***$_2$ at PEGMA), 3.92 (br, 2H, CO_2-C***H***$_2$ at TMSMA), 3.66 (s, 30H), 3.63-3.55 (s, 9H; m, 2H), 3.40 (s, 3H), 2.0-1.71 (br, 6H), 1.04 (br, 2H), 0.87 (br, 4H), 0.66 (br, 2H); ^{13}C-NMR (100 MHz, $CDCl_3$): δ = 177.5, 176.3, 71.8, 70.5,

68.3, 66.8, 63.8, 58.9, 50.6, 44.7, 21.5, 18.2, 5.3; FT-IR (cm^{-1}, neat): 2943, 2874, 1729, 1453, 1350, 1247, 1107, 950, 853, 822.

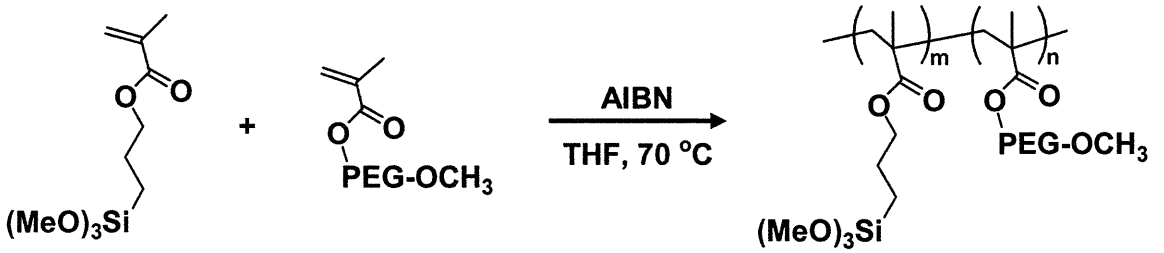

Scheme 3.1. Synthesis of Poly((trimethoxysilyl)propyl methacrylate-*r*-poly(ethylene glycol) methyl ether methacrylate) (Poly(TMSMA-*r*-PEGMA)).

3.2.4. Formation of Polymer Films

All substrates used herein such as Si/SiO_2 wafer, poly(dimethylsiloxane) (PDMS), and glass slide were first cleaned using detergent, and then rinsed sequentially with deionized water and methanol several times. Prior to forming the polymeric films, substrates were treated with an O_2 plasma at 0.15 Torr for 1 min to generate -OH groups as well as to clean the surfaces unless specially noted as 'no plasma treatment.' Polymeric self-assembled monolayers (PSAMs) of poly(TMSMA-*r*-PEGMA) onto those substrates were prepared by immersing the substrates in the copolymer solution in methanol (5-10 mg/mL) at ambient temperature for 1 h followed by washing with methanol. No ultrasonic washing procedure was required. The PSAMs were then cured at 120 °C for 15 min.

3.2.5. Protein Adsorption on Polymer Modified Surfaces.

Insulin, lysozyme, and fibrinogen were each dissolved at a concentration of 0.25 mg/mL in 10 mM phosphate buffer saline (PBS) solution (pH = 7.4). The PBS solution was prepared

by dissolving a Phosphate Buffered Saline Tablet (Sigma) in 200 mL of deionized water to obtain a solution that contained 10 mM sodium phosphate buffer, 2.7 mM KCl, and 137 mM NaCl. Polymer-coated and unmodified substrates (Si/SiO_2 wafers, glasses, and PDMS substrates) were immersed in the protein solution for 2 h, and were washed sequentially with PBS solution and water to remove non-adsorbed proteins and salts in the PBS solution. The samples were then blown dry in a stream of N_2.

3.2.6. Fibroblast Culture on Glass Substrates

Glass slides were cut into strips of *ca.* 1 cm × 1.5 cm and cleaned by an O_2 plasma. The polymer-coated glass slides were prepared by immersing the slides in the 10 mg/mL polymer solution in methanol for 2 h followed by rinsing with methanol and then by curing in 120 °C oven for 15 min. The polymer-coated glass slides were sterilized by UV radiation for 20 min. As a control surface, unmodified glass strips were also cleaned by an O_2 plasma and then sterilized by UV radiation. Subsequently each glass slide was placed in a 24-well plate, soaked in growth medium for 30 min and replaced with fresh medium. Each well was seeded with 100,000 NIH 3T3 fibroblasts and incubated at 37 °C, 5% CO_2 in Dulbecco's modified Eagle's medium, 90%; fetal bovine serum, 10%; penicillin, 100 units/mL; streptomycin, 100 μg/mL.

3.3. Results and Discussion

3.3.1. Preparation of Poly(TMSMA-r-PEGMA)

Poly(3-(trimethoxysilylpropyl) methacrylate-*r*-poly(ethylene glycol) methyl ether methacrylate), poly(TMSMA-*r*-PEGMA), was quantitatively synthesized by the radical polymerization of commercially available 3-(trimethoxysilyl)propyl methacrylate (TMSMA)

(1.0 equiv) and PEG methyl ether methacrylate (PEGMA) (1.0 equiv) in THF at 70 °C for 24 h. 0.01 equiv of AIBN was added as an initiator. The molecular weight of poly(TMSMA-*r*-PEGMA) was M_n = 26,000 with M_w/M_n = 1.88 as determined by gel permeation chromatography (GPC) relative to monodisperse polystyrene standards. The feed ratio of the two monomers was initially 1 to 1. By comparing the area under the peak at δ = 4.13 (CO_2-C***H***$_2$ at PEGMA) with that of the peak at δ = 3.92 (CO_2-C***H***$_2$ at TMSMA) in ^{1}H NMR spectrum, the molar ratio of the two monomer units in the copolymer was calculated to be the same as the corresponding feed ratio.

3.3.2. Formation and Charaterization of Polymeric Self-Assembled Monolayers

On Si/SiO$_2$ wafers. Polymeric self-assembled monolayers (PSAMs) of the polymer onto substrates exposing a SiO_2 surface were prepared from the copolymer solution in methanol (5-10 mg/mL). Immersing the cleaned Si/SiO_2 wafers in the 5 mg/mL polymer solution in methanol for 1 h generated the ultrathin polymer films with an average ellipsometric thickness of *ca.* 11 Å. Advancing and receding water contact angles of the PSAMs on a Si/SiO_2 wafer were 62° ± 1° and 46° ± 3°, respectively.

To examine the effects of immersion time and polymer concentration on the thickness of the PSAMs, O_2 plasma treated-Si/SiO_2 wafers were immersed in the polymer solution in methanol at various concentration and for various immersion time, followed by rinsing with methanol and dried under the stream of nitrogen. At a fixed polymer concentration of 5 mg/mL, the thicknesses of the films remained unchanged after immersion times up to 48 h (Figure 3.1a). On the other hand, it is known that monomeric trialkoxysilyl groups can give different coating thickness with different immersion times.[7,8] In addition, the formation of the PSAMs at a given time of 10 h was independent of the polymer concentrations up to 50

mg/mL (Figure 3.1b). This observation suggests that the adsorbed polymer layers can limit further attachment of additional polymer chains to the surface. Furthermore, we did not observe any thickness difference of the PSAMs after autoclaving for 1 h, annealing at 120 °C for 2 h, or incubation in PBS (pH 7.4) at 37 °C for 2 weekss.

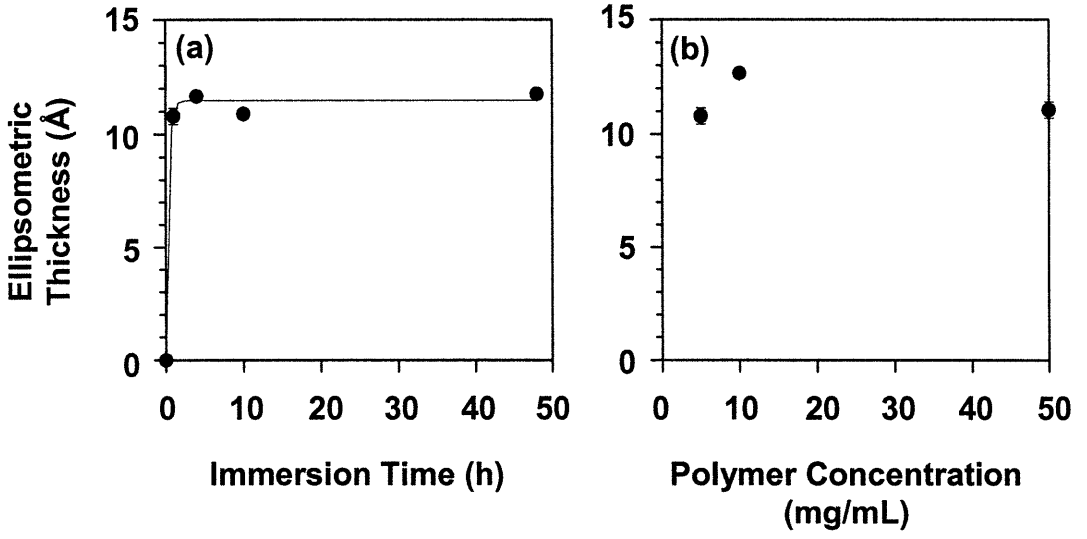

Figure 3.1. Thicknesses of PSAMs on Si/SiO_2 wafers as a function of (a) immersion time, and (b) concentration. The copolymer concentration in (a) was 5 mg/mL in methanol, and the immersion time in (b) was 10 h.

The surface topography of the PSAMs of the polymer on Si/SiO_2 wafers was examined by tapping mode atomic force microscopy (AFM). AFM height images of the PSAMs are presented in Figure 3.2. Unless specially noted, all PSAMs on the Si/SiO_2 wafers were prepared under the same conditions: immersion the polymer solution in methanol (5 mg/mL) for 1 h. Per each substrate, three different positions were taken. Figure 3.2a clearly shows the surface of the PSAMs on O_2 plasma treated-Si/SiO_2 wafers was very smooth with average roughness of 1.3 Å (root mean square) and had a topographically uniform pattern. Polymer aggregates were not detected for the O_2 plasma treated-substrate (Figure 3.2a), whereas randomly distributed polymer aggregates (about 30 nm wide and 5 nm high) could

be observed for the untreated-substrate (no plasma treatment) (Figure 3.2b). Such aggregation may be attributed to the crosslinking between unreacted trimethoxysilyl groups in the copolymer chains. It is expected that the O_2 plasma treatment generates more Si-OH groups on the surface of the substrate, resulting in a lower fraction of trimethoxysilyl groups that remained unreacted with the surface after the formation of the PSAMs in comparison to the untreated substrate (no plasma treatment). Therefore, this result indicates that plasma treatment enhances the uniformity of the PSAMs on Si/SiO_2 substrates.

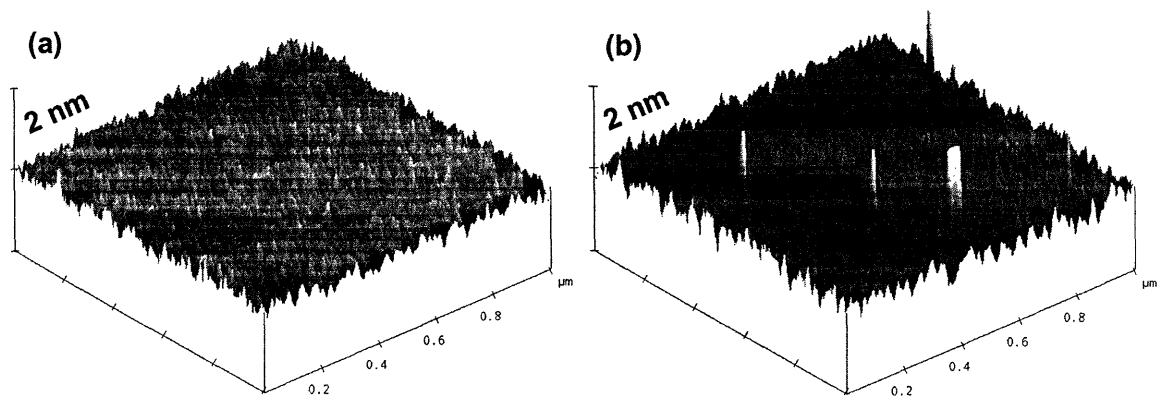

Figure 3.2. Tapping mode AFM height images of poly(TMSMA-*r*-PEGMA) SAMs: (a) on an O_2 plasma treated-Si/SiO_2 wafer and (b) on a detergent cleaned-Si/SiO_2 wafer (no plasma treatment).

Table 3.1. Elemental composition of the PSAMs on Si/SiO_2 wafer measured by XPS[a]

Substrate	Elemental Composition (%)		
	O	C	Si
Unmodified Si/SiO_2	38 ± <1	7 ± <1	55 ± <1
PSAMs on Si/SiO_2	34 ± <1	34 ± 3	32 ± 2

[a] Take-off angle was 55° from the surface normal.

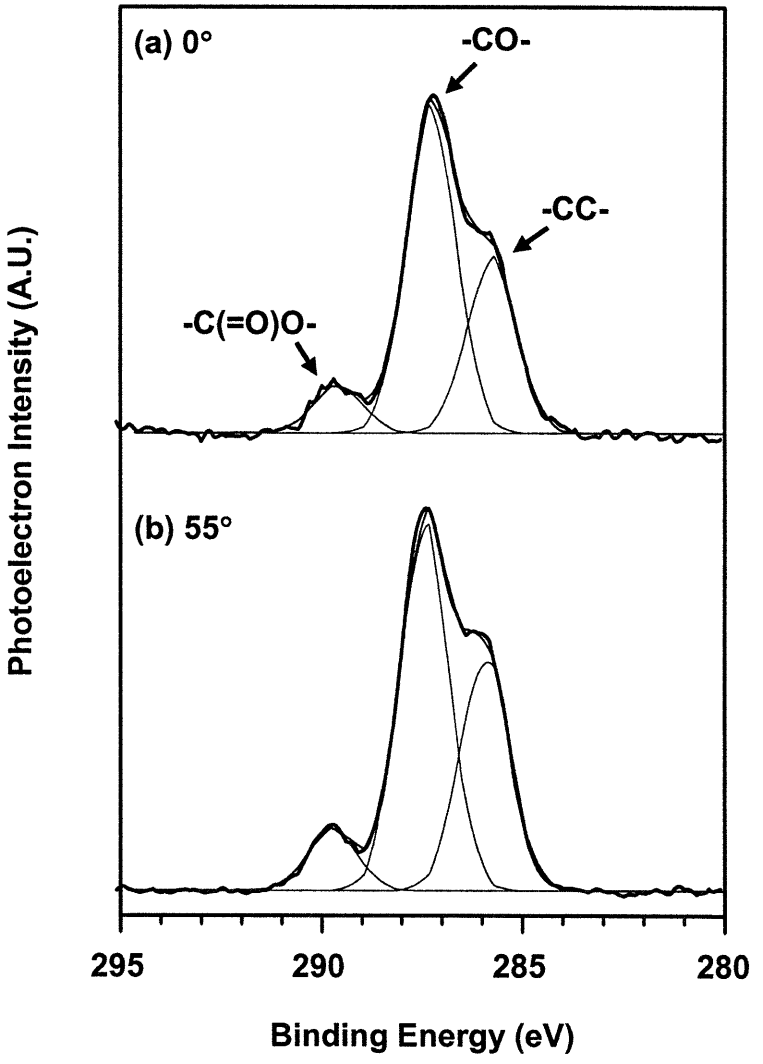

Figure 3.3. High resolution C(1s) X-ray photoelectron spectra of the PSAMs on Si/SiO_2 wafers at take-off angles of (a) 0° and (b) 55° from the surface normal.

Since poly(TMSMA-*r*-PEGMA) is a random copolymer, it is difficult to predict the structure of its self-assembled monolayers on oxide surfaces. However, thickness data seem to suggest that most of PEG side chains would stretch over the surface rather than align vertically on the surface, as the expected film thickness for the latter structure would be at least 20 Å. The polymer-coated films were also characterized by glancing angle X-ray photoelectron spectroscopy (XPS). Table 3.1 summarizes the elemental compositions of the

unmodified and the polymer-coated Si/SiO_2 surfaces as obtained from the survey scan. After the Si/SiO_2 was modified with the polymer, the carbon composition was increased by 25% and the silicon composition was decreased by 23%. Results of high resolution C(1s) XPS spectra further verify the formation of the PSAMs on Si/SiO_2 wafers (Figure 3.3 and Table 3.2). Three carbon peaks from hydrocarbon, ether carbon in the PEG chain, and ester carbon were observed from the C(1s) XPS spectra in Figure 3.3. The relative amount of those three carbon species characteristic of poly(TMSMA-*r*-PEGMA) were analyzed from the relative intensities of the corresponding peaks and were in good agreement with the stoichiometric ratios of the three carbon species (Table 3.2). The ratio of C-O in the PEG moieties to (C=O)O in the polymer backbone would increase with an increasing take-off angle in case the PEG chains align vertically from the surface. However, as take-off angle was changed from 0° to 55° from surface normal, the ratio slightly decreased, implying that the PEG chains lie horizontally over the surface as also suggested from the thickness data. Based on these findings, the self-assembled structure of the polymer onto a Si/SiO_2 support can be proposed as shown in Figure 3.4.

Table 3.2. High resolution C(1s) XPS composition at take-off angles of 0° and 55° from the surface normal

Take-Off Angle	Composition (%)		
	CH_2	C-O	C(=O)O
0°	30	61	9
55°	35	56	9

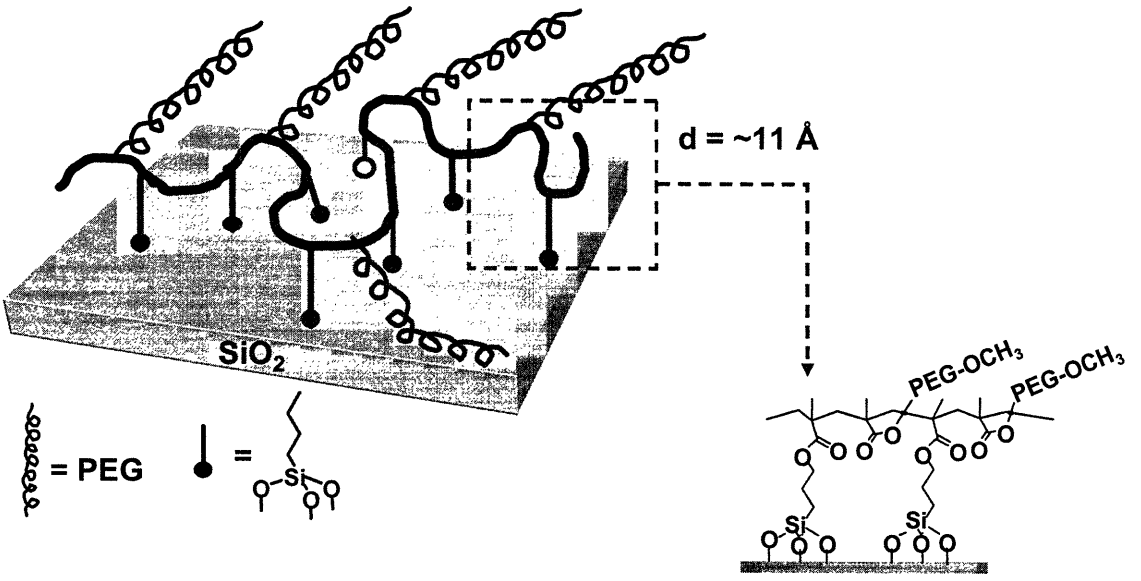

Figure 3.4. Schematic representation of the polymeric self- monolayer of poly(TMSMA-*r*-PEGMA) on a silicon dioxide surface.

On glass and PDMS substrates. PSAMs could be similarly prepared on glass and on PDMS substrates. Glass and PDMS substrate surfaces were first oxidized with an O_2 plasma, followed by subsequent immersion in the polymer solution of 10 mg/mL in methanol for 2 h. After rinsing with methanol and drying under N_2 stream, the substrates were annealed at 120 °C for 15 min. The resulting polymer films on glass and on PDMS were characterized by C(1s) XPS at a 55° take-off angle. Their C(1s) XPS spectra were showin in Figure 3.5. The hydrocarbon (-CC-) peak observed from C(1s) spectra of unmodified PDMS and glass could be attributed to methyl group in PDMS and to the hydrocarbon from dust adsorbed onto unmodified glass. On the other hand, the C(1s) spectra of the polymer coated surfaces could be resolved into three peaks from hydrocarbon, ether (-CO-), and ester (-C(=O)O-), which are characteristic of poly(TMSMA-*r*-PEGMA). Figure 3.5 demonstrates that PSAMs on the PDMS had higher hydrocarbon peak intensity than PSAMs on the Si/SiO_2 wafer (Figure 3.3)

and on the glass support, which can be due to the additional methyl moieties from PDMS substrate. However, the evident distinction of the spectra of the polymer coated surfaces from the unmodified surfaces and the existence of the three characteristic peaks of the polymer clearly confirms that both PDMS and glass surfaces were modified with poly(TMSMA-*r*-PEGMA).

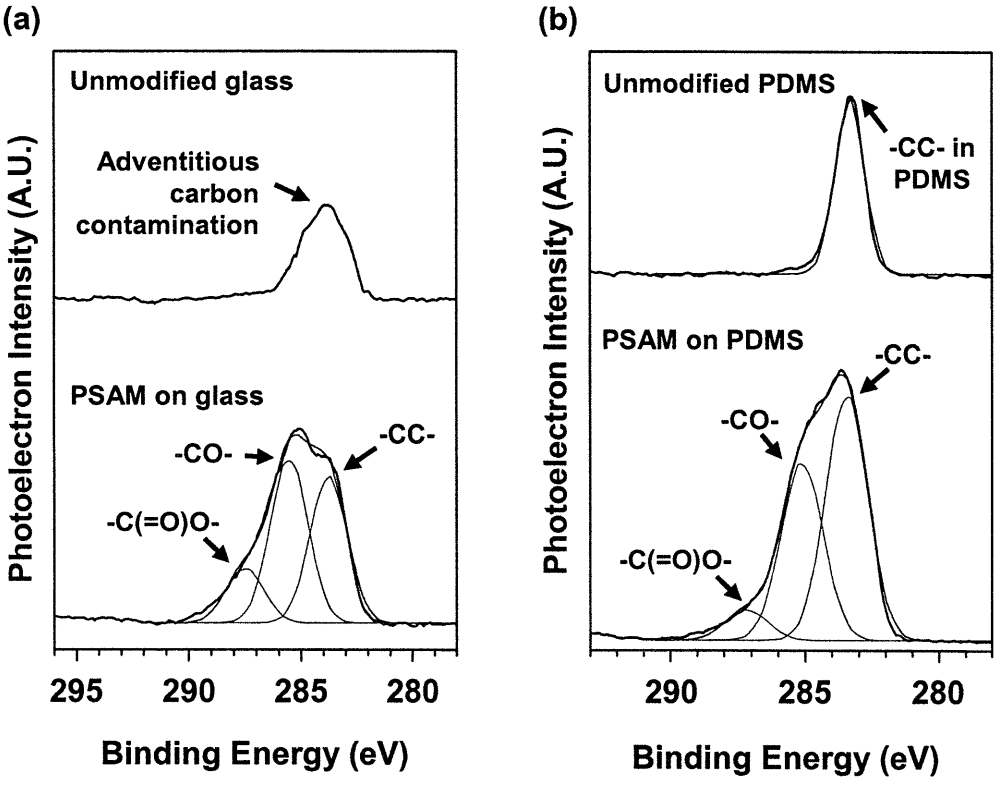

Figure 3.5. High resolution C(1s) XPS spectra of (a) glass and (b) PDMS before and after formation of the PSAM. The take-off angle was 55° from surface normal.

3.3.3. Protein Resistance of the Polymer Films

To evaluate the protein-resistant characteristics of the polymer films, polymer films were prepared from 5 mg/mL solution of poly(TMSMA-*r*-PEGMA) in methanol. The polymer-coated Si/SiO_2 wafers were immersed in several protein solutions (0.25 mg/mL in

PBS, pH 7.4) for 2 h. Figure 3.6 shows the degree of nonspecific protein adsorption onto the PSAMs as probed by the high resolution N(1s) XPS intensities. For all three proteins studied, the PSAMs showed significantly lower (up to 98 %) protein adsorption in comparison to the unmodified Si/SiO_2 wafer. For both a positively charged protein (Lysozyme, pI = 11.1) and a negatively charged protein (Insulin, pI = 5.4), the polymer-coated substrates were highly resistant to protein adsorption by > 95%. In addition, we observed about 98 % resistance toward fibrinogen (pI = 5.5) adsorption, which is abundant in blood plasma and serum and is a well-known protein for its stickiness.

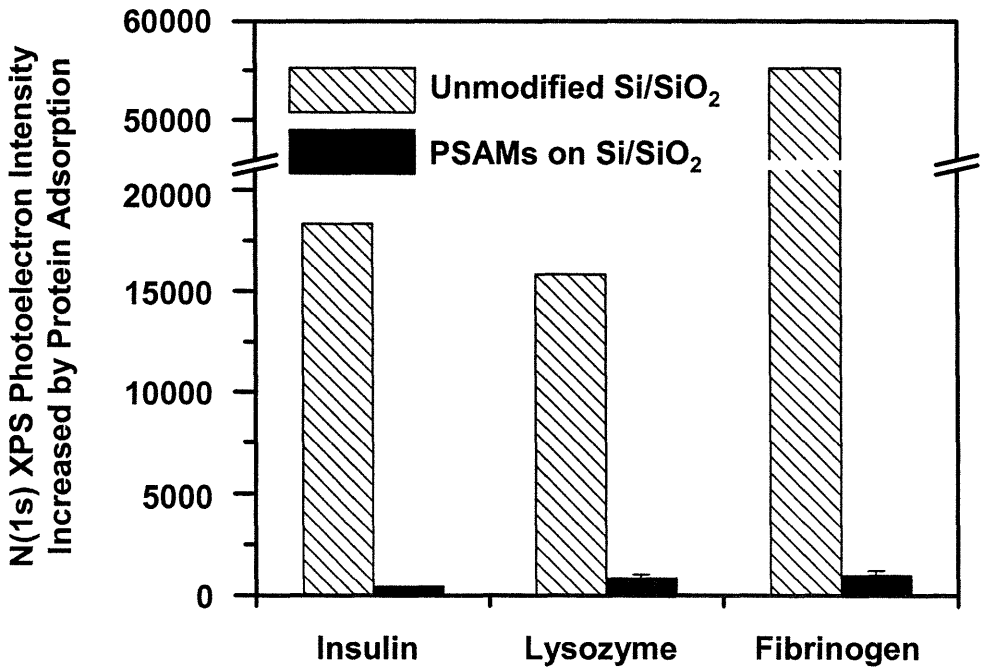

Figure 3.6. Protein adsorption on native (unmodified) and poly(TMSMA-*r*-PEGMA)-modifed Si/SiO_2 wafers. The relative amount of each protein on the surface is displayed using N(1s) XPS photoelectron intensity.

The nonspecific protein adsorption onto the PSAMs was also probed by the changes in ellipsometric thickness of the substrates before and after incubation in each protein solution (Figure 3.7). The thickness of the adsorbed protein films on unmodified Si/SiO_2 wafer was

ca. 20 Å for insulin and lysozyme and *ca.* 65 Å for fibrinogen. On the other hand, the detection limit and the thickness of adsorbed fibrinogen was only *ca.* 2 Å.

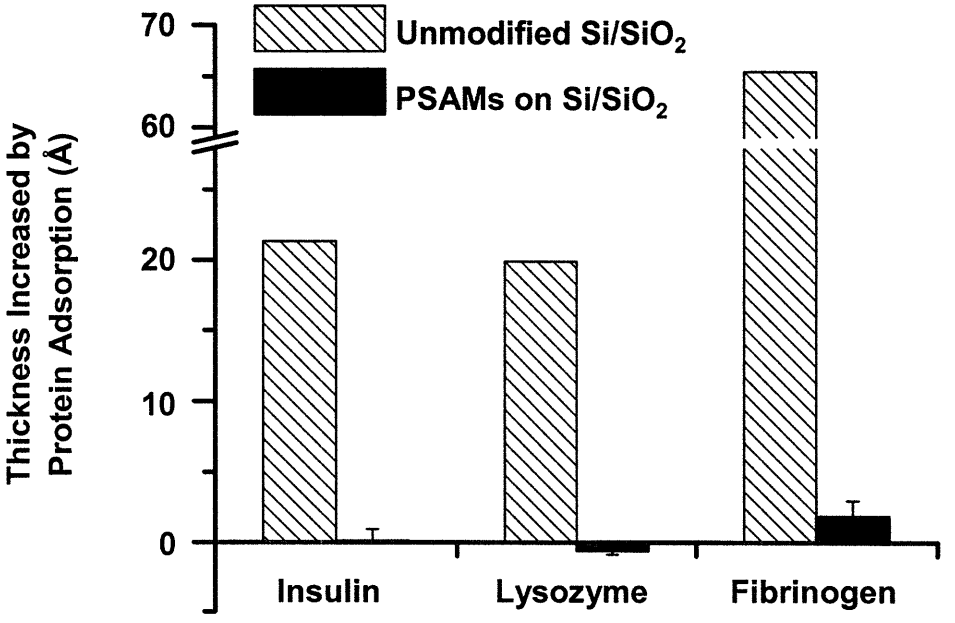

Figure 3.7. Ellipsometric thickness changes in the substrates after immersion into protein solutions (0.25 mg/mL in PBS, pH 7.4) at ambient temperature for 2 h.
thickness increased by insulin and lysozyme adsorbed onto the PSAM was below the

The degree of nonspecific protein adsorption onto PSAMs on PDMS and on glass was also obtained from the N(1s) XPS intensities (Figure 3.8). The polymer films on PDMS and on glass had lower protein resistances (*e.g.*, 81 % and 94 % for insulin, respectively) than on Si/SiO_2 wafers (95 %). As discussed in Chapter 2, this result is attributed to the large differences in the nonspecific protein adsorption on each unmodified substrate.

3.3.4. Non-biofouling Coating of Microfluidic Channels

Section 3.3.3 demonstrated that glasses and PDMS substrates can be rendered protein-resistant by forming ultrathin films of poly(TMSMA-*r*-PEGMA) on those surfaces. Because

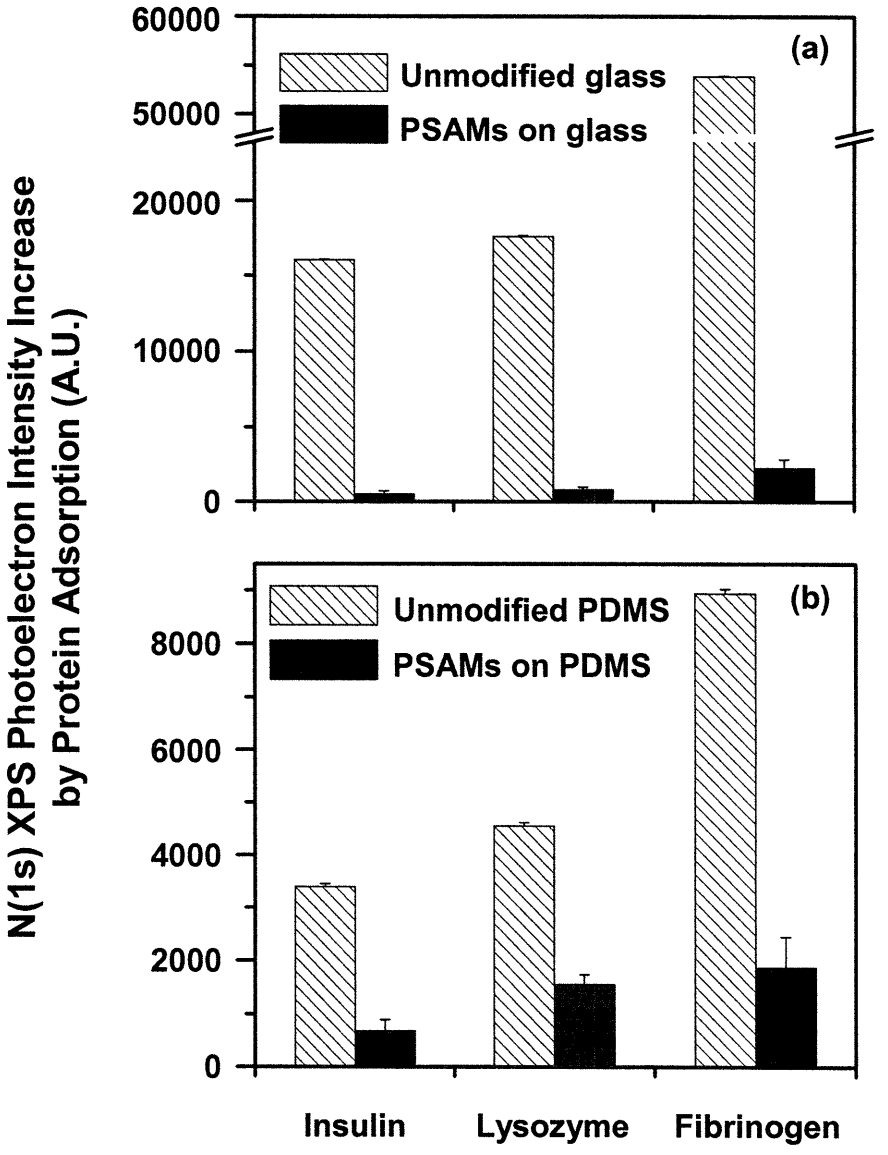

Figure 3.8. Protein resistance of (a) the unmodified and the polymer-coated PDMS and (b) the unmodified and the polymer-coated glass as evaluated by the increases in the N(1s) XPS photoelectron intensities upon protein adsorption.

most microfluidic channels are made of PDMS molds on glass supports, the present strategy can also be applied to the preparation of non-biofouling microfluidic channel walls. Those non-biofouling capillary channels are important in electrophoresis, microfluidics, and bio-MEMS devices. [9,10] To fabricate the microfluidic channels (80 μm height, 500 μm width), a model PDMS mold was bonded onto a glass slide using an O_2 plasma. Figure 3.9 shows one

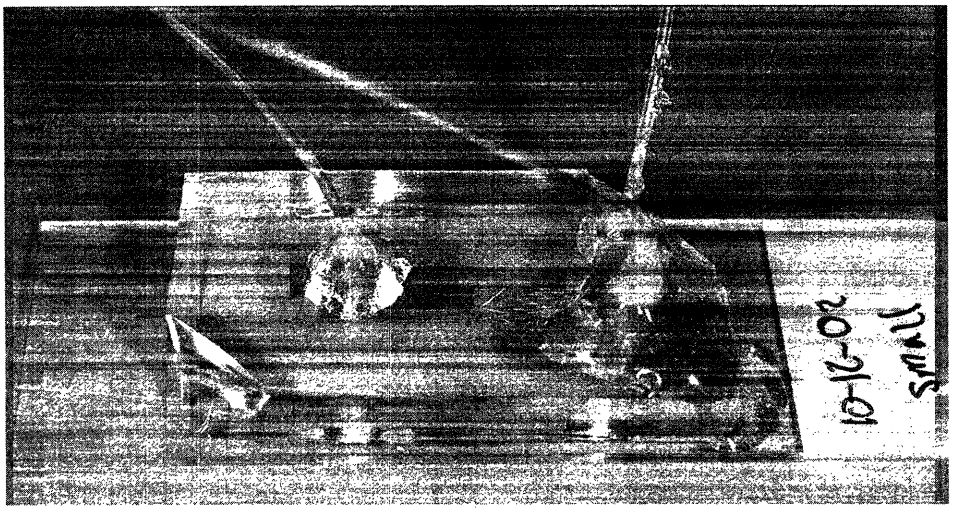

Figure 3.9. A representative microfluidic device with capillary tubing connected to channels.

example of the microfluidic device with capillary tubing connected to channels. The inlet tubes is connected to a syringe pump that can control the flow rate in the range of 0.001 mL/min to 20 mL/min. The inside of the microfluidic channel walls was coated by flowing the polymer solution in methanol (10 mg/mL) in through the inlet port using a syringe pump for 2 h at a rate of 2 μL/min. The use of methanol as solvent prevented the PDMS mold from swelling during the procedure. After washing the channel by flowing methanol for 10 min, FITC-BSA (0.1 mg/mL in PBS, pH 7.4) was flowed through the channel at a rate of 5 μL/min for 30 min. As a control experiment, FITC-BSA solution was directly flowed through the channel without prior coating with the polymer. Each channel was subsequently washed with PBS solution for 15 min. The PDMS and the glass parts were separated and fluorescence images were taken of each channel area. Figure 3.10 shows the fluorescence microscopy images of the PDMS and glass channel parts after the FITC-BSA adsorption onto polymer-coated and unmodified channels. As these images indicate, much less protein adsorption was observed on the polymer-coated channel walls on both glass (Figure 3.10b) and PDMS (Figure 3.10d) compared to those of unmodified glass and PDMS (Figure 3.10a and c).

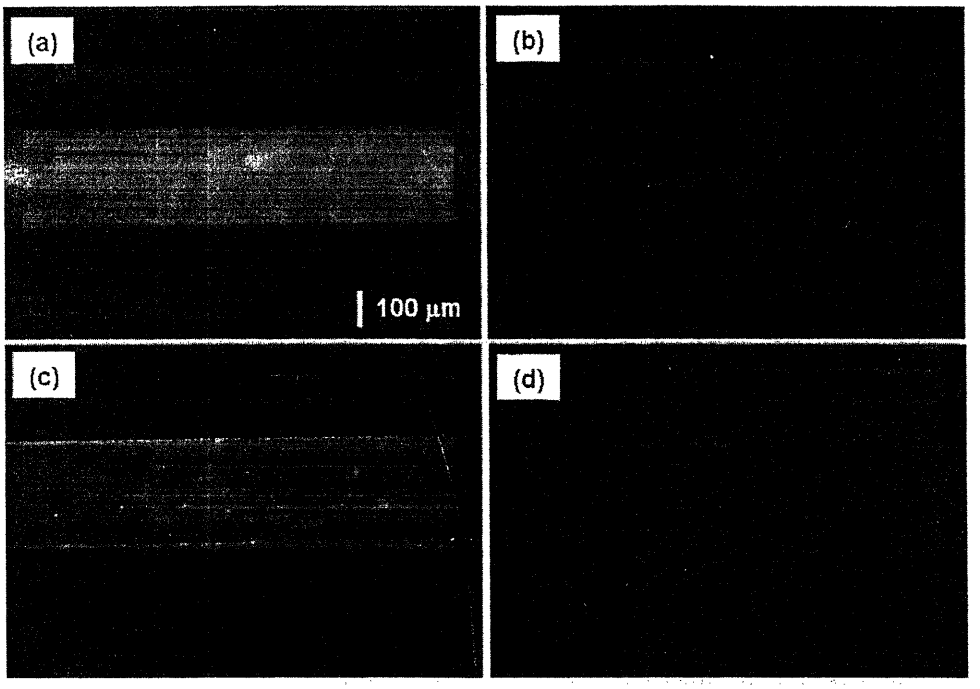

Figure 3.10. Fluorescence images on each part of capillary channel after flowing an aqueous solution of FITC-Bovine Serum Albumin (0.1 mg/mL, pH 7.4 PBS buffer) through the channel: (a) unmodified glass (b) polymer-coated glass; (c) unmodified PDMS and (d) polymer-coated PDMS. The scale bar indicates 100 μm.

3.3.5. Cell Adhesion on the Polymer Films

To investigate the cell-resistant properties of the PSAMs, we carried out cell culture experiments. NIH 3T3 fibroblasts, which tend to be very adhesive and can make confluent monolayers, were seeded on the unmodified glass and the polymer-coated glass. After 24 h, each glass substrate was gently washed with the same culture medium and was imaged by an optical microscope. On the unmodified glass slide, fibroblasts grew and formed confluent monolayers with a density of *ca.* 1.4×10^5 cells/cm^2 (Figure 3.11a). However, the polymer-coated glass slide was highly resistant to cell adhesion as well as to cell spreading (Figure 3.11b) with a density of *ca.* 4.3×10^3 cells/cm^2, which is only 3% of the cell density on unmodified glass. This result suggests that the polymer films are highly resistant to serum proteins in the cell culture medium and thus prevents fibroblasts from seeding on the surface.

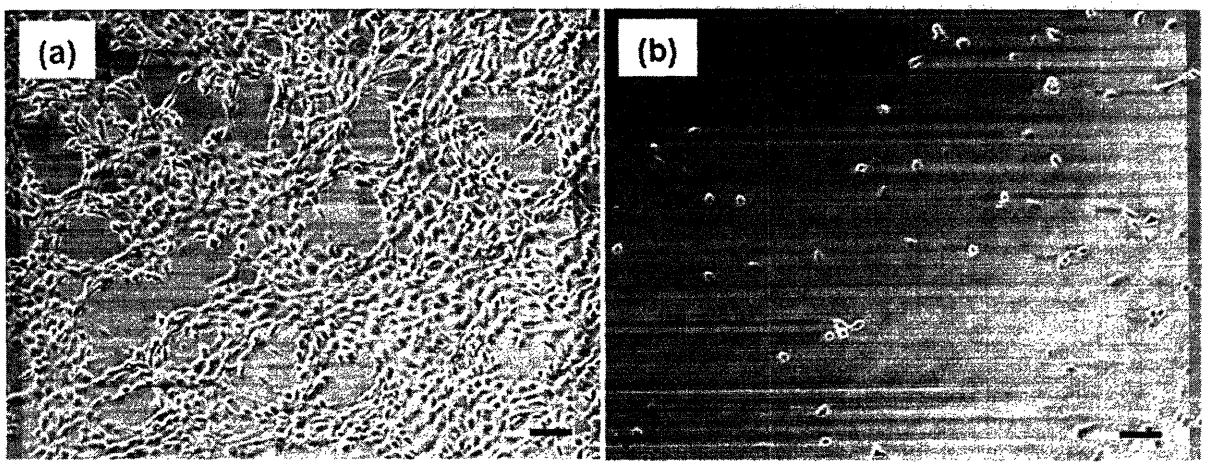

Figure 3.11. NIH 3T3 fibroblasts cultured on (a) unmodified glass and (b) the copolymer-coated glass for 24 h with an initial seeding density of 5.3×10^4 cells/cm^2. The scale bar indicates 100 μm.

3.4. Conclusion

Non-biofouling surfaces could be easily prepared on substrates exposing a SiO_2 surface by forming polymeric self-assembled monolayers of a surface-reactive graft copolymer of PEG. The polymer films were reproducibly generated at the ambient environments without special care for anhydrous conditions. The resulting ultrathin films of *ca.* 1 nm thickness showed a great reduction in protein adsorption (up to 98%) and cell adhesion. The present approach may be potentially applied to other substrates such as metal oxides (*e.g.*, Al_2O_3 and TiO_2) and polymer surfaces. The present system has advantages over the previous strategy in Chapter2 in that poly(TMSMA-*r*-PEGMA) films can be directly formed onto the bare substrates without prior formation of an adhesion promoting layer. Since functional units other than PEG, such as biotin and fluorocarbons, can also be incorporated into the polymer as monomer units, the combined copolymer system of the 'anchor part' (trialkoxysilane) and the 'function part' may have applications in the preparation of functional surfaces for medical and analytical devices.

3.5. References for Chapter 3

* This work was done in collaboration with Dr. Sangyong Jon, Chemical Engineering, MIT.

(1) Irvine, D. J.; Mayes, A. M.; Griffith, L. G. Nanoscale clustering of RGD peptides at surfaces using comb polymers. 1. Synthesis and characterization of comb thin films. *Biomacromolecules* **2001**, *2*, 85-94.

(2) Park, J.-W.; Thomas, E. L. A surface-reactive rod-coil diblock copolymer: Nano- and micropatterned polymer brushes. *J. Am. Chem. Soc.* **2002**, *124*, 514-515.

(3) Sun, F.; Castner, D. G.; Mao, G.; Wang, W.; McKeown, P.; Grainger, D. W. Spontaneous polymer thin film assembly and organization using mutually immiscible side chains. *J. Am. Chem. Soc.* **1996**, *118*, 1856-1866.

(4) Xia, N.; Hu, Y.; Grainger, D. W.; Castner, D. G. Functionalized poly(ethylene glycol)-grafted polysiloxane monolayers for control of protein binding. *Langmuir* **2002**, *18*, 3255-3262.

(5) Bearinger, J. P.; Terrettaz, S.; Michel, R.; Tirelli, N.; Vogel, H.; Textor, M.; Hubbell, J. A. Chemisorbed poly(propylene sulfide)-based copolymers resist biomolecular interactions. *Nat. Mater.* **2003**, *2*, 259-264.

(6) Johnson, P. A.; Levicky, R. Polymercaptosiloxane anchor films for robust immobilization of biomolecules to gold supports. *Langmuir* **2003**, *19*, 10288-10294.

(7) Plueddemann, E. P. *Silane coupling agents*; 2nd ed.; Plenum Press: New York, **1991**.

(8) Moon, J.-H.; Shin, J. W.; Kim, S. Y.; Park, J. W. Formation of uniform aminosilane thin layers: An imine formation to measure relative surface density of the amine group. *Langmuir* **1996**, *12*, 4621-4624.

(9) Folch, A.; Ayon, A.; Hurtado, O.; Schmidt, M. A.; Toner, M. Molding of deep polydimethylsiloxane microstructures for microfluidics and biological applications. *J. Biomech. Eng.* **1999**, *121*, 28-34.

(10) Albarghouthi, M. N.; Stein, T. M.; Barron, A. E. Poly-n-hydroxyethylacrylamide as a novel, adsorbed coating for protein separation by capillary electrophoresis. *Electrophoresis* **2003**, *24*, 1166-1175.

Chapter 4. Fabrication of Poly(ethylene glycol) Microstructures for Protein and Cell Patterning by Soft Lithography

4.1. Introduction

The ability to spatially control the cell positioning and organization on surfaces is vital to understanding the cell-surface interactions and to engineering the cellular processes such as adhesion, growth, or migration.[1-5] In addition to leading to a better understanding of the basic issues above, the selective localization of proteins and cells on microstructured device surfaces has practical applications for such as protein- or cell-based biosensors,[6] diagnostic assays,[7] high-throughput screening for drug discovery,[8-10] and tissue engineering templates[11].

The previous chapters in this thesis have discussed the protein- and cell- repelling property of poly(ethylene glycol) (PEG) and have demonstrated that PEG films that were coated to surface by various methods were effective in resisting protein and cell attachment. Therefore, patterning the background regions of the substrates with PEG on would drive proteins or cells onto specific regions. Thus, micropatterning of PEG is important to the patterned deposition of proteins or cells.

Microfabrication technologies, a collective term describing the conventional methods for creating microstructures and patterns, have been successfully applied to protein or cell patterning, because they can exercise spatial control over the attachment of proteins and cells to surfaces. Although optical lithography or photolithography is one of the most well-established microfabrication techniques[12,13] and has been tested for its potential for protein and cell patterning,[14-16] its usage with proteins and cells is generally limited by steps that require harsh organic solvents.[17] A biocompatible process in the photolithographic patterning of poly(ethylene glycol) (PEG) hydrogels has been reported. This process

generally involves three steps: spin coating a photopolymerizable PEG solution onto a substrate, exposing gel precursor through a photoresist, and developing the pattern using solvents such as water, toluene, or supercritical CO_2.[18-21] PEG microstructures fabricated by this process have been successfully applied to the fabrication of enzyme electrodes,[20] pH sensitive MEMS devices,[21] and optical sensors[19]. However, because it requires complex equipment, photolithography is too complicated and expensive a technique to be the mainstay for protein or cell. Moreover, photolithography has limited capability for incorporating specific chemical functionalities.

A possible evolution of microfabrication may be sought in soft lithography, a collective name for a set of lithographic techniques that involve the use of an elastomer such as polydimethylsiloxane (PDMS). It is well-suited for biological applications because it can be applied to biologically compatible surfaces and can be processed in an ordinary laboratory without clean room facilities. Up till now, many soft lithographic techniques have been employed to transfer solutions of biological components or to modify surfaces with a negative relief of the pattern. The earliest technique reported is microcontact printing (μCP),[17,22-31] where self-assembled monolayers (SAMs) terminated with PEG chains are created on background regions to provide bioinert surroundings[32,33] and thus to allow patterned deposition of proteins or cells onto selected regions.

Although μCP is a straightforward and versatile technique, it cannot be used to exercise topographical manipulation over a surface. To obtain topographical patterns, microfluidic networking,[11,34-36] and micromolding in capillaries (MIMIC)[35,37] have been employed. However, these techniques are restricted in that the mold should have an inner network structure and also in that feature sizes below 1 μm have been difficult to realize.[38] There also have been other strategies to generate patterns of proteins and cells on surfaces, such as

membrane-based lift-off,[39,40] manipulations of surface charge, hydrophilicity, acid/base interactions,[41] and topography,[1,4] and polymer templating using μCP[42-45]. Nevertheless, no soft lithographic technique has yet been available to pattern PEG hydrogels *directly* on the surface.

This chapter reports an addition to these emerging protein and cell patterning techniques. In particular, it discusses an application of a molding technique called capillary force lithography (CFL)[46,47] to the patterned deposition of proteins and cells. This CFL technique[46,47] combines the key feature of the imprint lithography of molding a polymer melt with the primary element of soft lithography of using an elastomeric mold. Capillary force lithography involves a molding process where a uniform PEG film is molded with a patterned poly(dimethylsiloxane) (PDMS) by way of capillarity and wettability of the polymer within the mold. A crosslinkable PEG derivative is first spun onto the substrates; the film is then brought in conformal contact with a patterned PDMS mold. The capillary force between PEG and PDMS drives the PEG, which has been in contact with the mold, into the empty space between the mold and the underlying substrate. This process then ultimately leads to the formation of PEG microstructures inside the void and the depletion of the polymer material in the region where PDMS mold has been in touch contact with the PEG film. In comparison with the PEG structures created by μCP, which is a two-dimensional patterning method, the molded PEG structure acts both as a non-biofouling region and as a physical barrier for the adhesion of proteins and cells. Such a barrier exhibits a unique regulation of surface patterning. Unlike microfluidic systems or MIMIC techniques, CFL can create discrete patterns as well as continuous inner network structures. Furthermore, CFL offers a general platform for patterning a broad range of materials since it can be applied to substrates such as glass, silicon, silicon dioxide and polymers. As a result, it may

be a valuable tool for fabricating protein chips and high-throughput cell screening devices because feature sizes can be easily controlled (~500 nm to ~500 μm) on a large area with suitably prepared PDMS molds.

4.2. Experimental Section

4.2.1. Materials

Poly(ethylene glycol) dimethacrylate (PEGDMA, Mw = 330) and 2,2-dimethoxy-2-phenylacetophenone (DMPA) were obtained from Aldrich (Milwaukee, WI). 3-Trichlorosilylpropyl methacrylate was purchased from Gelest, Inc. (Morrisville, PA). Fluorescein isothiocyanate-labeled bovine serum albumin (FITC-BSA) was a product of Fluka (Buchs, Switzerland). Fibronectin (FN) and phosphate buffered saline (PBS) tablets were provided by Sigma. NIH-3T3 murine embryonic fibroblasts and other cell culture supplies were obtained from American Type Culture Collection (ATCC, Manassas, VA). Fetal bovine serum, trypsin, and Dulbecco's modified Eagle's medium (DMEM) were supplied by Gibco Invitrogen Corporation (Carlsbad, CA). All other chemicals were obtained from Aldrich unless otherwise specified. All chemicals were used as received. Si(100) wafers were a product of North East Silicon Technologies, Inc. (NESTEC, New Bedford, MA).

PDMS molds were prepared by replica molding. First, the prepolymer and curing agent from Sylgard 184, a two-component silicon elastomer kit from Essex Chemical (Edison, NJ), were mixed in the 10:1 (w:w) ratio. After degassing the mixture under vacuum for 5 h to remove the air trapped inside, the mixture was cast against patterned silicon masters. The masters had complementary relief structures made of SU-8 photoresist, and were prepared using a photolithographic technique. The cast mixture was then incubated at 70 °C for 2 h.

The patterned PDMS mold was then separated from the master, cut, and cleaned with methanol. The prepared molds had protruding features with different lateral dimensions ranging from 10 to 50 μm and with step heights of 0.5 μm or 1.5 μm.

4.2.2. Characterization

Fourier Transform - Infrared Spectroscopy (FT-IR) spectra were used to monitor the progress of the crosslinking reaction of PEGDMA after UV illumination. A solution of 5 wt% PEGDMA and 0.05 wt% of DMPA in methanol was spin-coated on a KBr disk (25mm × 5mm) (Wilmad, Buena, NJ) for 30 s at 3000 rpm. The DMPA was added to the solution as a photoinitiator. FT-IR spectra of PEGDMA were recorded on a Digilab FTS 175 spectrometer (Bio-Rad; Cambridge, MA) with a narrow-band MCT detector at the spectral resolution of 1 cm^{-1}. We repeated the cycles of UV exposure and IR spectra collection until we attained static spectra over time. Thicknesses of the PEGDMA films coated on Si/SiO_2 wafers (North East Silicon Technologies, Inc.; New Bedford, MA) were measured with a Gaertner L116A ellipsometer (Gaertner Scientific Corp., Skokie, IL) equipped with a 632.8 nm He-Ne laser. A refractive index of 1.46 was used for all PEGDMA films, and a three-phase model was used to calculate thicknesses. A Ramé-Hart goniometer (Mountain Lakes, NJ) equipped with a video camera and a monitor was used to measure contact angles on drops of *ca.* 3 μL in volume in both the advancing and receding modes (*ca.* 1 μL/s). Reported values represent averages of at least three independent measurements. Atomic force microscopy (AFM) images were obtained in tapping mode in air on a NanoScope III Dimension (Veeco Instruments Inc., Woodbury, NY). The scan rate was 1 Hz, and 256 lines were scanned per sample. Tapping mode tips, NSC15 - 300 kHz, were obtained from MikroMasch (Portland). Data were processed using Nanoscope III 4.31r6 software (Veeco

Instruments Inc., Woodbury, NY). Optical and fluorescence images were taken with an inverted optical/fluorescence microscope equipped with a computer-aided image-capturing system (Axiovert 200, Zeiss).

4.2.3. Fabrication of PEG Patterns

Figure 4.1 outlines the fabrication process of the PEG microstructures on glass or Si/SiO_2 wafers. First, PEGDMA solutions in methanol were prepared at various concentrations ranging from 1 wt% to 100 wt%, *i.e.*, pure polymer. 1 wt% of DMPA with respect to the amount of PEGDMA was added in each solution as a photoinitiator. The solutions were stored in vials wrapped in aluminum foil and kept at -20 °C until use. Si/SiO_2 wafers and glass were used as substrates. Substrates were rinsed several times with acetone and ethanol and dried in a stream of nitrogen. Each PEGDMA solution was then spun using a spin-coater (Model CB 15, Headaway Research, Garland, TX) onto a substrate at 3000 rpm for 10 s. Immediately after the spin coating, the patterned PDMS molds were carefully placed onto the PEGDMA films for 0.5 h to make conformal contact.[47] While the PDMS molds were still in contact with the PEG films, the films were crosslinked by exposing them under a 365 nm, 15 mW/cm^2 low-power Black-light inspection lamp (ELC-251, Electro-Lite Corp., Danbury, CT). After 2 h of exposure to ultraviolet (UV) light, the molds were removed from the substrates.

4.2.4. Protein Adsorption

A PBS solution (pH = 7.4; 10 mM sodium phosphate buffer, 2.7 mM KCl, and 137 mM NaCl) was prepared by dissolving one PBS tablet in 200 mL of deionized water. FITC-BSA and fibronectin were each dissolved into PBS at concentrations of 0.25 mg/mL and 0.1 mg/mL, respectively. A few drops of each protein solution were evenly distributed onto the

patterned substrates and stored at room temperature for 30 min. The patterned substrates were rinsed sequentially with PBS and water, and blown dry in a stream of nitrogen; they were then imaged under a fluorescent microscope.

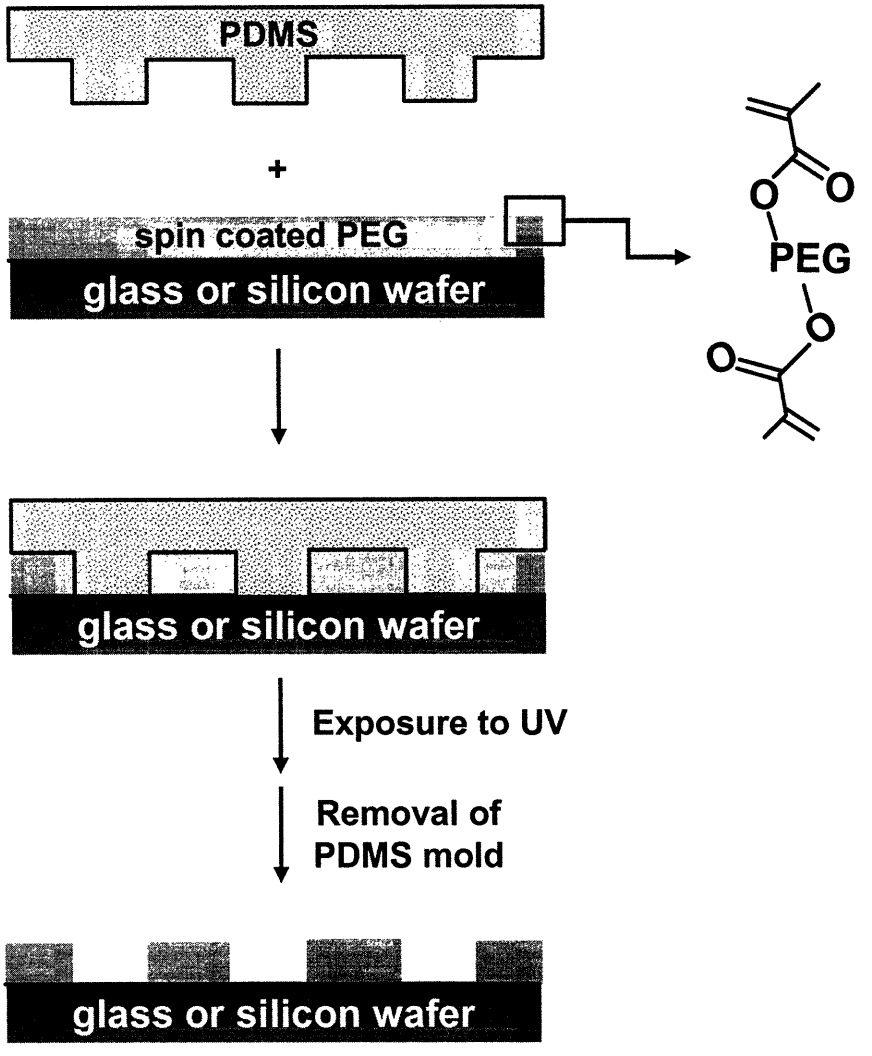

Figure 4.1. Schematic illustration of the PEG microstructure fabrication process. Initially, a uniform PEG film was prepared by spin coating PEGDMA. This PEG film was then molded by capillary force lithography, and crosslinked under UV to stabilize the pattern on the glass or Si/SiO_2 wafer support.

4.2.5. Cell Cultures

NIH-3T3 murine embryonic fibroblasts were maintained in Dulbecco's modified Eagle medium supplemented with 10% fetal bovine serum at 37 °C in a humidified atmosphere containing 5% CO_2/95% air. Once the cells were confluent, they were trypsinized using a trypsin-EDTA solution (0.25% trypsin) (Sigma) and passaged at a 1:5 subculture ratio. Fibronectin patterns were prepared on PEGDMA-patterned glass slides by incubating the slides in the fibronectin solution for 20 min followed by rinsing with PBS. The fibroblast suspension in the medium at a density of 1×10^6 cells/mL was then plated onto the fibronectin-patterned surfaces.

4.3. Results and Discussion

4.3.1. Fabrication and Characterization of PEG Microstructure

PEG microstructures were formed on glass and Si/SiO_2 wafers by capillary force lithography (CFL).[46,47] Details of CFL are described elsewhere.[46,48] Briefly, CFL describes capillarity-mediated molding of a liquid-like, mobile material. When a mobile polymer film has an acute contact angle (*i.e.*, < 90°) on the PDMS surface and is in conformal contact with a patterned PDMS mold, capillarity forces the polymer into the void space of the mold. During the capillary rise, the polymer in contact with the stamp becomes depleted and the underlying substrate gets exposed, leading to a negative replica of the mold. Figure 4.1 provides the schematic process flow of PEG microstructure fabrication using CFL.

In earlier studies of CFL using polystyrene (PS) and styrene-butadiene rubber (SBR), the mobility of the polymer was imparted thermally, *i.e.*, by heating the material above its glass transition temperature (T_g).[46,48] However, in the present system using PEGDMA,

raising the temperature above *ca.* 50 °C, the melting temperature of PEGDMA, induced instability and thus spontaneous dewetting patterns of spherical drops were observed. This instability is regarded as a result of both the high contact angle and the high mobility of the PEGDMA used. The contact angle of PEGDMA on PDMS was *ca.* 65° on a PDMS slab, whereas that of PS (Mw = 3,900) was 20-40° on the PDMS surface[49]. Besides, having a low molecular weight (Mw = 330) and having an oxygen element along the polymer backbone, the PEGDMA in the present system can be considered to be more liquid-like than the PS. Therefore, increasing the mobility of PEGDMA by raising the temperature triggered the instability of the patterns and thus was not suitable for assuring high-quality pattern transfer.

An alternative route to conveying polymer mobility is by using solvent.[47,50] This route consists of three steps: 1) forming a "wet film" by spin coating the concentrated polymer solution for a short time (< 15 s), 2) placing a patterned PDMS mold on the film and allowing the mold to absorb solvent, and 3) letting the mold and the substrate stay intact for 10 - 15 min and thereby allowing the solvent to evaporate. Considering the limitations of thermal activation stated above, this technique would be more useful in the present system of PEGDMA to ensure high pattern fidelity without noticeable defects or distortions. Therefore, the work in this chapter employed the "wet film" method.

To generate PEG microstructures, wet PEG films were formed by spin-coating the PEGDMA solution for 10 s, and immediately bringing the films in conformal contact with the PDMS mold. As the solvent (methanol) evaporates, PEGDMA in contact with the protruding PDMS features withdraws spontaneously and moves into the empty space of the PDMS mold by means of capillary action. According to the previously-cited report, this capillary action is completed within a few minutes.[47]

Spin-coated PEG films were 30 nm - 2 μm thick as measured by ellipsometry,

depending on the concentration of PEGDMA. After a 10-min annealing of the PEG microstructures under the PDMS molds, the PEG patterns were stabilized by crosslinking under a UV light. Due to its solubility in water, uncrosslinked PEG was completely depleted from the surface upon the slightest exposure to water. As the focus of this study was to form patterned arrays of biological species, water stability of the PEG microstructures was required. Therefore, in order to improve the stability of the PEG microstructure, PEGDMA, a polymerizable PEG derivative, was used instead of unmodified PEG and crosslinked for 2 h under the UV light and thus it was formed into PEG hydrogel.

Figure 4.2 shows representative AFM pictures of a polymer microstructure of 10 μm boxes on a Si/SiO_2 wafer. Polymer concentration was 50% in methanol. The topographical features demonstrate high pattern fidelity (Figure 4.2a, b, and c). A good contrast in the phase image in Figure 4.2d corresponds to two different kinds of interactions of the AFM tip with the surface, indicating that the substrate surface was completely exposed without any trace of PEG. The absence of residual polymers on the region where the substrate was brought in contact with the PDMS suggests that the interaction between the PEG and the substrate was sufficiently weak and that the PEG was mobile enough. The menisci formation at the protruding end of the polymer (Figure 4.2b) is characteristic of the capillary rise, which is attributed to the acute contact angle of *ca.* 65° at the PEGDMA/PDMS/air interface. The step height of the mold was 500 nm, which is nearly the same as the height from bottom to top of the cross-sectional image in Figure 4.2b. Use of concentrated solutions prevented the polymers from dewetting and facilitated the negative replica of the three-dimensional structure of the PDMS mold. Decrease in the PEGDMA concentration decreased this topological height of the PEG microstructure. Thus, the aspect ratio of PEG patterns could be controlled using different film thickness, *i.e.*, spin-coating solutions of different

concentrations, for a given feature size of the PDMS mold. Solutions at concentrations lower than 20 wt% in methanol eventually led to the formation of spherical drops by spontaneous dewetting. Comparison of PEG microstructures driven by CFL and dewetting processes has been discussed elsewhere.[51]

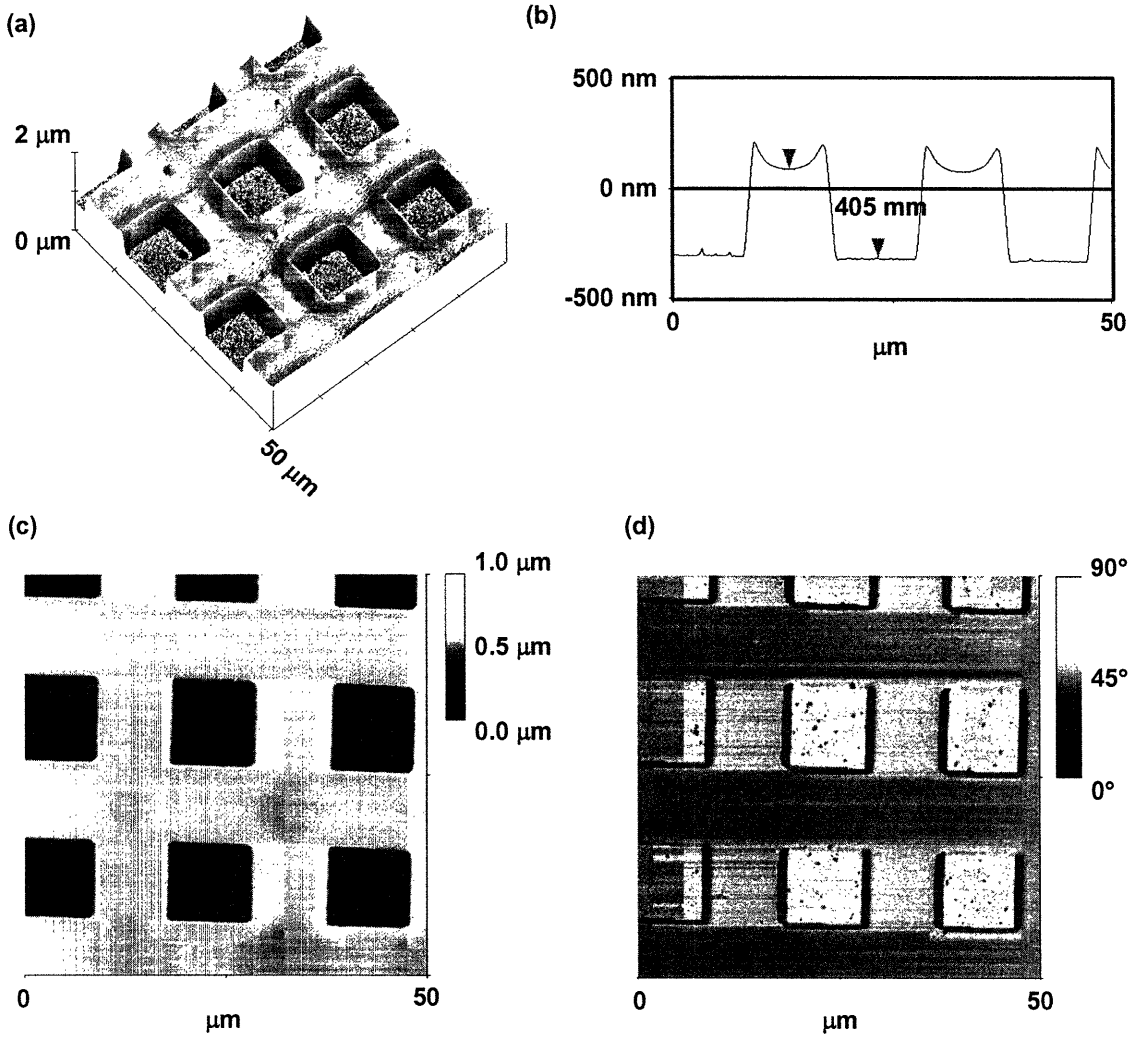

Figure 4.2. AFM images of a molded PEG microstructure with a 10 μm box pattern: (a) three-dimensional presentation, (b) cross-sectional view along the line in (a), (c) two-dimensional height image, and (d) two-dimensional phase image. A sharp contrast in the phase image indicates that the substrate surface is completely exposed. The scan size is $50 \times 50\ \mu m^2$.

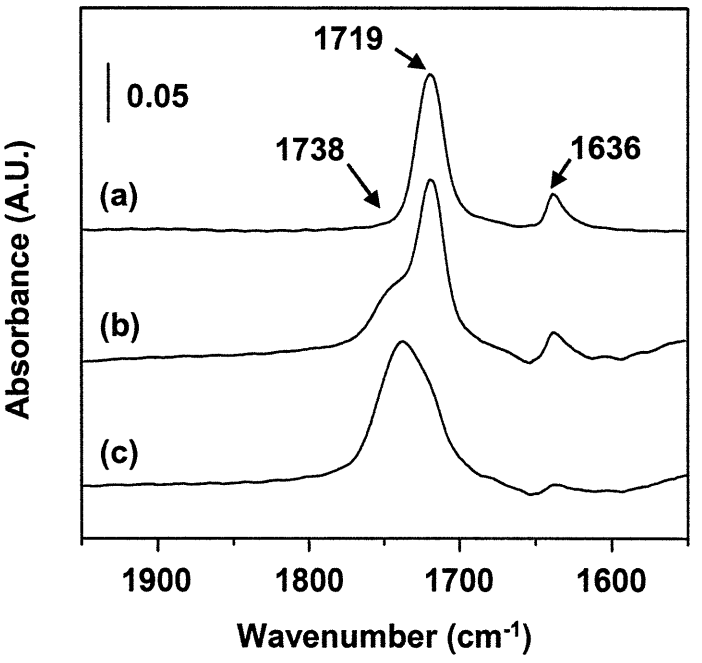

Figure 4.3. FT-IR spectra of a PEG (Mw = 300) film at different UV exposure times: (a) 0 h, (b) 2 h, and (c) 5 h.

To monitor the crosslinking of PEG films, Fourier transform infrared spectroscopy (FT-IR) spectra were obtained at different UV exposure times. The PEG chains are crosslinked by the reaction of the terminal C=C bond of methacrylates. This crosslinking converts the conjugated ester of methacrylates into saturated aliphatic esters. Thus the reaction progress can be monitored from the changes in IR peaks corresponding to the conjugated esters and the saturated aliphatic esters. Figure 4.3 provides the IR results around the ester region. The absorption IR spectrum of PEGDMA before exposure to a UV light features two distinct peaks at 1719 and 1636 cm^{-1}, which correspond to the (C=O)O stretching and the terminal C=C stretching in a methacrylate, respectively (Figure 4.3a). As the patterned PEG films were crosslinked by exposing the surface to UV light for 2 h, the IR spectrum of the PEG film after 2 h of UV exposure was also recorded (Figure 4.3b). After 2 h of polymerization reaction, a new peak arose at 1738 cm^{-1}, which is characteristic of (C=O)O stretching in a

saturated aliphatic ester. In addition, the peaks of the methacrylate (1719 and 1636 cm^{-1}) decreased compared to their initial intensities, indicating the saturation of the terminal C=C in the methacrylate and thus indicating the appearance of the crosslinked PEG chains. The degree of crosslinking after 2 h of the reaction can be calculated to be about 63% from the ratio of the peak intensities around 1636 cm^{-1} in Figure 4.3a and b. After 5 h of the crosslinking reaction, the peak of C=O stretching completely shifted to 1738 cm^{-1} and that of C=C (1636 cm^{-1}) is considerably suppressed, indicating that the film is completely crosslinked.

Despite the presence of 37% of uncrosslinked polymers, the patterned PEG film was stable enough not to be noticeably depleted even after 24 h of immersion in PBS. After being immersed in PBS for 24 h, the patterned PEG hydrogel absorbed a small amount of water and swelled in PBS so that air bubbles were spotted in and on the PEG hydrogel patterns. No bubbles were observed above the bare substrate region. However, the trapped air bubbles are also known to be important in resisting protein and cell adsorption, because the trapped air prevents the surrounding surfaces from contacting the protein solution.[39,40] At lower degrees of crosslinking, *i.e.*, when the PEG patterns were exposed to UV light for less than 1.5 h, the PEG patterns were depleted from the substrate as a result of the swelling stress at the interface of PEGDMA/substrate.

In the present study, PEG microstructures are attached to substrates "non-covalently." To investigate whether "covalent" anchorage of PEG to the substrate would improve the stability of PEG hydrogel microstructures, terminal acrylate groups were introduced onto substrates. The glass and Si/SiO_2 wafers were first cleaned in piranha solution[52] and then silanized by immersing in 3-trichlorosilylpropyl methacrylate solution in toluene for 6 h, followed by rinsing with dichloromethane and drying in a stream of nitrogen. The resulting

surface had terminal acrylate groups, which could be crosslinked with PEGDMA on the surface. However, the stability in water was not noticeably improved by this silanization.

4.3.2. Protein Patterning

The patterns discussed in this study consist of protruding PEG microstructures that have protein- and cell-repelling property and of the exposed glass bottoms that promote adhesion of proteins. To evaluate the ability of these patterned systems to aid selective deposition of proteins, the patterned PEG microstructures were immersed in PBS solutions of FITC-labeled BSA (FITC-BSA) and fibronectin (not FITC-labeled). After exposure to FITC-BSA and fibronectin solutions, the patterned surfaces are then imaged with fluorescence microscopy and optical microscopy, respectively. The protein- and cell-resistant property of PEG is well-known.[53] Hence, FITC-BSA and fibronectin are expected to be deposited only onto the exposed glass surface and not onto the PEG regions.

Figure 4.4a provides a result of an exemplary experiment that visualizes the localized and patterned deposition of proteins by fluorescent tagging. Bright regions denote FITC-BSA deposited onto the exposed glass bottoms of the 10 μm grooves, whereas the dark regions correspond to the protein-repellent PEG walls. The spatially well-resolved fluorescent image indicates that BSA was selectively deposited on the exposed glass surfaces. A well-defined patterned deposition of fibronectin was also observed on patterns of 10 μm boxes (Figure 4.4b). In this optical microscopy picture, bright regions correspond to PEG microstructures and dark regions refer to the exposed glass bottoms where fibronectin was adsorbed. PEG microstructures were formed only on the region in the right side of the vertical wavy boundary line in Figure 4.4b. Thus, the left region denotes the bare glass after exposure to fibronectin. The fact that this left region is also imaged dark indicates that the dark square

boxes in the patterned region denote the fibronectin-deposited bare glass regions, not the PEG patterned regions.

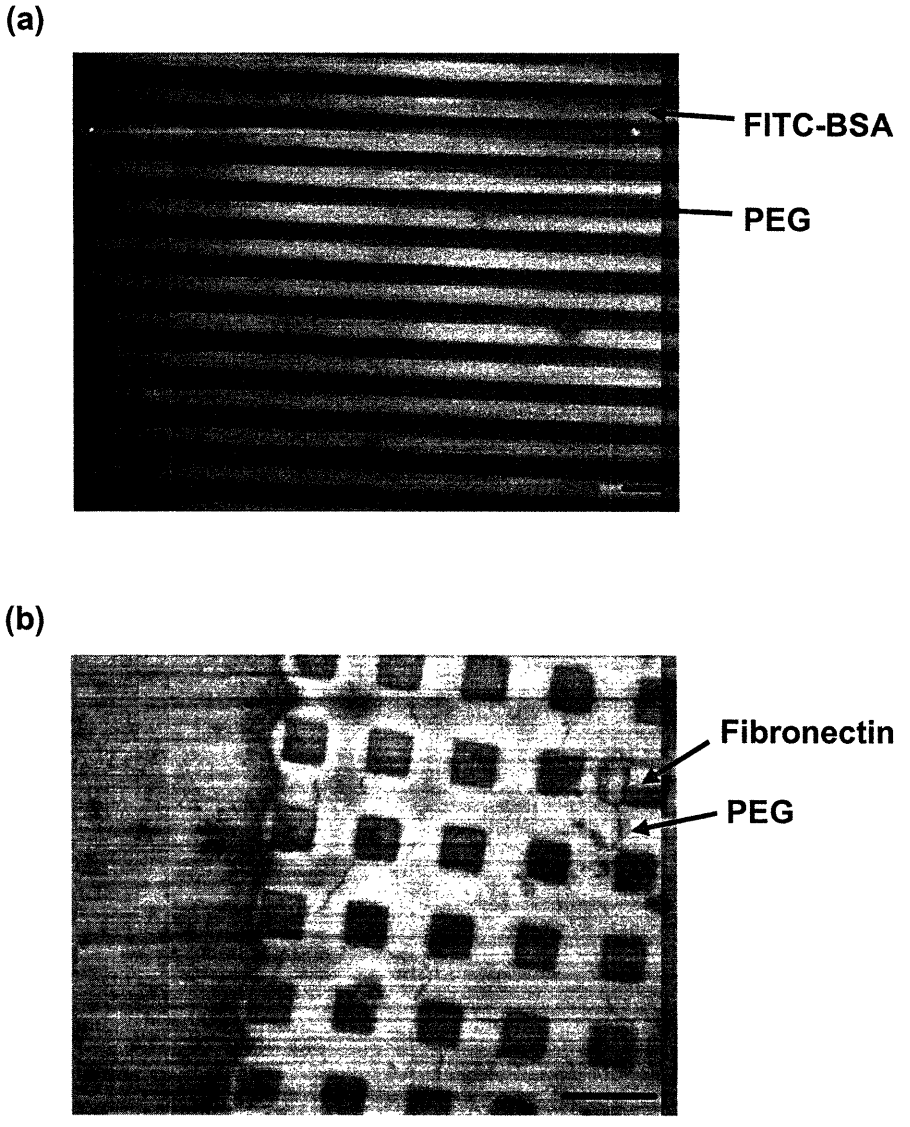

Figure 4.4. (a) A fluorescent micrograph of FITC-BSA that is selectively adsorbed on the 10 μm lines of PEGDMA surface. Sharp contrast is observed. (b) An optical micrograph of fibronectin (not fluorescein labelled) that is selectively adsorbed on the 10 μm boxes of PEGDMA surface. One can observe a drastic difference between the polymer and bare surface with the aid of the boundary line. The scale bars indicate 20 μm.

4.3.3. Cell Patterning

To examine the capability of the patterned PEG surfaces to attach cells selectively, cell culture experiments were performed on the PEG microstructure surfaces. The first step in cell patterning was to adsorb fibronectin onto the patterned surfaces. As an adhesive protein that mediates cell adhesion,[54-56] adsorbed fibronectin surface can aid the selective adhesion of cells by localizing the cells onto the fibronectin-coated regions. Section 4.2.4 verified that fibronectin was deposited only onto bare glass regions and not onto PEG microstructures. Thus, exposing the PEG patterned surfaces to the solution of fibronectin would result in selective localization of fibronectin onto bare glass bottoms and consequently would lead to the selective localization of cells onto bare glass bottoms.

After treating the PEG-patterned surfaces with a solution of fibronectin for 20 min, NIH-3T3 murine embryonic fibroblasts, which were suspended in medium at a concentration of 1×10^6 cells/mL, were seeded onto the surfaces. Fibroblasts are well-known anchorage-dependent mammalian cells that adhere indiscriminately to various substrates and form confluent monolayers. Figure 4.5 shows representative optical microscopy images of fibroblasts on various PEG microstructures after 4 h of cell culture. The cells were patterned across large areas in a well-defined manner. As expected, cells appear to deposit only on the exposed glass or Si/SiO_2 wafers, not on a PEG surface. The fibronectin coating on the underlying substrate regions facilitates the selective adhesion and spreading of cells within the bare glass regions; the PEG microstructures repelled the cells and thus drove cells to the fibronectin coated regions. The figure also shows that the number of cells on the surface can be controlled by varying the size of the barrier. Once the cells are immobilized on the surface, they spread and grow in size. Optical micrographs of fibroblasts plated on 15×75 μm^2 oval-shaped wells are provided in Figure 4.5a and b. The surfaces *inside* the wells are

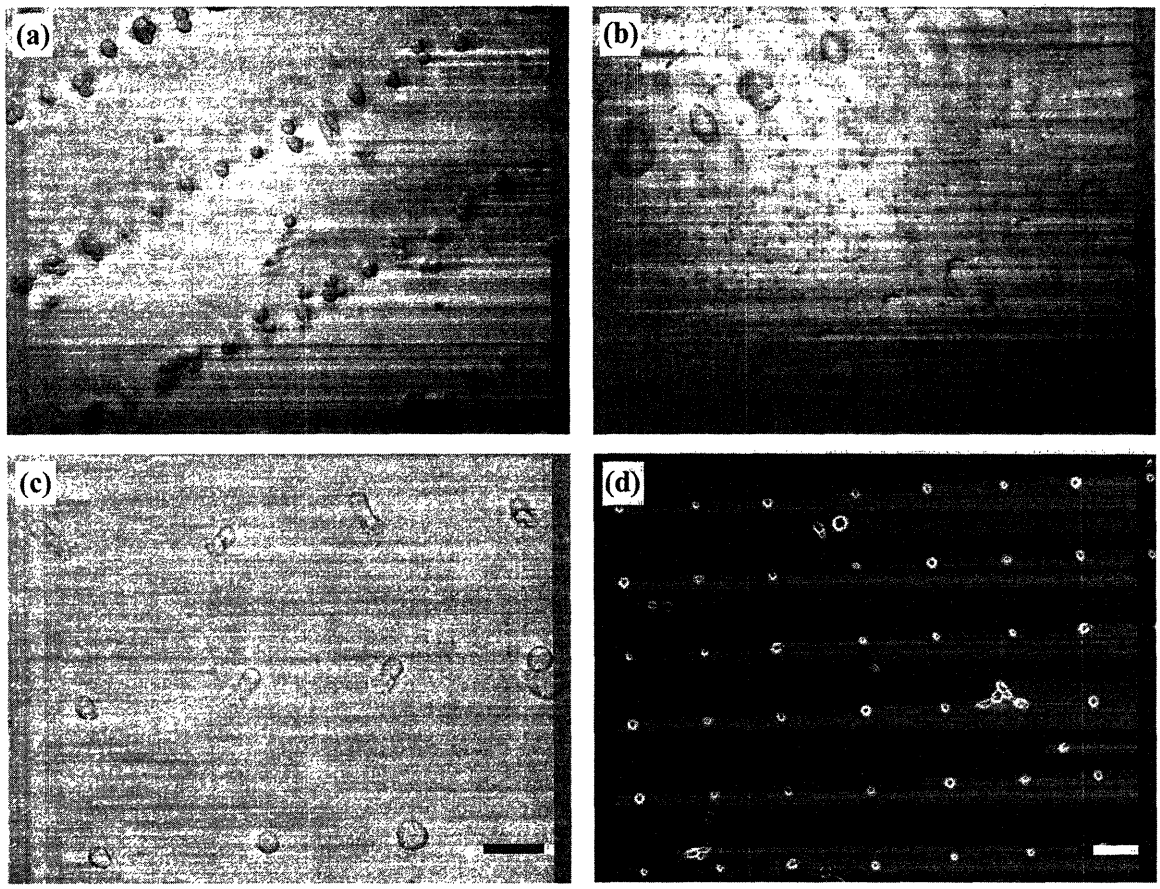

Figure 4.5. Optical micrographs of NIH-3T3 cells deposited on (a) 15 × 75 μm^2 ovals on glass, (b) the same as in (a) (magnified), (c) 25 μm circles on glass, and (d) 25 μm circles on silicon wafer. The PEGDMA barriers confine the cells at numbers strictly controlled by the pattern sizes. The scale bar indicates 50 μm.

comprised of fibronectin-coated glass substrate, and the surfaces *between* the wells are made of PEG microstructures. As Figure 4.5a suggests, each of the oval-shaped wells is occupied by one to three fibroblasts. The surface used in Figure 4.5c and d is composed of exposed glass (Figure 4.5c) or Si/SiO_2 wafer (Figure 4.5d) wells of 25 μm diameter circles and PEG walls surrounding the pattern. On both substrates, each circular well is occupied by only one isolated fibroblast. The initial cell size of NIH-3T3 is estimated to be about 10 μm. Thus, no cells were observed on patterned surfaces whose lateral dimensions are smaller than 10 μm. These results imply that the feature size can determine the number of adhered cells per well.

This may be applied to the fabrication of cell-based arrays for sensors and drug discovery.

Unlike PEG patterns of a few nm thickness such as PEG SAMs, the three-dimensional PEG microstructures confine the cells into fibronectin-coated bare substrate regions not only by the inertness of PEG molecules but also by acting as a physical barrier. A comparison of patterned fibroblast arrays on PEG patterns of monolayers and of microstructures revealed that cell patterns using PEG microstructures stayed stable for longer than 4 d whereas cell patterns from PEG monolayers started to form interconnected structures in 4 d.[57] Although a PDMS membrane has been previously used for physical confinement,[39,40] its application is limited in that the pattern sizes were typically on the order of a hundred micrometers and PDMS is not an inert material for cell adhesion. In this respect, it would be intriguing to examine the spreading behavior of individual cells in the presence of narrow and high aspect-ratio PEG walls, which could provide valuable information on cell culture in a confined, non-sticky geometry.

4.4. Conclusion

Capillary force lithography (CFL) was employed as a technique for general-purpose lithography for protein and cell patterning. By introducing PEGDMA as the patterned polymer, spatially well-resolved images of selective protein and cell attachment were obtained on a large area. This may open new pathways for fabricating protein chips and high-throughput cell screening devices. The number of cells in a given PEG barrier could be manipulated by varying the feature sizes. As the demand for precise control of cell positioning and functioning is increasing for applications ranging from cellular to tissue engineering and biosensors,[26,58] the technique discussed in this chapter could be increasingly useful for such purposes.

4.5. References and Notes for Chapter 4

* This work was done in collaboration with Dr. Kahpyang Suh, Chemical Engineering, MIT.

(1) Chen, C. S.; Mrksich, M.; Huang, S.; Whitesides, G. M.; Ingber, D. E. Geometric control of cell life and death. *Science* **1997**, *276*.

(2) Chen, C. S.; Mrksich, M.; Huang, S.; Whitesides, G. M.; Ingber, D. E. Micropatterned surfaces for control of cell shape, position, and function. *Biotechnol. Prog.* **1998**, *14*, 356-363.

(3) Folch, A.; Toner, M. Microengineering of cellular interactions. *Annu. Rev. Biomed. Eng.* **2000**, *02*, 227-256.

(4) Ito, Y. Surface micropatterning to regulate cell functions. *Biomaterials* **1999**, *20*, 2333-2342.

(5) Singhvi, R.; Kumar, A.; Lopez, G. P.; Stephanopoulos, G. N.; I., W. D.; Whitesides, G. M.; Ingber, D. E. Engineering cell shape and function. *Science* **1994**, *264*.

(6) Mrksich, M.; Whitesides, G. M. Patterning self-assembled monolayers using microcontact printing: A new technology for biosensors. *Trends. Biotechnol.* **1995**, *13*, 228-235.

(7) Colyer, C. L.; Tang, T.; Chiem, N.; Harrison, D. J. Clinical potential of microchip capillary electrophoresis systems. *Electrophoresis* **1997**, *18*, 1733-1741.

(8) You, A. J.; Jackman, R. J.; Whitesides, G. M.; Schreiber, S. L. A miniaturized arrayed assay format for detecting small molecule-protein interactions in cells. *Chem. Biol.* **1997**, *4*, 969-975.

(9) Ng, J. H.; Ilag, L. L. Biomedical applications of protein chips. *J. Cell. Mol. Med.* **2002**, *6*, 329-340.

(10) Figeys, D. Adapting arrays and lab-on-a-chip technology for proteomics. *Proteomics* **2002**, *2*, 373-382.

(11) Patel, N.; Padera, S.; Giles, H. W.; Cannizzaro, S. M.; Davies, M. C.; Langer, R.; Roberts, C. J.; Tendler, S. J. B.; Williams, P. M.; Shakesheff, K. M. Spatially controlled cell engineering on biodegradable polymer surfaces. *FASEB J.* **1998**, *12*, 1447-1454.

(12) Jeong, H. J.; Markle, D. A.; Owen, G.; Pease, F.; Grenville, A.; von Bünau, R. The future of optical lithography. *Solid State Technol.* **1994**, *37*, 39-47.

(13) Okazaki, S. Resolution limits of optical lithography. *J. Vac. Sci. Technol., B* **1991**, *9*, 2829-2833.

(14) Kleinfeld, D.; Kahler, K. H.; Hockberger, P. E. Controlled outgrowth of dissociated neurons on patterned substrates. *J. Neurosci.* **1988**, *8*, 4098-4120.

(15) Matsuda, T.; Sugawara, T. Development of surface photochemical modification method for micropatterning of cultured cells. *J. Biomed. Mater. Res.* **1995**, *29*, 749-756.

(16) Sorribas, H.; Padeste, C.; Tiefenauer, L. Photolithographic generation of protein micropatterns for neuron culture applications. *Biomaterials* **2002**, *23*, 893-900.

(17) Xia, Y.; Whitesides, G. M. Soft lithography. *Angew. Chem., Int. Ed.* **1998**, *37*, 550-575.

(18) Koh, W.-G.; Itle, L. J.; Pishko, M. V. Molding of hydrogel microstructures to create multiphenotype cell microarrays. *Anal. Chem.* **2003**, *75*, 5783-5789.

(19) Revzin, A.; Russell, R. J.; Yadavalli, V. K.; Koh, W. G.; Deister, C.; Hile, D. D.; Mellott, M. B.; Pishko, M. V. Fabrication of poly(ethylene glycol) hydrogel microstructures using photolithography. *Langmuir* **2001**, *17*.

(20) Lesho, M. J.; Sheppard, N. F. Adhesion of polymer films to oxidized silicon and its effect on performance of a conductometric ph sensor. *Sens. Actuators, B* **1996**, *37*, 61-66.

(21) Beebe, D. J.; Moore, J. S.; Bauer, J. M.; Yu, Q.; Liu, R. H.; Devadoss, C.; Jo, B. H. Functional hydrogel structures for autonomous flow control inside microfluidic channels. *Nature* **2000**, *404*.

(22) Bernard, A.; Renault, J. P.; Michel, B.; Bosshard, H. R.; Delamarche, E. Microcontact printing of proteins. *Adv. Mater.* **2000**, *12*, 1067-1070.

(23) Bernard, A.; Delamarche, E.; Schmid, H.; Michel, B.; Bosshard, H. R.; Biebuyck, H. Printing patterns of proteins. *Langmuir* **1998**, *14*, 2225-2229.

(24) James, C. D.; Davis, R. C.; Kam, L.; Craighead, H. G.; Isaacson, M.; Turner, J. N.; Shain, W. Patterned protein layers on solid substrates by thin stamp microcontact printing. *Langmuir* **1998**, *14*, 741-744.

(25) Mrksich, M.; Chen, C. S.; Xia, Y.; Dike, L. E.; Ingber, D. E. Controlling cell attachment on contoured surfaces with self-assembled monolayers of alkanethiolates on gold. *Proc. Natl. Acad. Sci.* **1996**, *93*.

(26) Craighead, H. G.; James, C. D.; Turner, A. M. P. Chemical and topographical patterning for directed cell attachment. *Curr. Opin. Solid. St. M.* **2001**, *5*, 177-184.

(27) Tan, J. L.; Tien, J.; Chen, C. S. Microcontact printing of proteins on mixed self-assembled monolayers. *Langmuir* **2002**, *18*, 519-523.

(28) Kane, R. S.; Takayama, S.; Ostuni, E.; Ingber, D. E.; Whitesides, G. M. Patterning proteins and cells using soft lithography. *Biomaterials* **1999**, *20*, 2363-2376.

(29) Lahann, J.; Choi, I. S.; Lee, J.; Jenson, K. F.; Langer, R. A new method toward microengineered surfaces based on reactive coating. *Angew. Chem., Int. Ed.* **2001**, *40*.

(30) Branch, D. W.; Corey, J. M.; Weyhenmeyer, J. A.; Brewer, G. J.; Wheeler, B. C. Microstamp patterns of biomolecules for high-resolution neuronal networks. *Med. Biol. Eng. Comput.* **1998**, *36*, 135-141.

(31) Wheeler, B. C.; Corey, J. M.; Brewer, G. J.; Branch, D. W. Microcontact printing for precise control of nerve cell growth in culture. *J. Biomech. Eng.-T. ASME.* **1999**, *121*, 73-78.

(32) Wang, Y. C.; Ferrari, M. Surface modification of micromachined silicon filters. *J. Mater. Sci.* **2000**, *35*, 4923-4930.

(33) Harris, J. M.; Zalipsky, S. *Poly(ethylene glycol): Chemisry and biological applications*; Am. Chem. Soc.: Washington D.C., **1997**.

(34) Takayama, S.; Ostuni, E.; Qian, X. P.; McDonald, J. C.; Jiang, X. Y.; LeDuc, P.; Wu, M.

H.; Ingber, D. E.; Whitesides, G. M. Topographical micropatterning of poly(dimethylsiloxane) using laminar flows of liquids in capillaries. *Adv. Mater.* **2001**, *13*.

(35) Papra, A.; Bernard, A.; Juncker, D.; Larsen, N. B.; Michel, B.; Delamarche, E. Microfluidic networks made of poly(dimethylsiloxane), Si, and Au coated with polyethylene glycol for patterning proteins onto surfaces. *Langmuir* **2001**, *17*, 4090-4095.

(36) Ng, J. M. K.; Gitlin, I.; Stroock, A. D.; Whitesides, G. M. Components for integrated poly(dimethylsiloxane) microfluidic systems. *Electrophoresis* **2002**, *23*, 3461-3473.

(37) Chiu, D. T.; Jeon, N. L.; Huang, S.; Kane, R. S.; Wargo, C. J.; Choi, I. S.; Ingber, D. E.; Whitesides, G. M. Patterned deposition of cells and proteins onto surfaces by using three-dimensional microfluidic systems. *Proc. Natl. Acad. Sci.* **2000**, *97*.

(38) Kim, E.; Xia, Y. N.; Whitesides, G. M. Polymer microstructures formed by molding in capillaries. *Nature* **1995**, *376*, 581-584.

(39) Ostuni, E.; Chen, C. S.; Ingber, D. E.; Whitesides, G. M. Selective deposition of proteins and cells in arrays of microwells. *Langmuir* **2001**, *17*, 2828-2834.

(40) Ostuni, E.; Kane, R.; Chen, C. S.; Ingber, D. E.; Whitesides, G. M. Patterning mammalian cells using elastomeric membranes. *Langmuir* **2000**, *16*, 7811-7819.

(41) Kumar, G.; Wang, Y. C.; Co, C.; Ho, C.-C. Spatially controlled cell engineering on biomaterials using polyelectrolytes. *Langmuir* **2003**, *19*, 10550-10556.

(42) Yamato, M.; Konno, C.; Utsumi, M.; Kikuchi, A.; Okano, T. Thermally responsive polymer-grafted surfaces facilitate patterned cell seeding and co-culture. *Biomaterials* **2002**, *23*, 561-567.

(43) Rowan, B.; Wheeler, M. A.; Crooks, R. M. Patterning bacteria within hyperbranched polymer film templates. *Langmuir* **2002**, *19*, 9914-9917.

(44) Hyun, J.; Ma, H.; Zhang, Z.; Beebe, T. P.; Chilkoti, A. Universal route to cell micropatterning using an amphiphilic comb polymer. *Adv. Mater.* **2003**, *15*, 576-579.

(45) Ghosh, P.; Amirpour, M. L.; Lackowski, W. M.; Pishko, M. V.; Crooks, R. M. A simple lithographic approach for preparing patterned, micron-scale corrals for controlling cell growth. *Angew. Chem., Int. Ed.* **1999**, *38*, 1592-1595.

(46) Suh, K. Y.; Kim, Y. S.; Lee, H. H. Capillary force lithography. *Adv. Mater.* **2001**, *13*, 1386-1389.

(47) Kim, Y. S.; Suh, K. Y.; Lee, H. H. Fabrication of three-dimensional microstructures by soft molding. *Appl. Phys. Lett.* **2001**, *79*, 2285-2287.

(48) Suh, K. Y.; Lee, H. H. Capillary force lithography: Large-area patterning, self-organization, and anisotropic dewetting. *Adv. Funct. Mater.* **2002**, *12*, 405-413.

(49) Suh, K. Y.; Park, J.; Lee, H. H. Controlled polymer dewetting by physical confinement. *J. Chem. Phys.* **2002**, *116*, 7714-7718.

(50) Kim, Y. S.; Lee, H. H.; Hammond, P. T. High density nanostructure transfer in soft molding using polyurethane acrylate molds and polyelectrolyte multilayers. *Nanotechnology* **2003**, *14*, 1140-1144.

(51) Suh, K. Y.; Langer, R. Microstructures of poly(ethylene glycol) by molding and dewetting. *Appl. Phys. Lett.* **2003**, *83*, 1668-1670.

(52) Cleaning by piranha solution was detailed in 2.2 in chapter 2.

(53) Whitesides, G. M.; Ostuni, E.; Takayama, S.; Jiang, X.; Ingber, D. E. Soft lithography in biology and biochemistry. *Annu. Rev. Biomed. Eng.* **2001**, *3*, 335-373.

(54) Akiyama, S. K.; Yamada, K. M. The interaction of plasma fibronectin with fibroblastic cells in suspension. *J. Biol. Chem.* **1985**, *2690*, 4492-4500.

(55) Maciag, T.; Kadish, J.; Wilkins, L.; Stemerman, M. B.; Weinstein, R. Organizational-behavior of human umbilical vein endothelial cells. *J. Cell Biol.* **1994**, *94*, 511-520.

(56) Tidwell, C. D.; Ertel, S. I.; Ratner, B. D.; Tarasevich, B. J.; Atre, S.; Allara, D. L. Endothelial cell growth and protein adsorption on terminally functionalized, self-assembled monolayers of alkanethiolates on gold. *Langmuir* **1997**, *13*, 3404-3413.

(57) Khademhosseini, A.; Jon, S.; Suh, K. Y.; Tran, T.-N. T.; Eng, G.; Yeh, J.; Seong, J.; Langer, R. Direct patterning of protein and cell resistant polymeric based self-assembled monolayers and microstrutures. *Adv. Mater.* **in press**.

(58) Chovan, T.; Guttman, A. Microfabricated devices in biotechnology and biochemical processing. *Trends. Biotechnol.* **2002**, *20*, 116-122.

Chapter 5. Preparation and Modification of Tri(Ethylene Glycol)-Terminated Self-Assembled Monolayers Exposing Hydroxyl Groups

5.1. Introduction

Bioanalytical or biomedical devices made of immobilized protein arrays (biochips) offer an attractive experimental alternative to traditional devices that have biological components in solution phase. The major advantages of biochips include the possibility of miniaturization and parallel operation, to name a few. In such solid-state devices that interface with biological species, the sensitivity and specificity of such devices are greatly affected by the way that biological species, such as proteins, are immobilized onto the devices substrates. For solid-state systems that incorporate such species as receptors or other active elements, the structural integrity of these species is often greatly affected by their local interactions with the underlying surfaces, where effects that cause nonspecific adsorption can alter their activity and binding abilities through structural changes effected by the surface. Hence the performance of such devices can be improved by promoting the specific molecular interactions and simultaneously suppressing nonspecific adsorption events. However, the ability to provide the required biocompatibility (*i.e.*, "*inertness*") to a surface for avoidance of unwanted non-specific adsorption while including sites for immobilization (*i.e.*, "*reactivity*") can be opposing requirements for a surface.

A demonstrated strategy for achieving this goal is the use of self-assembled monolayers (SAMs) that express oligo(ethylene glycol) (oEG) groups at their surfaces. Prime and Whitesides demonstrated that SAMS formed from the assembly of oligo(ethylene glycol)-terminated (oEG-terminated) alkanethiols, $HS(CH_2)_{11}(OCH_2CH_2)_mOR$ (m = 3~7, R = CH_3 or H) onto gold formed densely-packed monolayers that presented the ethylene glycol (EG)

units on surfaces[1] and were resistant against the nonspecific adsorption of many proteins. Mixed monolayers of oEG-terminated and unsubstituted alkanethiols on gold showed that thiols with longer sequences of the oEG were more effective at resisting protein adsorption at lower surface compositions.[2,3] Another study of mixed SAMs of oEG-functionalized alkanethiols with hydrophobic terminus and OH terminus suggested that protein adsorption depended on the density of hydrophobic groups at the surface and on the concentration of protein.[4]

The protein resistance of oEG SAMs depended on the molecular conformation of oEG moieties, as helical and amorphous conformations provided protein resistance to the SAMs, whereas an all-trans conformation for the oEG terminus (as found with SAMs on silver when m = 3 and R = CH_3) caused protein adsorption.[5,6] These differences in behavior were attributed to a stronger interaction between the oEG layer and water in the former conformations than in the all-trans state. These issues have been the subject of a variety of computational[6-8] and experimental[9,10] studies.

The basic structure of these films - an underlying alkyl region that provides dense packing within the SAM and an outer region that provides an oEG surface - has served as a foundation for incorporating reactive agents on this inert background matrix. For example, mixed SAMs incorporating a biotin cap on the oEG terminus within either an oEG-terminated alkanethiol or a simple unsubstituted alkanethiol have been used for immobilizing streptavidin onto gold.[8,11,12] oEG-terminated alkanethiols ($HS(CH_2)_n(EG)_mX$) that include an amino group,[13] a carboxylic acid,[14,15] or an maleimide[16] have provided surfaces for coupling proteins to be gold surfaces.

The specificity of the gold surface for the thiol functionality and the chemical compatibility of the thiol group with various functionalities has allowed the facile

introduction of these and other reactive groups within oEG containing SAMs on this surface. For other substrates (for example, metal oxides), different reaction chemistries are required for the preparation of SAMs, often placing limits on the chemical functionalities that can be included in an adsorbate. A particular case is the use of organotrichlorosilanes for modifying glass and other metal oxides where the head group employed for surface attachment (*i.e.*, $SiCl_3$) is chemically incompatible with a variety of species, thereby placing restrictions on the functional groups that may be present in the adsorbate. This limiting feature in composition is countered by enhancements in film stability. For example, thiol-based SAMs on gold readily desorb at elevated temperatures and undergo a destabilizing oxidative degradation that limits their use.[17-20] In contrast, SAMs on glass and other metal oxides formed from organotrichlorosilanes are covalent bonded to the support and are stable at much higher temperatures, through procedures such as autoclaving and sonication, and show long-term stabilities in air.[21]

The preparation of oEG-terminated SAMs on glass and Si/SiO_2 substrates was detailed elsewhere.[22] These SAMs were formed by the adsorption of oEG-terminated alkyltrichlorosilanes ($CH_3O(CH_2CH_2O)_3(CH_2)_{11}SiCl_3$; EG_3OMe silane) that included a methoxy cap on the oEG group for compatibility with the trichlorosilane moiety. As these SAMs contained three EG units, it will be denoted as EG_3 instead of oEG throughout this chapter and the next chapter. The resulting films were ~2-3 nm in thickness, expressed a densely packed methoxy-capped EG_3 surface, and provided a dramatic retardation in the non-specific adsorption of various proteins. Further, these films retained their protein-resistant properties through immersion in boiling water, contact with a hydrocarbon solvent at 90 °C for 1 h, and heating in an oven at 120 °C each for 1 h. These adsorbates provided a convenient approach for generating robust films on glass that retarded protein adsorption.

However, they lacked an ability to allow further modification as the subsequent attachment of receptor agents or biological species onto this matrix.

The objective of this work is to improve the EG_3-coated SiO_2 surface by advancing from a merely protein-resistant surface (EG_3OMe SAM) to a building block surface that imparts reactive sites (hydroxy-capped EG_3 surface; EG_3OH SAM), and allows receptor biomolecules to be specifically and stably assembled onto a surface whose resistance to nonspecific protein deposition is equivalent to or better than that of the EG_3OMe SAM. We report the generation of SAMs on SiO_2 surfaces that provide the following: (1) a terminal -OH group that allows possible subsequent on-surface modification, (2) a tri(ethylene glycol) surface that provides non-fouling characteristics, and (3) an underlying alkyl domain that aids in dense packing within the film. This chapter details the preparation, protein resistance, and characteristics of this film and its use as a support for immobilizing a binding protein and an immunoglobulin.

5.2. Experimental Section

5.2.1. Materials

11-Bromo-1-undecene (99 %) was obtained from Pfaltz & Bauer. Potassium hydroxide, sulfuric acid, 35% $H_2O_2(aq)$ were from Mallinckrodt. Lysozyme (EC 2326204), fibrinogen (EC 2325986), hexokinase (EC 2326115), insulin (EC 2342912), and protein A were from Sigma. Goat anti-rabbit immunoglobulin G (IgG) was obtained from Pierce. $LiAlH_4$ was obtained as a 1.0 M stock solution in anhydrous ether (Aldrich). All other materials were obtained from Aldrich. Gold substrates were prepared by the sequential thermal evaporation of 50 Å of Cr and 1500 Å of Au onto Si(100) (North East Silicon Technologies, Inc.; New Bedford, MA) in a vacuum chamber operating at ~10^{-6} Torr.

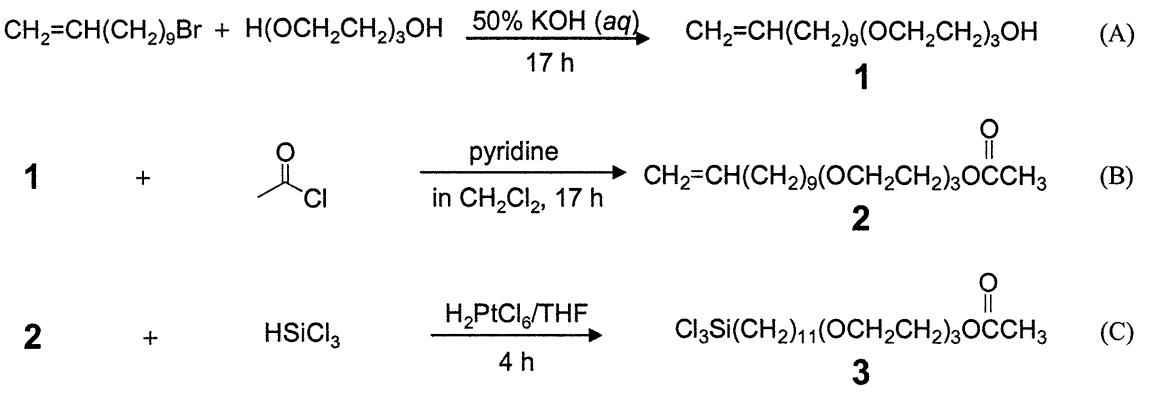

Scheme 5.1. Synthesis of acetyl[(1-trichlorosilyl)undec-11-yl]tri(ethylene glycol).

The adsorbate employed for formation of the EG_3OH SAM was prepared by the three-step synthesis shown in Scheme 5.1. **(A)** 11.0 mmol of KOH in 50 wt% aqueous solution was stirred with 51.5 mmol tri(ethylene glycol) for 30 min at 100 °C under a flow of N_2, and then 8.58 mmol of 11-bromoundec-1-ene was added. After 17 h of reaction, the mixture was extracted six times with hexane, and the collected extracts were concentrated using a rotary evaporator. The purified product of **1** was obtained by chromatography (eluent: ethyl acetate) as a colorless oil in an isolated yield of ~70%. **(B)** 6.6 mmol of **1** and 9.9 mmol of pyridine were mixed for 30 min under N_2, and were cooled to 0 °C in an ice bath. 13.2 mL of a 0.5 M solution of acetyl chloride in CH_2Cl_2 were added dropwise to the mixture at 0 °C. After stirring for 17 h at room temperature, the mixture was rinsed sequentially with double-distilled water, 1.0 M HCl (*aq*), saturated $NaHCO_3$ (*aq*), and 5 M NaCl (*aq*), followed by concentration using a rotary evaporator. Additional material was obtained by back extraction of the aqueous rinses with hexane and their concentration using a rotary evaporator. The combined concentrates were purified by column chromatography using ethyl acetate as eluent and gave product **2** as a colorless oil in 75 % yield. **(C)** 0.05 g of 0.12 M H_2PtCl_6 in dry tetrahydrofuran (THF) was mixed with 5.8 mmol of **2** and trichlorosilane ($HSiCl_3$) 17.4

mmol in a N_2 glove box and then stirred for 4 h. The final product (**3**), EG_3OAc, was obtained as a colorless oil in >95% yield by vacuum distillation at 260 °C. ^{1}H-NMR (400 MHz, $CDCl_3$): δ 1.2-1.5 (*m*, 16 H), 1.55 (*m*, 4 H), 2.06 (*s*, 3 H), 3.43 (*t*, 2 H), 3.5-3.75 (*m*, 14 H), 4.20 (*t*, 2 H).

5.2.2. Formation of Self-Assembled Monolayers on SiO_2

Preparation of acetate-terminated siloxane monolayers from $Cl_3Si(CH_2)_{11}EG_3OAc$. Si wafers were cleaned by immersion in 'piranha' solution (7/3 v/v mixture of conc. H_2SO_4 and 30 % aqueous H_2O_2) for 1 h at 80 °C. (CAUTION: 'Piranha' solution reacts violently with many organic materials and should be handled with care.) The substrates were rinsed with deionized 7water, dried in a stream of N_2, and cut into 1 × 3 cm^2 slides. Optical constants were measured on the bare slides using ellipsometry, and the values for a particular slide were used for calculating the thicknesses of SAMs and protein layers formed on its surface. The clean substrates were then immersed in ~5 mM solutions of **3** in anhydrous toluene for various reaction conditions to establish synthetic parameters, with reactions in 2 mM anhydrous toluene for 48 h being a preferred route. Derivatized substrates were rinsed sequentially with dichloromethane and acetone, and blown dry in a stream of N_2 prior to characterization and use. In this chapter the following chapters, we refer to these films by their tail group (for example, an EG_3OAc SAM) for simplicity. For experiments employing attenuated total reflection infrared spectroscopy (ATR-IR), silicon trapezoidal plates were cleaned using the same method and were derivatized by immersion in 5 mM solutions of **3** in anhydrous toluene at room temperature for one day and then at 60 °C for another day.

Formation of hydroxyl-terminated monolayers (EG_3OH layers) from EG_3OAc SAM. Si wafers and Si ATR plates derivatized with **3** were immersed into 0.1 and 1.0 M $LiAlH_4$

solutions in dry ether for various reaction times in order to determine optimal conditions for reducing the terminal acetate to a hydroxyl group. Reacted slides were rinsed sequentially with 10 mM HCl (*aq*), deionized water, and acetone, and dried in a stream of N_2 before characterization and further use. The preferred condition was an exposure to 1.0 M $LiAlH_4$ in anhydrous ether for 5 min.

Preparation of hydroxyl standard on gold substrate. Gold substrates were rinsed with acetone, dried under N_2, and then immersed into 2 mM solutions of $HS(CH_2)_{11}OH$ in ethanol for 24 h at room temperature to produce hydroxyl-terminated SAMs. These films provided a reference standard exposing 4.61×10^{14} hydroxyl groups/cm^2.

5.2.3. Surface Characterization

Ellipsometry. The thicknesses of the monolayer films and of adsorbed protein layers were measured with a Gaertner L116A ellipsometer (Gaertner Scientific Corporation, IL) at a 70° angle of incidence. A refraction index of 1.46 was used for all films, and a three-phase model was used to calculate thicknesses.

Contact angle measurements. A Ramé-Hart goniometer (Mountain Lakes, NJ) equipped with video camera and monitor was used to measure contact angles in both the advancing and receding modes (~1 μL/s) on drops of ~3 μL in volume. Reported values represent averages of at least three independent measurements.

X-ray photoelectron spectroscopy (XPS). XPS measurements were performed on a Surface Science Instrument Model X-100 using a monochromatic Al Kα x-ray source and a concentric hemispherical analyzer. The take-off angle for the detector was 35° from the surface plane. Spectra were fit with 100 % Gaussian peaks and a linear baseline.

Fourier Transform – Infrared/ Attenuated Total Reflection Spectroscopy (FT-IR/ATR). FT-IR/ATR spectra were collected on a Digilab FTS 175 spectrometer (Bio-Rad, Cambridge, MA) with a narrow-band MCT detector. Trapezoidal Si(100) and Si(111) ATR plates of 50 mm × 10 mm × 2 mm thickness (Harrick Scientific, Ossining, NY) were used. The spectral resolution was 1 cm^{-1} and 512 or 1024 scans were collected for each spectrum. Reference spectra were obtained from silicon ATR plates cleaned in piranha solution.

5.2.4. Protein Adsorption on Tri(ethylene glycol)-Modified Surfaces

The examined proteins were each dissolved at a concentration of 0.25 mg/mL in 10 mM phosphate buffer saline (PBS) solution (pH = 7.4). The PBS solution was prepared by dissolving a Phosphate Buffered Saline Tablet (Sigma) in 200 mL of deionized water to obtain a solution that contained 10 mM sodium phosphate buffer, 2.7 mM KCl, and 137 mM NaCl. Substrates were immersed in the protein solution for 24 h, washed sequentially with PBS solution and water, and blown dry in a stream of N_2.

5.2.5. Reactions on $Si/SiO_2/EG_3OH$ Monolayer

Reaction with trifluoroacetic anhydride (TFAA). EG_3OH surfaces were placed into a 2% (v/v) TFAA solution in hexane for 2 min under N_2, rinsed with hexane, and blown dry with N_2. This process produced trifluoroacetate-terminated EG_3 surfaces ($Si/SiO_2/O_{3/2}Si(CH_2)_{11}EG_3O(C{=}O)CF_3$). For comparison, SAMs of $HS(CH_2)_{11}OH$ on gold were similarly reacted with TFAA for conversion to $Au/S(CH_2)_{11}O(C{=}O)CF_3$. The surface density of reactive -OH groups on the EG_3OH SAM was determined by comparing F(1s) intensities in XPS to that from a $Au/S(CH_2)_{11}OH$ monolayer that was similarly modified with TFAA.

Immobilization of biomolecules. Scheme 5.2 illustrates the reaction steps for attaching protein A to the surface using 1,1-carbonyl diimidazole (CDI) as a crosslinker. The substrates presenting EG_3OH surfaces were washed well with anhydrous CH_2Cl_2, dried under N_2, and kept at 130 °C in a convection oven for 1 h. They were immersed in 0.5 M CDI in anhydrous acetonitrile (ACN) at room temperature for 1.5 h, followed by rinses with anhydrous ACN and 0.1 % HCl (*aq*). The CDI-coated surfaces were then contacted with a 0.5 mg/mL solution of protein A in a carbonate buffer (pH 9.0) at 4 °C for 24 h. After rinsing the surface with PBS, the samples were stored in PBS solution at 4 °C until use. The activity of the resulting protein A surfaces were examined by contacting the surface with 0.25 and 0.75 mg/mL solutions of Goat anti-rabbit IgG in PBS for 30 min and measuring the nitrogen signals from the sample by XPS.

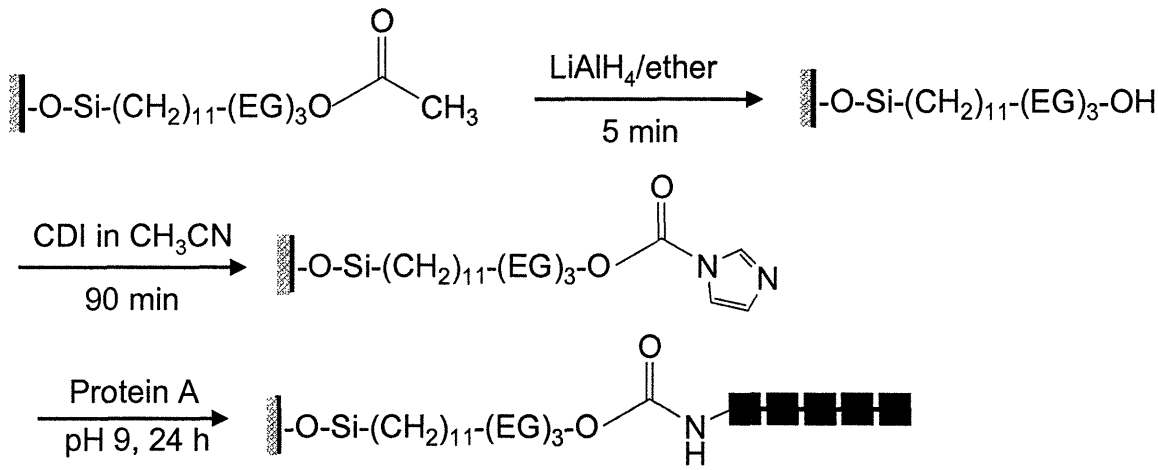

Scheme 5.2. Attachment of protein A to EG_3OH monolayer. CDI = 1,1-carbonyl diimidazole.

5.3. Results and Discussion

5.3.1. Formation and Characterization of $Si/SiO_2/O_{3/2}Si(CH_2)_{11}(OCH_2CH_2)_3OH$ Monolayer

Synthesis of $Cl_3Si(CH_2)_{11}EG_3OAc$. Our goal was to prepare a densely packed monolayer on a Si/SiO_2 surface that would expose a hydroxyl-terminated oEG functionality. In order to provide compatibility between the targeted OH terminus and the $SiCl_3$ head group used for surface attachment, we masked the hydroxyl as an acetate that could be cleaved after film formation. Scheme 1 shows the three-step synthesis used for the preparation of acetyl[(1-trichlorosilyl)undec-11-yl]tri(ethylene glycol) (**3**; EG_3OAc); the individual steps are based on previously reported procedures.[1,23,24] In the first step, the reaction of 11-bromoundec-1-ene, a five-fold excess of triethylene glycol, and KOH produced undec-1-en-11-yltri(ethylene glycol) (**1**) in ~70 % yield. The hydroxyl group (-OH) of **1** was protected by conversion into an acetate ($-OC(=O)CH_3$) (**2**) using acetyl chloride. Lastly, silanization of **2** using $HSiCl_3$ and H_2PtCl_6 as catalyst gave **3** in roughly quantitative yield. The final compound was stored in a N_2 glove box to avoid the effects that water might have to degrade and possibly polymerize the compound. Satisfactory results such as those presented here were obtained using freshly distilled samples of **3** and samples stored for up to a year in the glove box.

Formation of SAMs from 3. Figure 5.1 shows the ellipsometric thicknesses of monolayers formed by the self-assembly of $Cl_3Si(CH_2)_{11}(OCH_2CH_2)_3OC(=O)CH_3$ onto Si/SiO_2 surfaces as a function of reaction time. The EG_3OAc films were formed from solutions of **3** in anhydrous toluene, and the figure shows data obtained at 25 and 60 °C using concentrations ranging from 3 to 6 mM. We observed little effect on thickness over this concentration range while changes in temperature provided a greater difference, with thicker

EG_3OAc layers forming on the SiO_2 surface at the higher temperature. For example, it took ~40 h for the adsorption process to achieve a final thickness at 25 °C, while it took only 7 h at 60 °C. At 25 °C, the kinetics for the EG_3OAc SAM are slower than those reported for simple *n*-alkyltrichlorosilanes such as $C_{18}H_{37}SiCl_3$ where full coverages are obtained in 6 h from 0.25 mM solutions in heptane.[25] The seemingly slow formation of EG_3OAc films may be a result of a lesser interaction between EG units than between alkyl chains and provide a smaller driving force for assembly.

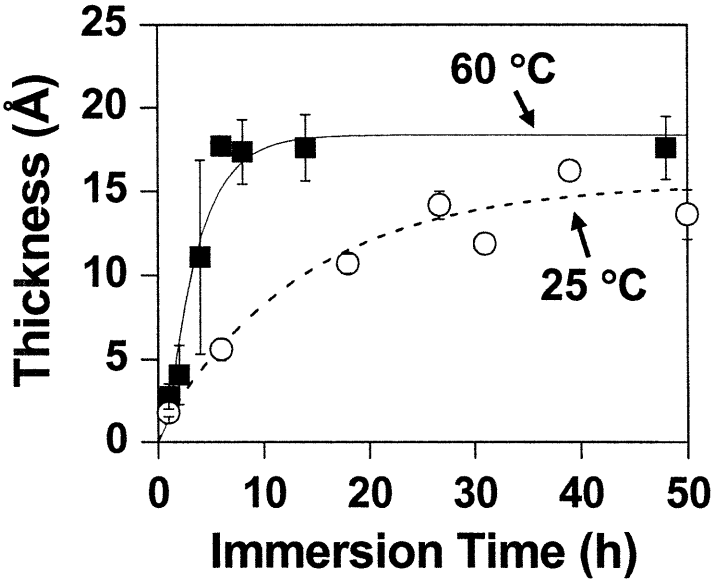

Figure 5.1. Kinetics of monolayer formation for reaction of $Cl_3Si(CH_2)_{11}(OCH_2CH_2)_3OC(=O)CH_3$ in anhydrous toluene onto Si/SiO_2 surfaces; concentrations ranged from 3 to 6 mM and showed no discernible effect on the kinetics. Open circles are ellipsometric thicknesses of the film formed at 25 °C and filled squares are thicknesses at 60 °C. The curves represent first-order kinetic fits to the data.

The limiting ellipsometric thickness of EG_3OAc SAMs formed under these conditions was 19 Å. This value is ~60% of the expected thickness if a densely packed monolayer with an extended chain configuration formed from **3** (i.e., ~31 Å). We investigated the use of

other solvents (N,N-dimethylformamide, CH_2Cl_2, and tetrahydrofuran) as a means to generate well-defined films and observed that adsorptions conducted from toluene gave the thickest films. The tendency of EG moieties to coil[26-28] as well as the various observations of reduced packing and disorder within alkylsiloxane films incorporating functional groups[29,30] may be responsible for the thickness of films formed from **3** being less than that expected for a purely *trans*-extended structure of **3**.

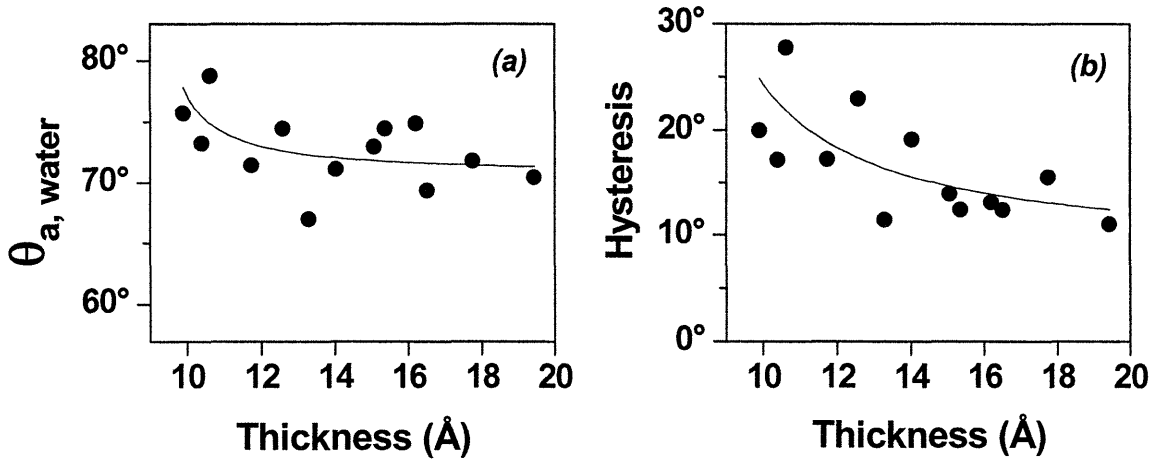

Figure 5.2. Wetting properties of EG_3OAc film as a function of its film thickness: (a) Advancing water contact angle (θ_a), and (b) contact angle hysteresis (θ_a - θ_r) for water. Lines represent guides to the eye.

A critical issue for providing protein resistance for films derived from **3** will be the completeness of their coverage of the surface with EG_3 functionalities. The regularity and the hydrophilicity of the films were assessed using wetting measurements. Figure 5.2 shows the advancing water contact angle ($\theta_a(H_2O)$) and the water contact angle hysteresis ($\Delta\theta = \theta_a$-θ_r) of EG_3OAc films of varying thickness. The data points in Figure 5.2 are the results of different preparations employing various concentrations, solvents, temperatures, and immersion times. In general, the water contact angle and water contact angle hysteresis were

highest for the thinner films and showed a decrease with increasing ellipsometric thickness. These decreases are compatible with the formation of more closely packed EG_3-exposing films. Specifically, the highest water contact angles suggest a lack of coverage by the EG_3 chains as the interactions between the probe liquid (water) and the $-(CH_2)_n-$ chain would result in a less wettable surface while higher surface coverages of EG_3 groups would produce a more wettable surface. The lower levels of contact angle hysteresis for water on the surfaces of the thicker EG_3OAc films would suggest a more homogenous surface. Water is sensitive to the composition of the outermost 5 Å of a surface[31] and changes in hysteresis and in wetting can suggest changes in structure, composition, and homogeneity in this region. For the EG_3OAc films, the decrease in water contact angle hysteresis with increasing film thickness is compatible with the formation of a films with better organization and superior homogeneity. The thickest EG_3OAc films exhibited water contact angles of 70° and hystereses of 10°, and these values provided a useful guide as to the quality of films formed in our work.

Reduction of EG_3OAc to EG_3OH. The acetate groups that terminate the EG_3OAc films were converted to hydroxyl groups by their reduction on the surface by $LiAlH_4$. In detail, the EG_3OAc films on Si/SiO_2 substrates were immersed into 0.1 M or 1.0 M solutions of $LiAlH_4$ in anhydrous ether for various times, followed by sequential rinsing with anhydrous ether, 0.1 M HCl(*aq*), deionized water, and ethanol. The resulting films were characterized by infrared spectroscopy, XPS, and wetting measurements.

Figure 5.3 shows representative high-resolution XPS spectra of the C(1s) regions for an EG_3OAc SAM (*i.e.*, before deprotection) and an EG_3OH SAM (here, after deprotection for 5 min in 1.0 M $LiAlH_4$/ether). The spectrum in Figure 5.3a was fitted with three peaks: one for aliphatic carbons (C_1), one for carbons participating in an ether linkage (i.e., C-O-C) (C_2),

and one for the carboxyl carbon of the acetate group (i.e., C(=O)O) (C_3). In Figure 5.3b, the complete loss of the peak at ~290 eV (C_3) for the carboxyl carbon suggests a complete reduction of the acetate group, presumably to a hydroxyl terminus. This assignment was confirmed by the reaction of this surface with trifluoroacetic anhydride (TFAA), and these results are discussed later in this article.

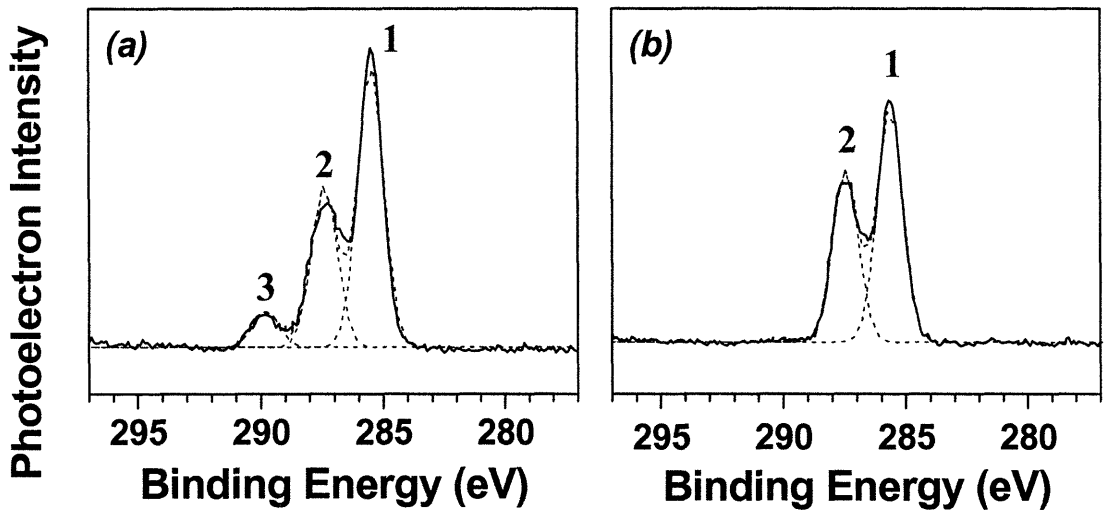

Figure 5.3. Representative XPS spectra for the C(1s) region of (a) acetate- and (b) hydroxyl- terminated tri(ethylene glycol)-containing alkylsiloxane monolayers on Si/SiO_2. The hydroxyl-terminated surface was prepared by reducing the acetate-terminated EG_3 monolayer (EG_3OAc) to its hydroxyl counterpart (EG_3OH) by immersing the acetate-terminated surface in 1.0 M $LiAlH_4$/ether for 5 min. Dashed lines represent Gaussian peak fits to the data. Peaks 1: $-(\underline{C}H_2)$-, 2: -$\underline{C}$-O-, 3: $CH_3\underline{C}(=O)$-O-.

In Figure 5.3, the intensity of the C_2 peak arising from the oEG chain is nearly the same in both Figure 5.3a and b, denoting that the reduction of the acetate by $LiAlH_4$ did not noticeably affect or degrade the EG group, at least through 5 min of exposure to 1.0 M $LiAlH_4$. Table 5.1 summarizes the relative area ratios for the three C(1s) peaks that comprise the spectra in Figure 3a and b, and compares these values with those based on stoichiometry. For both the EG_3OAc and EG_3OH films, the relative area ratios from XPS are similar to the

stoichiometric values. For the species expected to be at the outer surface (i.e., C_3 of the terminal acetate in EG_3OAc and C_2 of the oEG chain in EG_3OH), we observe XPS values that are slightly higher than expected from stoichiometry. These deviations are compatible with structures where the acetate group in the EG_3OAc film (based on the ratio C_3/C_1 for EG_3OAc) and the oEG chain in the EG_3OH film (based on the ratio C_2/C_1 for EG_3OH) are localized near the outer surface as would be expected for attachment of the films by the -$SiCl_3$ moiety and an exclusion of the tail groups from the region near the substrate surface.

Table 5.1. Relative areas of the three C(1s) peaks for EG_3OAc and EG_3OH monolayers calculated from: (a) XPS experimental data (Figures 5.3a and b), (b) expected XPS intensities based on atomic composition. C_1: -CC-, C_2: C-O, and C_3: -C(=O)O-

	Relative areas of C(1s) peaks				
	EG_3OAc			EG_3OH	
	C_1	C_2	C_3	C_1	C_2
(a) Experimental	1.00	0.56	0.13	1.00	0.73
(b) Atomic composition	1.00	0.64	0.09	1.00	0.70

We further confirmed the attachment of **3** to form the EG_3OAc film by infrared spectroscopy. Figure 5.4 shows infrared data from an ATR silicon crystal that was modified to expose an EG_3OAc film and subsequently reacted with $LiAlH_4$, and then with trifluoroacetic anhydride (TFAA). In Figure 5.4a for the EG_3OAc film, the spectra contain a strong absorption peak at around 1745 cm^{-1} that corresponds to the carbonyl stretching band for the acetate in the EG_3OAc monolayer. Figure 5.4b shows this region after immersion of the Si crystal in 1.0 M $LiAlH_4$/ether for 5 min. The spectrum for this sample shows a complete loss of the ester absorption, indicating a loss of the acetate groups by this reaction.

To verify that the $LiAlH_4$ reduction produces an EG_3OH film exposing surface -OH groups, the crystal was immersed in a 2 vol % TFAA solution in hexane for 2 min. The infrared spectrum for this sample (Figure 5.4c) exhibits an absorption around the carbonyl region, indicating a generation of $OC(=O)CF_3$ groups, presumably by the reaction of TFAA with surface -OH groups.

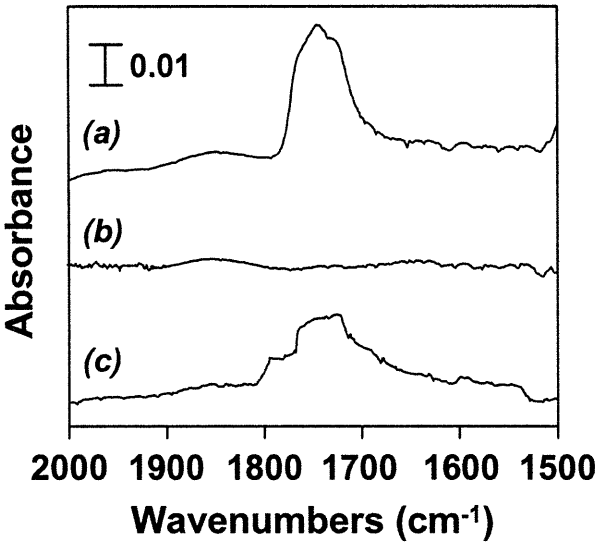

Figure 5.4. ATR/FT-IR spectra of: (a) $Si/SiO_2/O_{3/2}Si(CH_2)_{11}(EG)_3OC(=O)CH_3$, (before deprotection), (b) $Si/SiO_2/O_{3/2}Si(CH_2)_{11}(EG)_3OH$, (after deprotection), and (c) $Si/SiO_2/O_{3/2}Si(CH_2)_{11}(EG)_3O(C=O)CF_3$, prepared by derivatizing $Si/SiO_2/O_{3/2}Si(CH_2)_{11}(EG)_3OH$ with trifluoroacetic anhydride (TFAA).

The reaction of TFAA with the $LiAlH_4$-reduced EG_3OAC film was further investigated by XPS. Figure 5.5 shows representative F(1s) spectra for an EG_3OAc SAM and an EG_3OH SAM after each SAM was treated with TFAA. In the latter case, the reaction product of EG_3OH and TFAA (i.e., $EG_3OC(=O)CF_3$) shows an intense F(1s) signal (Figure 5.5a), whereas the treated EG_3OAc film shows no F(1s) peak. The results confirm the generation of an -OH on the oEG surface by the $LiAlH_4$ reduction.

Figure 5.6 shows an XPS spectrum of the C(1s) region for an EG_3OH SAM after its

reaction with TFAA to form $EG_3O(C{=}O)CF_3$. In the figure, peaks C_3 and C_4 are not present in the spectrum for the untreated EG_3OH and represent chemical species arising from the reaction of the $LiAlH_4$-generated –OH terminus with TFAA. Specifically, we assign C_3 to -**C**(=O)O- and C_4 to the **C**F_3- arising from the TFAA treatment. We note that for treatment of EG_3OAc films with TFAA, we observed XPS spectra similar to those in Figure 5.3a for the native EG_3OAc sample with no signal at the binding energy for C_4. The results further confirm the generation of reactive –OH groups on the oEG chains by the reduction of the EG_3OAc films by $LiAlH_4$ and the ability to have them undergo chemical modification.

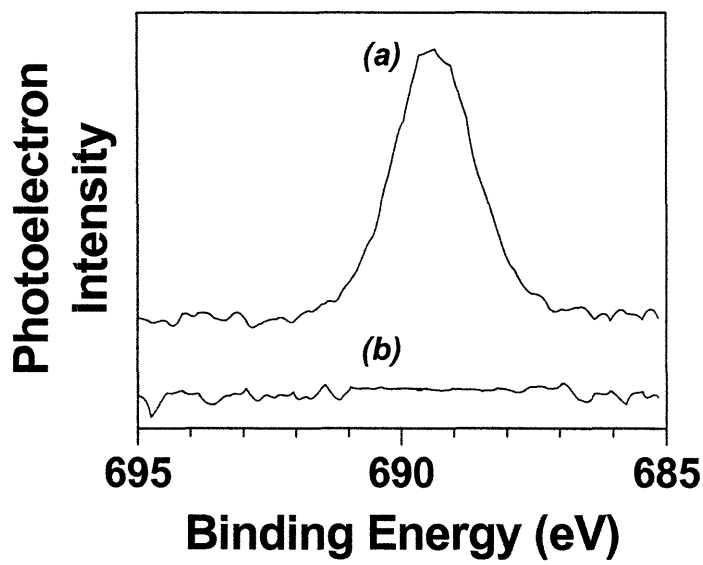

Figure 5.5. XPS spectra of the F(1s) region for monolayers of (a) EG_3OH and (b) EG_3OAc after treatment with TFAA. The absence of a F(1s) peak in (b) shows that the EG_3OAc surface is inert toward TFAA.

To determine the surface density of reactive OH groups on the EG_3OH SAM, we compared F(1s) signals from the TFAA-treated EG_3OH SAM to those produced by a TFAA-treated SAM of $HS(CH_2)_{11}OH$ on Au. We selected this alkanethiolate SAM on gold as a reference as each molecule within a closely packed n-alkanethiolate monolayer on gold

occupies ~21.4 Å^2/molecule,[32] corresponding to a surface density of 4.61×10^{14} molecules/cm^2. Assuming similar conversions of -OH to -OC(=O)CF_3 for both the Si/SiO_2/EG_3OH and Au/S$(CH_2)_{11}$OH SAMs, the surface density of OH tail groups in the EG_3OH SAM, ϕ, can be determined as:

$$\phi = \frac{\text{Area of F(1s) for } EG_3OC(=O)CF_3}{\text{Area of F(1s) for Au/HS}(CH_2)_{11}OC(=O)CF_3} \times \left(4.61 \times 10^{14} \text{ molecules/cm}^2\right) \quad (5.1)$$

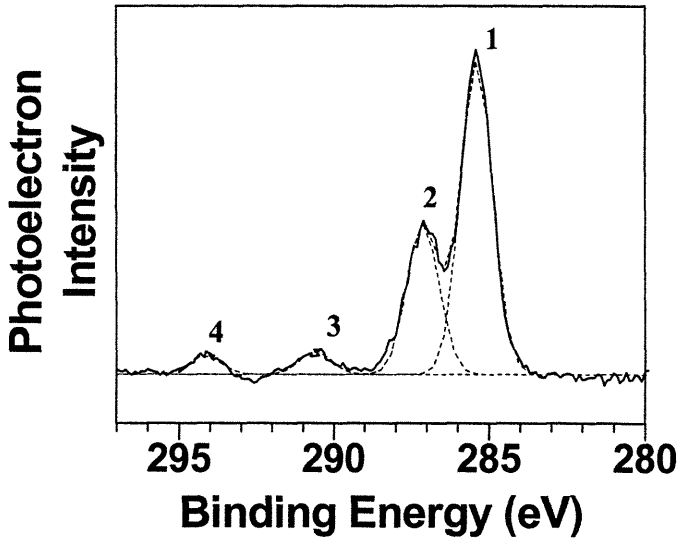

Figure 5.6. XPS spectrum of the C(1s) region for Si/SiO_2/$O_{3/2}$Si$(CH_2)_{11}(OCH_2CH_2)_3OC(=O)CF_3$ as prepared by reacting an EG_3OH-terminated monolayer with TFAA. Peaks 1: -(CH_2)-, 2: -(CH_2O)-, 3: -C(=O)O-, and 4: CF_3-.

Figure 5.7 shows the surface density of OH tail groups in a EG_3OAc SAM for various reduction times using two different $LiAlH_4$ concentrations. The SiO_2/EG_3OAc SAM substrates were immersed into 0.1 and 1.0 M $LiAlH_4$ solutions in anhydrous ether for 0 to 40 min, later reacted with TFAA, and then examined by XPS to obtain F(1s) intensities. We compared the F(1s) intensities on the modified EG_3OAc SAMs to those from a TFAA-treated Au/S$(CH_2)_{11}$OH SAMs to estimate the surface density of EG_3OH tail groups by eq 5.1 across

various deprotection conditions. For substrates immersed in a 0.1 M $LiAlH_4$ solution, the F(1s) intensity increased linearly with deprotection time; however, the F(1s) intensity for the reacted EG_3OAc surfaces was only 9 % of that from the gold reference surface. In contrast, the F(1s) intensity for EG_3OAc surfaces reacted with 1.0 M $LiAlH_4$ reached ~60 % of the F(1s) signal from the gold reference, corresponding to a EG_3OH surface density of 2.7×10^{14} molecules/cm^2. This value was obtained within 1 to 5 min of exposure to the 1.0 M $LiAlH_4$ solution. We note that a 15-s exposure of the EG_3OAc SAM to the 1.0 M $LiAlH_4$ solution produced a F(1s) intensity that was only ~ 20 % of the reference, suggesting that a contact time of ~1 min or more was required for reduction of the acetate terminus.

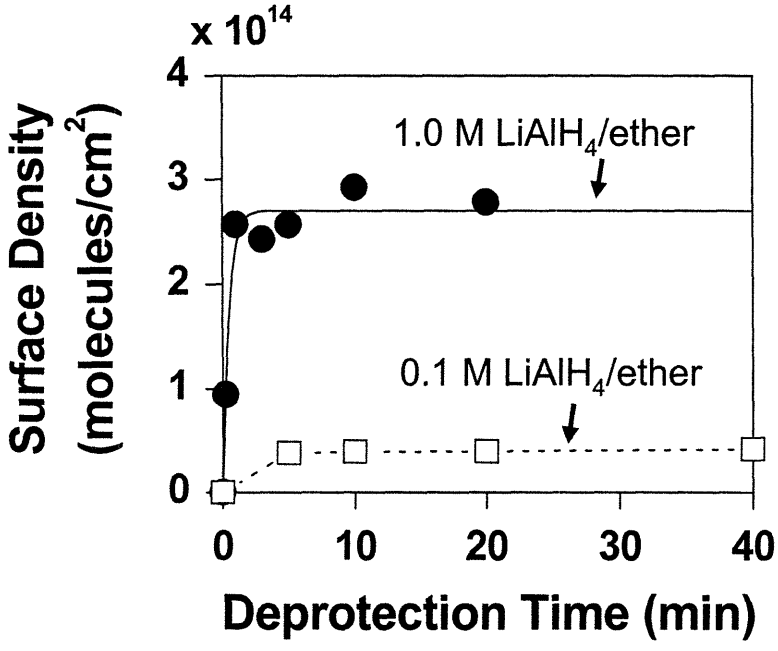

Figure 5.7. Surface density of EG_3OH termini as a function of deprotection time for EG_3OAc SAMs to two different $LiAlH_4$ concentrations. Surface densities were determined by comparing the F(1s) intensity from EG_3OH-containing samples and from $Au/S(CH_2)_{11}OH$ as reference after treating these surfaces with TFAA. Lines are guides to the eye.

After deprotection of the acetate terminus, the ellipsometric thickness for the EG_3OAc SAMs decreased by ~3 Å and $\theta_a(H_2O)$ changed from ~73° to ~63°. In both cases, the

decreases in thickness and in $\theta_a(H_2O)$ with reduction time reach limiting values after about 20 min of $LiAlH_4$ exposure (Figure 5.8). Based on the molecular structure of EG_3OAc and assuming a densely packed layer with perpendicularly oriented, fully-extended chains, the reduction of the terminal acetate to a hydroxyl group should cause a decrease of ~2.5 Å in film thickness. Figure 5.8a shows that reductions by 1.0 M $LiAlH_4$ solutions for times up to ~5 min produced decreases in film thickness of less than this value, whereas longer reductions produced thickness decreases slightly larger than this value. At shorter times, we presume that some of the unreacted acetate groups remain in the monolayer, whereas at longer times, exposures to 1.0 M $LiAlH_4$ solutions result in film decomposition. By C(1s) XPS, a substrate that was in contact with 1.0 M $LiAlH_4$ solution for 3 min exhibited a small C_3 peak indicative of remaining acetate. Decomposition of the SAM by extended exposure to the 1.0 M $LiAlH_4$ solution (150 min) was evidenced by a general decrease in all C(1s) intensity. As optimum between the need to reduce the acetate terminus while minimizing decomposition to the EG SAM, we selected 5 min of exposure to the 1.0 M $LiAlH_4$ solution as our preferred condition for generating the EG_3OH surface.

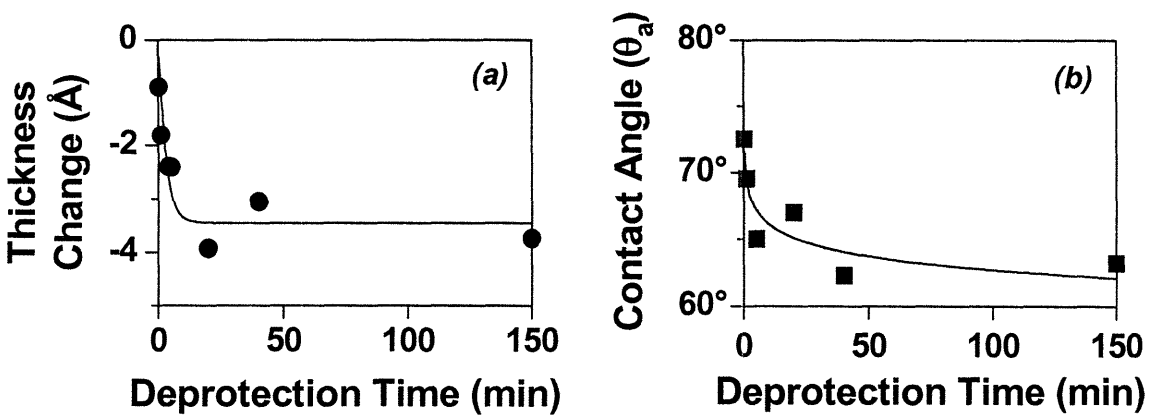

Figure 5.8. (a) Ellipsometric thickness change and (b) advancing contact angles of water on EG_3OH SAM as a function of exposure time of the acetate-terminated EG_3 SAM to 1.0 M $LiAlH_4$/ether.

5.3.2. Protein Resistance of EG_3OAc, EG3OH, and EG_3OCH_3 SAMs

Protein adsorption experiments on the EG_3OH-modified SiO_2 wafers showed that the coating resulted in significant reductions in non-specific protein adsorption as compared to silanating procedures that hydrophobize the surface by reaction with *n*-octadecyltrichlorosilane ($CH_3(CH_2)_{17}SiCl_3$) as a means to reduce protein adsorption. Figure 5.9 shows thickness results for the non-specific adsorption of four different proteins on the EG_3 SAMs: the EG_3OCH_3 SAM as an 'inert' surface, the EG_3OAc SAM as a 'protected' hydroxyl surface, and the EG_3OH SAM as a reactive OH surface. Data for a hydrophobized surfaces are included for comparison. Regardless of the terminal functionality (-OH, -OMe, and -OAc), the three EG_3–type SAMs showed no significant change in film thickness after 24-h contact with 0.25 mg/mL insulin, lysozyme, and hexokinase solutions, in contrast to the behavior for the C_{18} SAM. As an example of when the EG_3 films were not fully able to suppress the non-specific adsorption of a protein, Figure 5.9 also shows data for fibrinogen, where the prevention of its nonspecific adsorption was not possible. We note, however, that the EG_3 coatings were able to reduce the adsorption of fibrinogen by ~70 % from that on bare glass and by ~50% from that on hydrophobized glass employing an octadecyltrichlorosilane (OTS) treatment. Moreover, the EG_3OH surface was the best among the three EG_3 derivatives in terms of fibrinogen resistance.

The similarities of the three EG_3 films in terms of their protein resistant characteristics and their related molecular structures - they differ only in their terminal group - suggest that these three derivatives will be a useful key set for the preparation of mixed monolayers that offer protein-resistant properties and present tailorable compositions of 'reactive' and 'inert' functionality. Such systems are targeted for the construction of surfaces with controlled adsorption and recognition properties useful in biosensing and other diagnostic applications.

With these directions in mind, we examined a general strategy for chemically modifying the EG_3OH SAM.

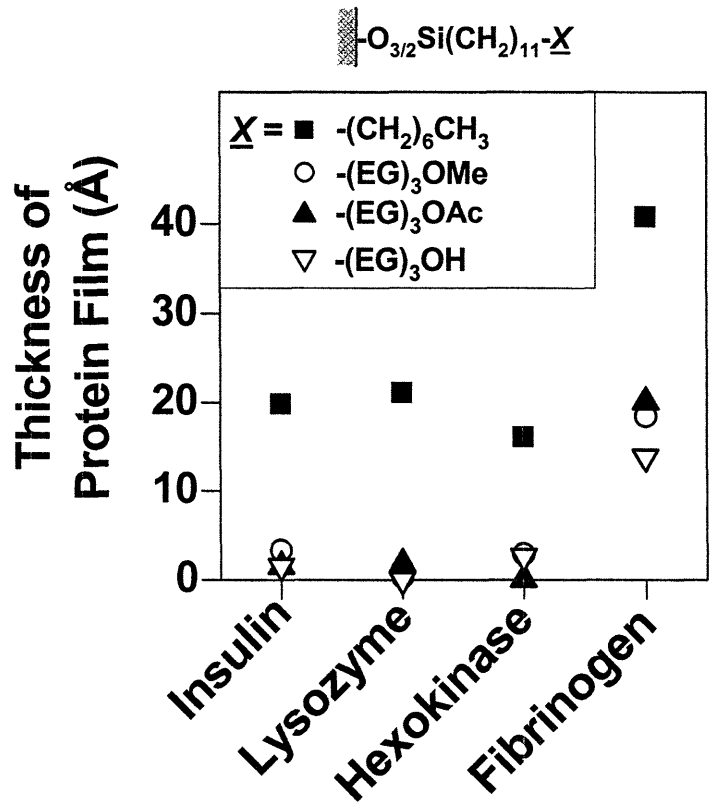

Figure 5.9. Ellipsometric thickness increases upon exposure of a C_{18} SAM, and three different EG_3 SAMs (EG_3OMe, EG_3OAc, and EG_3OH) to various protein solutions (0.25 mg/mL in PBS, pH 7.4) for 24 h. For comparison, the thickness increases onto untreated Si/SiO_2 surfaces were ~ 20 Å for insulin, lysozyme, and hexokinase, and ~ 65 Å for fibrinogen.

5.3.3. Subsequent Modification of the EG_3OH SAM Surface for Immobilization of Biomolecules

A goal in this work is to generate a chemically reactive, stable, protein resistant coating for glass and metal oxide surfaces that provides a platform for attaching agents to these thin films. Figure 5.10 illustrates a procedure for immobilizing protein A on the EG_3OH surface using carbonyl diimidazole (CDI) as a crosslinker. Protein A was selected for this study as it

provides a general strategy for linking and orienting immunoglobulins.[33,34]

We monitored the progress of the various reaction steps in Figure 5.10 by measuring XPS N(1s) peak intensities at various stages through the process. The N(1s) signal provided a convenient method for monitoring changes at the film surface as an EG_3O/CDI layer would have two nitrogen elements per molecule, and attachment of Protein A or an immunoglobulin would be expected to provide further increases in nitrogen levels. Thus, increases in N(1s) intensity after a reaction step are indicative of the attachment of the corresponding reagent during the stages in Figure 5.10.

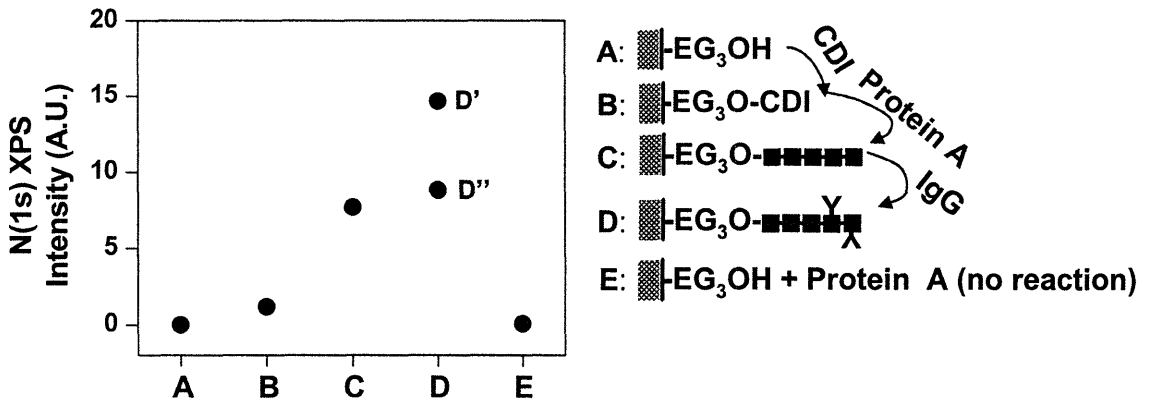

Figure 5.10. N(1s) XPS intensities from EG_3OH SAMs on Si/SiO_2 through a stepwise synthetic process to immobilize protein A and IgG. The rightmost data point (E) shows that protein A does not adsorb onto the native EG_3OH surface (i.e., no CDI pre-treatment). Immunoglobulin immobilization was conducted for 30 min using either 0.25 mg/ml (D') or 0.75 mg/mL (D") of IgG in PBS at pH 7.4. See text for details.

In Figure 5.10, the initial EG_3OH surface displayed no identifiable N(1s) intensity. Treatment with CDI resulted in a N(1s) signal that suggested an ~30% reaction by surface EG_3OH groups based on a comparison of the intensity to an amino-treated SAM on SiO_2 used as reference. The N(1s) intensity further increased when this surface was then treated with Protein A and again with a model IgG that became bound by the immobilized Protein A

molecules. The greater increase in N(1s) signal due to attachment of Protein A than by reaction with CDI is compatible with the greater number of nitrogen atoms present in the protein (~500 *vs.* 2). We note that the XPS data do not exhibit an increase in N(1s) signal that scales with the number of nitrogen atoms in Protein A and CDI as steric constraints would be expected to limit the number of attached Protein A molecules to the CDI surface. The ellipsometric thickness increase upon attachment of Protein A to the CDI surface was 1.5 nm. To insure that the N(1s) signal from due to the exposure of the CDI surface to Protein A was the result of specific attachment, Figure 5.10E also shows data for an EG_3OH surface (*i.e.*, no CDI activation) that was treated with Protein A for 24 h. We observed no identifiable N(1s) signal for this sample suggesting the lack of non-specific adsorption for Protein A onto the native EG_3OH surface and the requirement of CDI treatment for localizing Protein A on the surface. This result suggests that the EG_3OH film presents an "inert" surface towards unwanted non-specific protein adsorption, and that its hydroxyl-termination can provide a means for specifically immobilizing proteins and other species onto this surface.

Figure 5.10D shows the results for linking a model IgG to the Protein A surface. Our initial exploration for this immobilization exhibited a sensitivity to the IgG concentration. For example, the increase in N(1s) signal for treating the Protein A surface with IgG at 0.25 mg/mL was small, with treatment using IgG at 0.75 mg/mL generating a much greater change. The observed differences with concentration suggest that higher concentrations are required for saturating the Protein A binding sites with IgG. The data clearly demonstrate our abilities to link agents to the EG_3OH SAM through the reactive OH tail group, and to use generated Protein A surfaces on the EG_3OH SAM as a potentially generic linking agent for attaching immunoglobulins to these inert surfaces.

The developed silane-based EG_3OH system appears to provide characteristics that can offer notable uses as a flexible platform for biosensor construction. We anticipate that their robust anchoring, dense packing of these films, and their presentation of a chemically reactive and modifiable surface with protein resistant characteristics will make the EG_3OH system particularly useful for biological and sensing applications such as those that employ microsystems, technologies such as waveguide-based biosensors that require immobilization and binding events extremely close (a few nanometers) to the transducer surface, and for other applications that require responsive thin films with antifouling properties.

5.4. Conclusions

The self-assembly of $CH_3C(=O)O(CH_2CH_2O)_3(CH_2)_{11}SiCl_3$ (***3***) onto Si/SiO_2 substrates (and presumably onto related oxide surfaces) provides the ability to generate densely packed, hydroxyl-terminated, oligo(ethylene glycol)-expressing surfaces. The molecule adsorbed spontaneously onto the Si/SiO_2 surface to generate an acetate-terminated tri(ethylene glycol) surface that is subsequently deprotected chemically using $LiAlH_4$ to generate a chemisorbed hydroxyl-terminated tri(ethylene glycol)–expressing film. Both the EG_3OAc and EG_3OH films exhibit low levels of non-specific protein adsorption and provide notable enhancements in antifouling characteristics as compared to hydrophobizing treatments using octadecyltrichlorosilane in related chemical modification procedures. A key advance provided by the EG_3OH film is its ability to incorporate terminal sites on the siloxane film that allow subsequent chemical modification and attachment. Specifically, we have used the EG_3OH surface for immobilizing biomolecules onto these hydroxyl-terminated "inert" surfaces. The attachment of Protein A onto this surface and its binding to an immunoglobin provide demonstrations of this ability, with the attachment of Protein A offering broad

abilities to immobilize a variety of immunoglobulins on these surfaces as recognition elements for sensing. The EG_3OH platform offers key attributes for the design of biosensing and diagnostic components that are the subject of current study in our laboratory.

5.5. References for Chapter 5

(1) Pale-Grosdemange, C.; Simon, E. S.; Prime, K. L.; Whitesides, G. M. Formation of self-assembled monolayers by chemisorption of derivatives of oligo(ethylene glycol) of structure $HS(CH_2)_{11}(OCH_2CH_2)_mOH$ on gold. *J. Am. Chem. Soc.* **1991**, *113*, 12-20.

(2) Prime, K. L.; Whitesides, G. M. Self-assembled organic monolayers - model systems for studying adsorption of proteins at surfaces. *Science* **1991**, *252*, 1164-1167.

(3) Prime, K. L.; Whitesides, G. M. Adsorption of proteins onto surfaces containing end-attached oligo(ethylene oxide) - a model system using self-assembled monolayers. *J. Am. Chem. Soc.* **1993**, *115*, 10714-10721.

(4) Ostuni, E.; Grzybowski, B. A.; Mrksich, M.; Roberts, C. S.; Whitesides, G. M. Adsorption of proteins to hydrophobic sites on mixed self-assembled monolayers. *Langmuir* **2003**, *19*, 1861-1872.

(5) Harder, P.; Grunze, M.; Dahint, R.; Whitesides, G. M.; Laibinis, P. E. Molecular conformation in oligo(ethylene glycol)-terminated self-assembled monolayers on gold and silver surfaces determines their ability to resist protein adsorption. *J. Phys. Chem. B* **1998**, *102*, 426-436.

(6) Wang, R. L. C.; Kreuzer, H. J.; Grunze, M. Molecular conformation and solvation of oligo(ethylene glycol)- terminated self-assembled monolayers and their resistance to protein adsorption. *J. Phys. Chem. B* **1997**, *101*, 9767-9773.

(7) Wang, R. L. C.; Kreuzer, H. J.; Grunze, M. The interaction of oligo(ethylene oxide) with water: A quantum mechanical study. *Phys. Chem. Chem. Phys.* **2000**, *2*, 3613-3622.

(8) Nelson, K. E.; Gamble, L.; Jung, L. S.; Boeckl, M. S.; Naeemi, E.; Golledge, S. L.; Sasaki, T.; Castner, D. G.; Campbell, C. T.; Stayton, P. S. Surface characterization of mixed self-assembled monolayers designed for streptavidin immobilization. *Langmuir* **2001**, *17*, 2807-2816.

(9) Zwahlen, M.; Herrwerth, S.; Eck, W.; Grunze, M.; Hähner, G. Conformational order in oligo(ethylene glycol)-terminated self-assembled monolayers on gold determined by soft x-ray absorption. *Langmuir* **2003**, *19*, 9305-9310.

(10) Kim, H. I.; Kushmerick, J. G.; Houston, J. E.; Bunker, B. C. Viscous "interface" water adjacent to oligo(ethylene glycol)-termianted self-assembled monolayers. *Langmuir* **2003**, *19*, 9271-9275.

(11) Jung, L. S.; Nelson, K. E.; Campbell, C. T.; Stayton, P. S.; Yee, S. S.; Perez-Luna, V.; Lopez, G. P. Surface plasmon resonance measurement of binding and dissociation of wild-

type and mutant streptavidin on mixed biotin-containing alkylthiolate monolayers. *Sens. Actuators, B* **1999**, *54*, 137-144.

(12) Jung, L. S.; Nelson, K. E.; Stayton, P. S.; Campbell, C. T. Binding and dissociation kinetics of wild-type and mutant streptavidins on mixed biotin-containing alkylthiolate monolayers. *Langmuir* **2000**, *16*, 9421-9432.

(13) Chirakul, P.; Perez-Luna, V. H.; Owen, H.; Lopez, G. P. Synthesis and characterization of amine-terminated self-assembled monolayers containing diethylene glycol linkages. *Lagmuir* **2002**, *18*, 4324-4330.

(14) Herrwerth, S.; Rosendahl, T.; Feng, C.; Fick, J.; Eck, W.; Himmelhaus, M.; Dahint, R.; Grunze, M. Covalent coupling of antibodies to self-assembled monolayers of carboxy-functionalized poly(ethylene glycol): Protein resistance and specific binding of biomolecules. *Langmuir* **2003**, *19*, 1880-1887.

(15) Lahiri, J.; Isaacs, L.; Tien, J.; Whitesides, G. M. A strategy for the generation of surfaces presenting ligands for studies of binding based on an active ester as a common reactive intermediate: A surface plasmon resonance study. *Anal. Chem.* **1999**, *71*, 777-790.

(16) Houseman, B. T.; Gawalt, E. S.; Mrksich, M. Maleimide-functionalized self-assembled monolayers for the preparation of peptide and carbohydrate biochips. *Langmuir* **2003**, *19*, 1522-1531.

(17) Bensebaa, F.; Ellis, T. H.; Badia, A.; Lennox, R. B. Thermal treatment of n-alkanethiolate monolayers on gold, as observed by infrared spectroscopy. *Langmuir* **1998**, *14*, 2361-2367.

(18) Bhatia, R.; Garrison, B. J. Phase transitions in a methyl-terminated monolayer self-assembled on au{111}. *Langmuir* **1997**, *13*, 765-769.

(19) Schlenoff, J. B.; Li, M.; Ly, H. Stability and self-exchange in alkanethiol monolayers. *J. Am. Chem. Soc.* **1995**, *117*, 12528-12536.

(20) Schoenfisch, M. H.; Pemberton, J. E. Air stability of alkanethiol self-assembled monolayers on silver and gold surfaces. *J. Am. Chem. Soc.* **1998**, *120*, 4502-4513.

(21) Kluth, G. J.; Sung, M. M.; Maboudian, R. Thermal behavior of alkylsiloxane self-assembled monolayers on the oxidized si(100) surface. *Langmuir* **1997**, *13*, 3775-3580.

(22) Lee, S.-W.; Laibinis, P. E. Protein-resistant coatings for glass and metal oxide surfaces derived from oligo(ethylene glycol)-terminated alkyltrichlorosilanes. *Biomaterials* **1998**, *19*, 1669-1675.

(23) Margel, S.; Vogler, E. A.; Firment, L.; Watt, T.; Haynie, S.; Sogah, D. Y. Peptide, protein, and cellular interactions with self-assembled monolayer model surfaces. *J. Biomed. Mater. Res.* **1993**, *27*, 1463-1476.

(24) Wenzler, L. A.; Moyes, G. L.; Raikar, G. N.; Hansen, R. L.; Harris, J. M.; Beebe, T. P.; Wood, L. L.; Saavedra, S. S. Measurements of single-molecule bond rupture forces between self-assembled monolayers of organosilanes with the atomic force microscope. *Langmuir* **1997**, *13*, 3761-3768.

(25) Richter, A. G.; Yu, C. J.; Datta, A.; Kmetko, J.; Dutta, P. Using x-rays to characterize

the process of self-assembly in real time. *Colloids Surf. A* **2002**, *198*, 3-11.

(26) Maxfield, J.; Shepherd, I. W. Conformation of poly(ethylene oxide) in the solid state, melt and solution measured by Raman scattering. *Polymer* **1975**, *16*, 505-509.

(27) Yamauchi, T.; Hasegawa, A. Determination of peg concentration in its aqueous solution using differential scanning calorimetry. *J. Appl. Polym. Sci.* **1993**, *49*, 1653-1658.

(28) Yang, R.; Yang, X. R.; Evans, D. F.; Hendrickson, W. A.; Baker, J. Scanning tunneling microscopy images of poly(ethylene oxide) polymers: Evidence for helical and superhelical structures. *J. Phys. Chem.* **1990**, *94*, 6123-6125.

(29) Tillman, N.; Ulman, A.; Schildkraut, J. S.; Penner, T. L. Incorporation of phenoxy groups in self-assembled monolayers of trichlorosilane derivatives: Effects on film thickness, wettability, and molecular orientation. *J. Am. Chem. Soc.* **1988**, *110*, 6136-6144.

(30) Tillman, N.; Ulman, A.; Elman, J. F. A novel self-assembled monolayer film containing sulfone-substituted aromatic group. *Langmuir* **1990**, *6*, 1512-1518.

(31) Laibinis, P. E.; Bain, C. D.; Nuzzo, R. G.; Whitesides, G. M. Structure and wetting properties of w-alkoxy-n-alkanethiolate monolayers on gold and silver. *J. Phys. Chem.* **1995**, *99*, 7663-7676.

(32) Ulman, A. *An introduction to ultrathin organic films: From langmuir-blodgett to self-assembly*; Academic Press, **1991**.

(33) Gersten, D. M.; Marchalonis, J. J. Rapid, novel method for solid-phase derivatization of igg antibodies for immune-affinity chromatography. *J. Immunol. Methods* **1978**, *24*, 305-309.

(34) Lu, B.; Smyth, M. R.; O'Kennedy, R. Oriented immobilization of antibodies and its applications in immunoassays and immunosensors. *Analyst* **1996**, *121*, R29-R32.

Chapter 6. Mixed Self-Assembled Monolayers of Tri(ethylene glycol)-Terminated Alkyltrichlorosilane for the Selective Immobilization of Proteins

6.1. Introduction

6.1.1. Motivation and Overview

The high selectivity of antibodies against their target antigens has been a key characteristic property that has motivated the development of methods for immobilizing antibodies for use in various applications, such as in microarrays for therapeutics and screening,[1-3] diagnostic immunoassays and immunosensors,[4,5] and affinity chromatography[6,7]. When used as recognition elements in immunosensors, the sensitivity and specificity of such devices are often greatly affected by the conformation and orientation of the antibodies on the transducer surfaces. The orientation of the antibodies and their configurational heterogeneity on the surface is governed by the ways in which the antibodies are immobilized. Therefore, immobilization strategies play a paramount role in maintaining the binding activity of antibodies when attached to a support.

The binding of an immunoglobulin G (IgG, a class of antibody) to a covalently attached molecule of protein A has beenused by various groups for immobilizing IgG molecules with a control over their orientations.[8-10] Figure 6.1and Figure 6.2 provide schematic illustrations of a protein A and an IgG molecule with descriptions of their fragments; these molecules are further discussed in Section 6.1.2. The salient feature of protein A is that this protein specifically binds to the F_c fragment of an IgG, orienting the F_{ab} fragments of the IgG in such a way that they can be accessible for antigen binding. Thus, the binding of IgG molecules to protein A-functionalized surfaces can be a versatile strategy for creating IgG immobilized

arrays. Therefore, optimizing the binding activity of the protein A-coated surfaces is important in the construction of IgG surfaces.

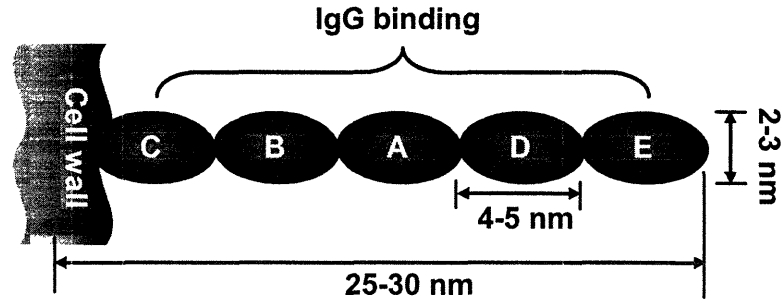

Figure 6.1. Schematic illustration of a staphylococcal protein A molecule.

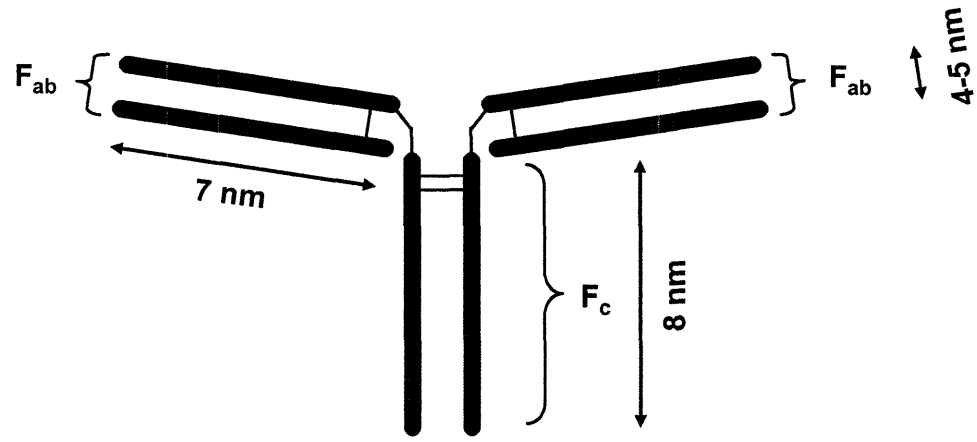

Figure 6.2. Schematic illustration of an immunoglobulin G (IgG) molecule. The IgG molecule consists of three distinct fragments. There are two F_{ab} fragments that lie at the outermost end of the top two branches and provide antigen binding sites, and an F_c fragment that is located in the base of the molecule.

The potential of self-assembled monolayers (SAMs) for achieving molecular-level control over surface properties has been widely recognized.[11-13] In addition, the functionality and composition of the surfaces can further be manipulated by forming *mixed* SAMs where the composition of two (or more) different adsorbates comprising the SAM can be

systematically varied.[14] SAMs on gold have been widely applied for generation of well-defined surfaces with biological components.[15-18] In contrast, the functionalization of SiO_2-based surfaces with SAMs expressing biological species has been less studied, even though silicon and silicon dioxide are the most commonly used substrates in the fabrication of solid-state devices.[19] This lack of exploration is due in part to the chemical incompatibility of the adsorbates commonly used for derivatizing Si and SiO_2 surfaces and the functionalities present in many biological compounds.

In the preceding chapter, we detailed the formation of a SAM on SiO_2 surfaces presenting oligo(ethylene glycol) moieties with a "hydroxyl" terminus (EG_3OH SAM; "*reactive*" EG_3 surface). We also demonstrated that this EG_3OH surface can be used to functionalize silicon dioxide surfaces with protein A, and that such surfaces can capture IgG molecules. In the previous study, the SAMs on SiO_2 surfaces that presented oligo(ethylene glycol) moieties with a "methoxy" terminus (EG_3OMe SAM; "*inert*" EG_3 surface) were found resistant against the nonspecific adsorption of various proteins.[20] This set of "*reactive*" and "*inert*" EG_3 terminated adsorbates has the same main chemical structure but different terminal groups. As detailed in the previous chapter, the main structures have an EG_3 termination and contain 11 alkyl chains, and include a trichlorosilyl group for surface attachment (*i.e.*, $Cl_3Si(CH_2)_{11}(OCH_2CH_2)_3$-X; where X is OCH_3 for the "inert" adsorbate, or X is $OC(=O)CH_3$ for the "reactive" adsorbate). The EG_3 termination imparts the protein resistance, while the long alkyl chain helps to assemble the molecules into densely packed monolayers. The termination on the EG_3 unit tunes the surface to be "*reactive*" or "*inert*" by having different functionalities. Thus, SiO_2 surfaces prepared from mixtures of these two adsorbates may allow the formation of well-defined films containing both defined alkyl and EG_3 regions whose surface reactivity can be systematically varied in terms of reactive site

density across all compositions.

This chapter focuses on the generation of protein A surfaces on these mixed silane-derived surfaces for optimization of protein A activity. Specifically, this chapter discusses the construction of protein A surfaces that can prevent the nonspecific adsorption of proteins other than the target IgG molecules and can bind to IgG with a maximum surface density and binding efficiency. To realize this goal, a precise manipulation in the coverage of protein A on the surface is required. Specifically, this chapter details the generation of protein A surfaces at various controlled surface densities. It demonstrates that the amount of protein A on the surface can be controlled using the mixed SAMs of the EG_3OH component on the surface. This chapter also shows that the IgG capturing activity of the protein A surface depends both on the amount of immobilized protein A and on the level of steric hindrance imposed on the protein A by surrounding closely packed molecules.

6.1.2. Protein A and IgG

Protein A, the common abbreviation for "staphylococcal protein A," is a cell wall constituent of the bacterium *Staphylococcus aureus*. It is well known for its binding ability to various mammalian IgG molecules through non-immune interactions that involve the F_c fragment of IgG[21] and avoid interactions with the antigen-binding fragments (Figure 6.2), thereby, maintaining the binding ability of the IgG for antigens.

Protein A has five homologous IgG binding units, E, D, A, B, and C (Figure 1.1), all of which have α-helical structure and interact with the hinge region in F_c.[22,23] An exact three-dimensional structure of protein A is not yet available; nonetheless, from the structural analysis of the binding pocket B by X-ray crystallography and the electron density profile, the fragment B may be viewed as a cylinder with a diameter of *ca.* 2.5 nm and a height of *ca.*

4.5 nm.[24-26] The structure of the other IgG binding fragments in protein A is similar to that of the fragment B, as they have similar amino acid sequence and secondary structure.[22,23] Each of the five fragments in protein A is able to bind to the F_c portion of an IgG. The binding between protein A and IgG is strong as the equilibrium dissociation constant (K_d) of IgG and the fragment B in protein A has been reported to be 10-60 nM.[27]

Immunoglobulin G (IgG) is the most abundant antibody in normal serum. IgG molecules have molecular weights of *ca.* 150,000 g/mol and consist of three distinct domains comprosing two F_{ab} fragments and one F_c fragment (Figure 6.2). An IgG can bind up to two antigens through its F_{ab} fragments, which lie at the outermost end of the top two branches. The F_c fragment in an IgG is located in the base of the molecule, and the binding site in the F_c fragment for fragment B of protein A is reported to be near the center of the F_c fragment.[25] To give a sense of scale, Figure 6.2 provides the dimensions of the F_{ab} and the F_c fragments as obtained from the X-ray crystallographic results[28,29]. In solution, the two F_{ab} fragments can rotate around the center of the molecule, and thus the IgG can elongate to take "T-shape" when they contain high net charges.[28-30]

6.2. Experimental Section

6.2.1. Materials

All the reagents were obtained from Aldrich (Milwaukee, WI) unless noted otherwise. 11-Bromo-1-undecene (99 %) was obtained from Pfaltz & Bauer (Waterbury, CT). 3-aminopropyltriethoxysilane (APTES) was from Gelest (Morrisville, PA). Potassium hydroxide, sulfuric acid, 35% $H_2O_2(aq)$ were from Mallinckrodt. Sodium hydride (NaH) was received from Aldrich as 60% dispersion in mineral oil and was used without purification. Acetone and ethanol were from EM Scientific. Hexokinase (EC 2326115) and

protein A were from Sigma. Phosphate buffer saline (PBS) was prepared by dissolving one PBS tablet (Sigma) into 200 mL of double-distilled water. This procedure produced a buffered solution at pH 7.4 that consists of 10 mM sodium phosphate buffer, 2.7 mM KCl, and 137 mM NaCl.

Goat anti-rabbit immunoglobulin G (IgG) was obtained from Pierce. Gold pellets (Au, 99.99%), chromium (Cr) coated tungsten filaments, and n-type Si(100) wafers were purchased from American Precious Metals (East Rutherford, NJ), R. D. Mathis and Co. (Long Beach, CA), and North East Silicon Technologies (New Bedford, MA). Gold substrates were prepared by the sequential thermal evaporation of 50 Å of Cr and 1500 Å of Au onto Si(100) in a vacuum chamber operating at ~10^{-6} Torr.

$Cl_3Si(CH_2)_{11}(OCH_2CH_2)_3OC(=O)CH_3$ (EG_3OAc silane), the adsorbate employed for the formation of EG_3OH film, was prepared by the three-step synthesis, which was detailed in Chapter 5. Scheme 6.1 shows the two-stsep synthesis used for the preparation of $Cl_3Si(CH_2)_{11}(OCH_2CH_2)_3OCH_3$ (EG_3OMe silane) SAM. The individual steps are based on direct modifications of the previously reported procedures.[20,31] **(A)** 8.7 mmol of NaH was dispersed in 30 mL of anhydrous dimethylformamide (DMF). Subsequently, 26.0 mmol of $H(OCH_2CH_2)_3OCH_3$ was mixed with NaH/DMF dispersion for 30 min, and then 8.6 mmol of $CH_2=CH(CH_2)_9Br$ was added dropwise. After being stirred at room temperature under nitrogen atmosphere for 7 h, the reaction mixture was extracted four times with hexane, and the collected extracts were concentrated by a rotary evaporator. The purified product of ***1*** was obtained by flash chromatography on silica gel (eluent: hexane, followed by hexane/ethyl acetate 9:1, and lastly 5:5) as a colorless oil in an isolated yield of ~ 80 %. **(B)** 50 mg of 0.12 M H_2PtCl_6 in anhydrous tetrahydrofuran (THF) was mixed with 5.8 mmol of ***1*** and 17.4 mmol of $HSiCl_3$ in a N_2 glove box and then stirred for 2 h. The final product ***2***,

EG_3OMe silane, was obtained in > 95 % yield after removal of unreacted $HSiCl_3$ under the vacuum. ^{1}H-NMR (400 MHz, $CDCl_3$): δ 1.2-1.5 (*m*, 16 H), 1.56 (*m*, 4 H), 3.38 (*s*, 3 H), 3.45 (*t*, 2 H), 3.5-3.75 (*m*, 12 H).

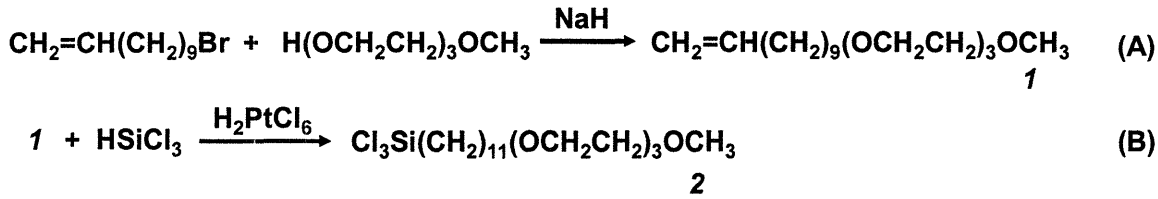

Scheme 6.1. Synthesis of methyl[(1-trichlorosilyl)undec-11-yl]tri(ethylene glycol).

6.2.2. Formation of Mixed Monolayers on SiO_2

Preparation of mixed self-assembled monolayers (SAMs) of EG_3OAc/EG_3OMe. Si/SiO_2 wafers were cut into 1 × 3 cm^2 slides and cleaned by immersion in 'piranha' solution (7/3 v/v mixture of conc. H_2SO_4 and 30 % aqueous H_2O_2) for 1 h at 80 °C. (CAUTION: 'Piranha' solution reacts violently with many organic materials and should be handled with care.) The substrates were rinsed with deionized water, dried in a stream of N_2, and put into a glove box. Mixed SAMs were prepared by in the glove box immersing the cleaned substrates for 24 h into a toluene solution of EG_3OAc silane and EG_3OMe silane in the desired ratio. The total concentration of EG_3OAc and EG_3OMe silane mixture was kept constant at 2 mM. The derivatized substrates were taken out to the air, sequentially rinsed with dichloromethane and acetone, and blown dry in a stream of N_2 prior to characterization and use. In this chapter, we refer to these films by their tail group (*e.g.*, an EG_3OAc SAM) for simplicity.

Formation of mixed monolayers of EG_3OH/EG_3OMe from EG_3OAc/EG_3OMe mixed SAMs. The optimum operating condition for reducing EG_3OAc to EG_3OH was discussed in

Chapter 5. Briefly, mixed SAMs of EG_3OAc/EG_3OMe were placed in an 1.0 M $LiAlH_4$ solution in dry ether for 5 min to reduce the terminal acetate of EG_3OAc component to a hydroxyl group. Reacted slides were rinsed sequentially with 10 mM HCl (*aq*), deionized water, and acetone, and dried in a stream of N_2 before characterization and further use.

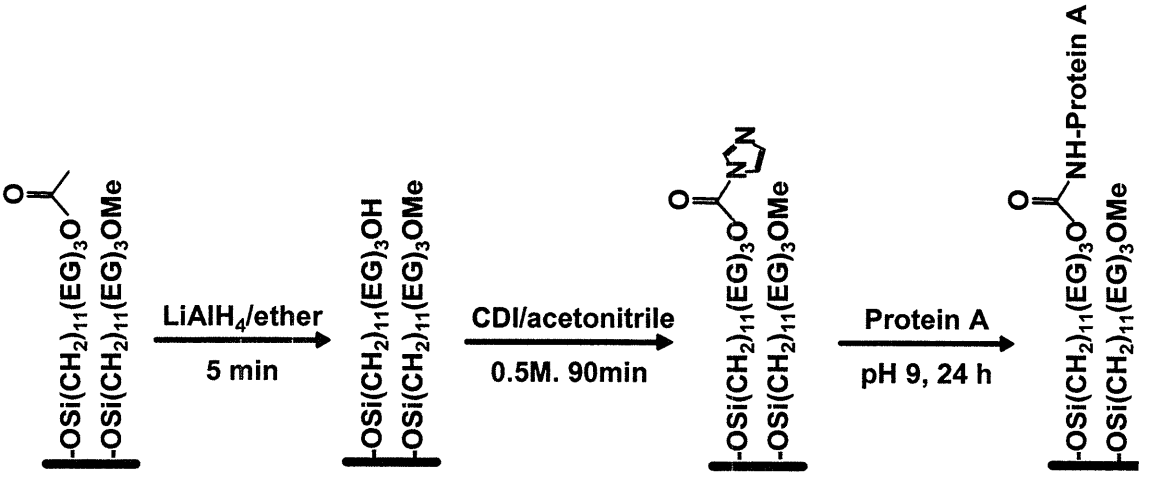

Scheme 6.2. Immobilization of protein A to EG_3OAc/EG_3OMe mixed SAMs. CDI = 1,1-carbonyl diimidazole, and ACN = acetonitrile.

6.2.3. Immobilization of Protein A onto Mixed Monolayers

Scheme 6.2 illustrates the reaction steps for attaching protein A to the surface using 1,1-carbonyl diimidazole (CDI) as a crosslinker. The substrates presenting EG_3OH/EG_3OMe mixed monolayer surfaces were washed well with anhydrous CH_2Cl_2, dried under N_2, and kept at 130 °C in a convection oven for 1 h. Subsequently, they were immersed in 0.5 M CDI in anhydrous acetonitrile (ACN) at room temperature for 1.5 h, followed by rinses with anhydrous ACN and 0.1 % HCl (*aq*). The CDI-coated surfaces were then contacted with a 0.5 mg/mL solution of protein A in a carbonate buffer (pH 9.0) at 4 °C for 24 h. After rinsing the surface with PBS, the samples were stored in PBS solution at 4 °C until use. The

activity of the resulting protein A were examined by incubating the protein A surfaces with goat anti-rabbit IgG in PBS at 0.75 mg/mL for 30 min followed by washing with PBS and drying, and measuring the nitrogen signals from the sample by XPS. As a control experiment to assess the specificity of protein A surfaces to IgG binding, N(1s) intensities of protein A surfaces were also measured after immersing the protein A surfaces into a 0.75 mg/mL solution of hexokinase in PBS for 30 min and then rinsing with PBS buffer and drying under nitrogen.

6.2.4. Surface Characterization

Ellipsometry. The thicknesses of the surfaces were measured with a Gaertner L116A ellipsometer (Gaertner Scientific Corporation, IL) at a 70° angle of incidence. A refraction index of 1.46 was used for all films, and a three-phase model was used to calculate thicknesses. The intrinsic error range from the equipment was ±2 Å.

X-ray photoelectron spectroscopy (XPS). Peak intensities of high resolution N(1s) XPS spectra were used to monitor the reaction progress at various reaction steps in Scheme 6.2. XPS measurements were performed on a Surface Science Instrument Model X-100 using a monochromatic Al Kα x-ray source and a concentric hemispherical analyzer. Per one sample, two measurements were taken at two different elliptical spots of spot size 1.0 mm × 1.7 mm. The take-off angle for the detector was 35° from the surface plane. Spectra were fit with 100 % Gaussian peaks and a linear baseline.

Preparation of surfaces for characterization

To estimate the amount of EG_3OH and proteins on the surface, a hydroxyl standard on gold substrate and an amine standard on Si/SiO_2 wafers were prepared and reacted with trifluoroacetic anhydride (TFAA).

Hydroxyl standard on gold substrate. Gold substrates were rinsed with acetone, dried under N_2, and then immersed into 2 mM solutions of 11-mercapto-1-undecanol in ethanol for 24 h at room temperature to produce hydroxyl-terminated SAMs on gold. The samples were then rinsed with ethanol and dried with a stream of nitrogen. As discussed in Chapter 5, these films, $Au/S(CH_2)_{11}OH$ provided a reference exposing 4.61×10^{14} hydroxyl groups/cm^2, *i.e.*, 4.61×10^{14} molecules/cm^2.

Amine standard on Si/SiO_2 wafers. APTES SAM on Si/SiO_2 wafers, *i.e.*, $Si/SiO_2/O_{3/2}(CH_2)_3NH_2$, was used as an amine standard. Wafers were cleaned in piranha solution and then immersed into 15 mM APTES solution in anhydrous toluene at room temperature for 15 min. Afterwards, the substrates were rinsed with CH_2Cl_2 and sonicated sequentially in CH_2Cl_2 and acetone for 15 min each, and blown dry with N_2. Finally, the substrates were cured in a convection oven at 130°C for 15 min.

Reaction with trifluoroacetic anhydride (TFAA). Hydroxyl standard, *i.e.*, $Au/S(CH_2)_{11}OH$, was placed into a 2% (v/v) TFAA solution in hexane for 2 min under N_2, rinsed with hexane, and dried under N_2. This process produced a trifluoroacetate surface of $Au/S(CH_2)_{11}O(C=O)CF_3$. Mixed monolayers of EG_3OH/EG_3OMe were similarly reacted with TFAA for conversion to $EG_3OC(=O)CF_3/EG_3OMe$. The surface density of reactive -OH groups on the EG_3OH/EG_3OMe mixed monolayers was determined by comparing F(1s) XPS intensities of $EG_3OC(=O)CF_3/EG_3OMe$ to that of a $Au/S(CH_2)_{11}O(C=O)CF_3$.

Likewise, an amine standard, *i.e.*, $Si/SiO_2/O_{3/2}(CH_2)_3NH_2$, surface was reacted with TFAA to generate a fluorinated surface of $Si/SiO_2/O_{3/2}(CH_2)_3NHC(=O)CF_3$. The surface density of amine groups on the amine standard was determined by comparing the F(1s) XPS intensity of the $Si/SiO_2/O_{3/2}(CH_2)_3NHC(=O)CF_3$ surface to that of the $Au/S(CH_2)_{11}O(C=O)CF_3$ surface. High resolution N(1s) XPS intensity was also obtained for

future use in the estimation of the amount of adsorbed proteins.

6.3. Results and Discussion

6.3.1. Formation and Characterization of Mixed Monolayers

A goal in this chapter was to investigate the effect of surface reactivity on the ability of protein A to bind IgG. To control the surface reactivity, mixed monolayers exposing EG_3OH and EG_3OMe termini were employed. As explained in Chapter 5, the hydroxyl group of the EG_3OH component was masked as an acetate (EG_3OAc), driving formation of the SAM and subsequently reduced to -OH after film formation. The mixed EG_3OAc/EG_3OMe silane system was chosen because the structural similarity of the two components was likely to result in well-mixed films with a consistent structured underlayer, *i.e.*, no single-component domain formation. This structural uniformity was confirmed both by the similar thickness of 20-21 Å and contact angle hysteresis of 13°-15° by water across all mmixed SAMs regardless of their solution composition (Table 6.1).

Table 6.1. Surface characterization of mixed SAMs of EG_3OAc/EG_3OMe silanes

EG_3OAc / EG_3OMe (w/w)	Ellipsometric Thickness (Å)	Water contact angle[a]		
		θ_a	θ_r	Hysteresis (θ_a - θ_r)
0 / 100	21	68°	53°	15°
40 / 60	20	71°	57°	14°
100 / 0	21	73°	60°	13°

[a]θ_a: advancing angle and θ_r: receding angle.

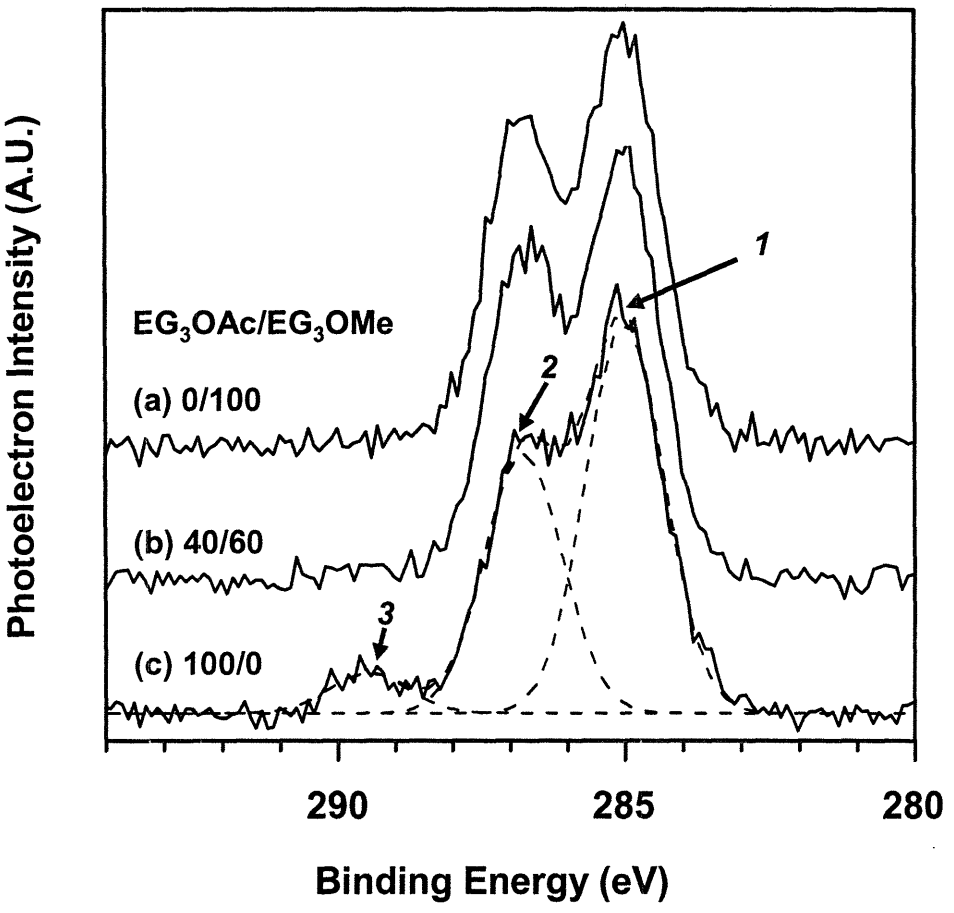

Figure 6.3. High resolution C(1s) XPS spectra of SAMs formed from EG_3OAc/EG_3OMe silane solutions mixture of selected compositions at a 55° take-off angle from surface normal. Dashed lines represent Gaussian peak fits to the data. Each spectrum was adjusted to have peak *1* at 285.0 eV.

Figure 6.3 presents high resolution C(1s) XPS spectra of SAMs prepared from EG_3OAc/EG_3OMe silane solutions at various compositions: 0/100, 40/60, and 100/0 by weight. An example of typical peak fitting for these spectra is presented for the 100% EG_3OAc SAM (Figure 6.3c). The three peaks correspond to the following functional groups: peak *1* to aliphatic hydrocarbon C-C, peak *2* to C-O (*i.e.*, EG carbons), and peak *3* to C(=O)O. As expected, peak *3* was not detected in the 100% EG_3OMe SAM (Figure 6.3a) and was highest for the 100% EG_3OAc SAM (Figure 6.3c). The mixed SAM formed from a

40/60 (w/w) EG_3OAc/EG_3OMe silane solution mixture had an intermediate intensity for peak *3* (Figure 6.3b).

The generation of the EG_3OH surface required reduction of the EG_3OAc SAM formation, and Chapter 5 discussed the reduction of the terminal acetate group in the EG_3OAc SAM to an OH group by contact with a $LiAlH_4$ solution in ether. In order to demonstrate that the $LiAlH_4$ treatment did not significantly affect the EG_3OMe SAM, the effects of $LiAlH_4$ exposure to the EG_3OMe SAM were investigated. Figure 6.4 shows that the C(1s) spectrum of the EG_3OMe SAM showed little change after exposure to $LiAlH_4$ for the conditions used to reduce the EG_3OAc terminus. Thus, we conclude that the exposure of the mixed SAMs to $LiAlH_4$ solution would affect only the EG_3OAc group.

Consequently, mixed monolayers of EG_3OH/EG_3OMe were produced through the coadsorption of EG_3OAc and EG_3OMe silanes and the subsequent reduction of EG_3OAc to EG_3OH by $LiAlH_4$. Reduction of EG_3OAc to EG_3OH by $LiAlH_4$ led to a decrease in ellipsometric thicknesses, and the decrease in thickness was approximately proportional to the EG_3OAc silane composition in the solution. For example, the thickness decreased by 4 Å, 2 Å, and ~ 0 Å for films prepared using the solutions for generating mixed SAMs that contained 100%, 40%, and 0% of EG_3OAc silanes, respectively.

After the reduction of the EG_3OAc group to an EG_3OH terminus, the surface reactivity of the mixed SAM was probed by measuring the surface density of reactive OH groups in the film. In order to label the surface OH with a tag that would provide a distinct, readily quantified peak in XPS, the surfaces were reacted with trifluoroacetic anhydride (TFAA) to produce a F(1s) signal that was used for detection. Once labeled with TFAA, the XPS spectra of the EG_3OH-containing SAMs exhibited an F(1s) peak at a binding energy of 689 eV. Using the F(1s) XPS peak intensity on $Au/S(CH_2)_{11}O(C{=}O)CF_3$ as a reference surface

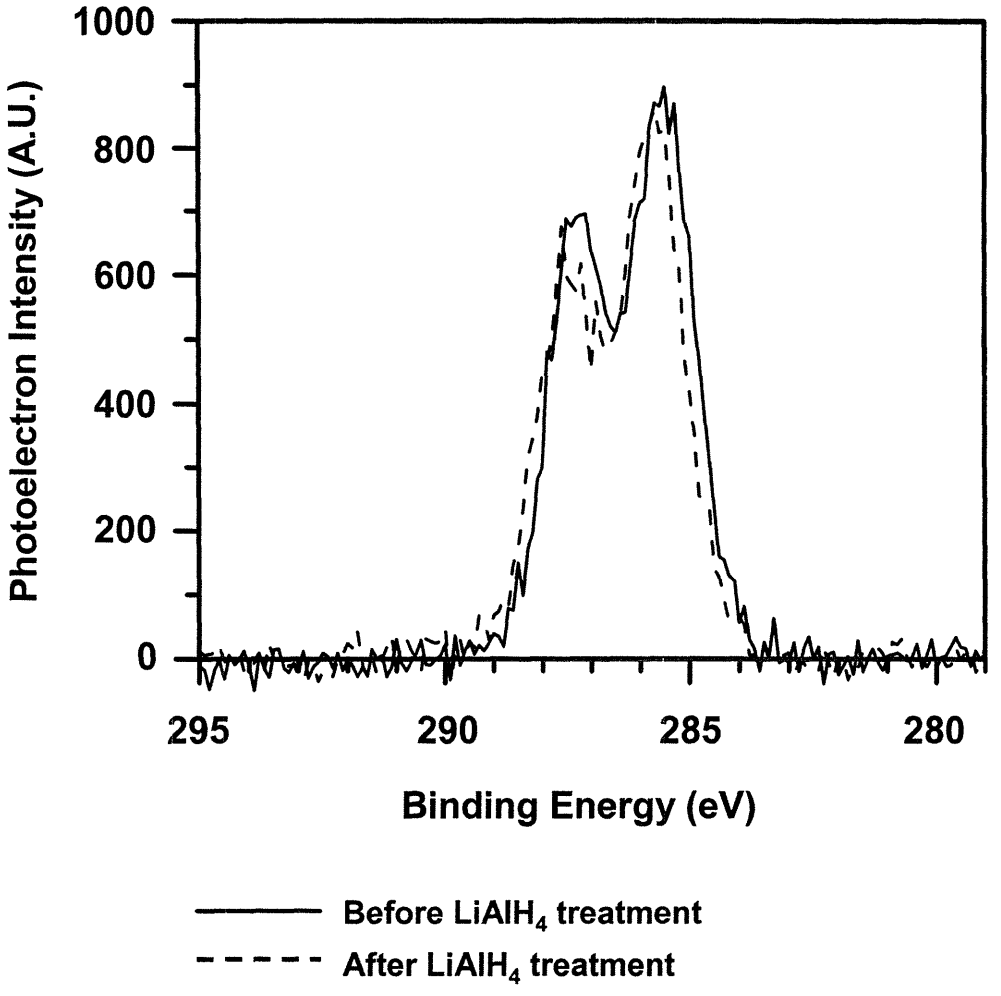

Figure 6.4. High resolution C(1s) XPS spectra of EG_3OMe SAM before and after exposure to 1.0 M solution of $LiAlH_4$/ether for 5 min followed by sequential rinsing with anhydrous ether, 0.1 M HCl (*aq*), acetone, and CH_2Cl_2.

exposing 4.61×10^{14} groups/cm^2,[12] the surface densities of reactive OH groups in the mixed EG_3OH/EG_3OMe monolayers were determined by comparing the F(1s) peak intensities of the TFAA-treated EG_3OH/EG_3OMe mixed monolayers to that of the reference. Using equation (6.1), the surface density of reactive OH group was determined and examined as a function of the EG_3OAc silane composition in the solution used to generate the mixed SAMs (Figure 6.5).

$$\phi_{EG_3OH} = \frac{\text{F(1s) area for } EG_3OC(=O)CF_3}{\text{F(1s) area for } Au/S(CH_2)_{11}OC(=O)CF_3} \times \left(4.61 \times 10^{14}/\text{cm}^2\right) \qquad (6.1)$$

By preparation of mixed monolayers from reactive and inert EG_3 silanes in different ratios, reactive OH groups could be diluted at the surface. FromFigure 6.5, it is evident that the relationship between the solution and surface composition of reactive EG_3 groups is close to linear.

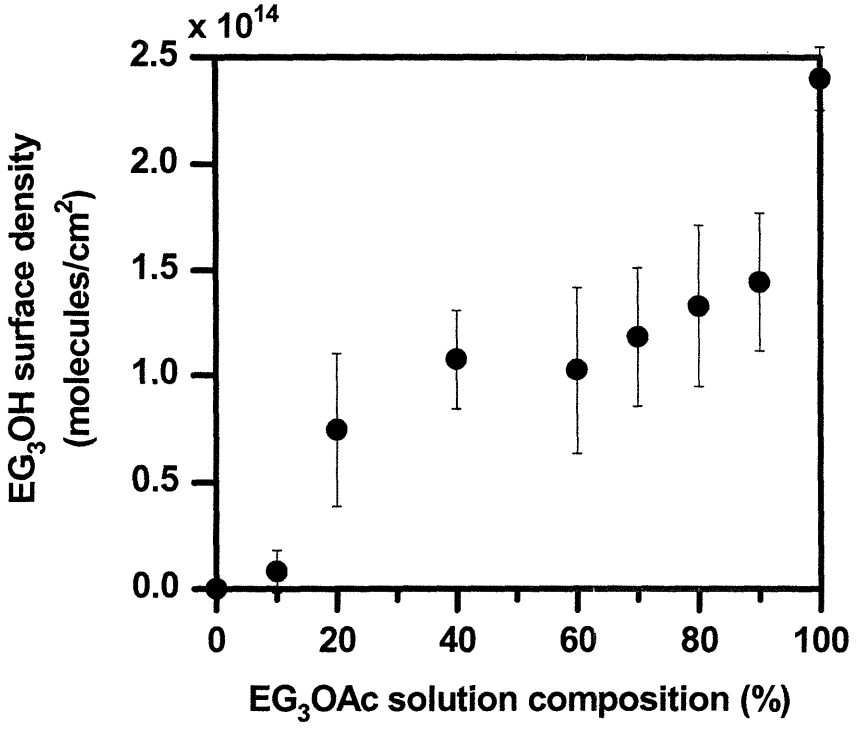

Figure 6.5. Surface density of EG_3OH termini as a function of solution composition of EG_3OAc in EG_3OAc/EG_3OMe mixed SAM. Surface densities were determined by comparing the F(1s) XPS intensity from the EG_3OH/EG_3OMe surfaces to that from $Au/S(CH_2)_{11}OH$ as a reference after treating these surfaces with TFAA.

6.3.2. Functionalization of Si/SiO_2 Surfaces with Protein A

Protein A was immobilized to mixed monolayers of EG_3OH/EG_3OMe through urethane bond formation with EG_3OH with 1,1,-carbonyldiimidazole (CDI) coupling reagents as described in Scheme 6.2. To assess the extent of CDI coupling and the surface density of protein A, the amine standard ($Si/SiO_2/O_{3/2}(CH2)_3NH_2$; APTES SAM) surface was characterized by XPS. Amine standard was prepared from a 15 mM APTES solution in

toluene. This process produced an amine-terminated silane film with 6 Å thick, and 40° and 23° advancing and receding water contact angles, respectively. The amine standard was then labeled with TFAA for F(1s) XPS measurement. From the discussion in Chapter 5, a hydroxyl standard surface is shown to have 4.61×10^{14} molecules/cm^2. Hence, the surface density of the amine standard could be calculated based on the F(1s) intensities of TFAA-labeled amine standard surface, $Si/SiO_2/O_{3/2}(CH2)_3NHC(=O)CF_3$, and TFAA-labeled hydroxyl standard surface, $Au/S(CH_2)_{11}O(C=O)CF_3$, by the following equation:

$$\phi_{APTES} = \frac{\text{F(1s) area for } Si/SiO_2/O_{3/2}/(CH_2)_3NHC(=O)CF_3}{\text{F(1s) area for } Au/S(CH_2)_{11}OC(=O)CF_3} \times \left(4.61 \times 10^{14}/\text{cm}^2\right) \quad (6.2)$$

From eq (6.2), the amount of APTES SAM, i.e., the amount of nitrogen elements, was determined to be 1.93×10^{14} molecules (elements) /cm^2.

N(1s) XPS peak intensity of the APTES SAM was also measured and used as a reference of nitrogen element for quantifying nitrogen-containing surfaces. For example, the surface density of EG_3O-CDI from 100% EG_3OH surface could be calculated to be 0.90×10^{14} molecules/cm^2 by comparing the N(1s) XPS intensity of the sample with that of APTES SAM (eq 6.3).

$$\phi_{EG_3O-CDI} = \frac{\text{N(1s) area for } EG_3O-CDI}{\text{N(1s) area for APTES SAM}} \times \left(1.93 \times 10^{14}/\text{cm}^2\right) \times \frac{1}{2} \quad (6.3)$$

The division by two in the last part of eq (6.3) is based on the fact that one EG_3O-CDI surface molecule has two nitrogen atoms (Scheme 6.2). On a 100% EG_3OH surface, the extent of reaction of EG_3OH and CDI coupling could be accordingly determined to be 34 - 38 %, by comparing the amount of EG_3O-CDI with that of EG_3OH.

The amount of protein A could be estimated likewise. One protein A molecule has approximately 405 nitrogen atoms, assuming one nitrogen per one amino acid. Thus the

surface density of protein A on mixed monolayers of EG_3OH/EG_3OMe was calculated by eq (6.4), a direct modification of eq (6.3).

$$\phi_{Protein\ A} = \frac{\text{N(1s) area increased by Protein A}}{\text{N(1s) area for APTES SAM}} \times \left(1.93 \times 10^{14}/\text{cm}^2\right) \times \frac{1}{405} \qquad (6.4)$$

The amount of protein A in units of molecules/cm^2 on 100% EG_3OAc surface can be converted to ~ 41 ng/cm^2. Assuming that specific gravity of protein A is 1 mg/cm^3, 41 ng/cm^2 corresponds to 4.1 Å, which is in good agreement with the ellipsometric thickness on a 100% EG_3OAc surface increased by protein A immobilization. Thus surface density of protein A on mixed monolayers could be reasonably determined by eq (6.4) and was plotted as a function of solution composition of EG_3OAc/EG_3OMe silane mixture (Figure 6.6).

Figure 6.6 shows the general trend of the increase in protein A surface density proportional to the weight percent of EG_3OAc in the solution mixture, and proportional to the increasing composition of reactive EG_3OH component. Figure 6.6 illustrates that the surface coverage of protein A can be controlled by manipulating the surface reactivity, and thus by using the appropriate silane solution compositions. Nonspecific adsorption of protein A onto an inert EG_3 surface, *i.e.*, a surface consisting of 0% EG_3OAc silane, was less than 5 % of the amount of protein A attached to 100% EG_3OAc surface. In Chapter 5, EG_3 surfaces were shown to have similar protein resistances regardless of the terminal group. Therefore we can conclude that nonspecific adsorption of protein A has little effect on the attachment of protein A to mixed monolayers.

Maximum protein A attachment happens at the maximum surface reactivity (Figure 6.6). This linearity implies that the reaction occurs at the uppermost surface and does not require a full insertion of protein molecules into the film. However, when it comes to immunoglobulin

G (IgG) binding to a protein A surface, all the binding sites in protein A are not exposed to the uppermost surface. Consequently, IgG molecules need to diffuse inside the film to bind with protein A and thus sufficient space in the protein A array should be provided for IgG binding. Based on the dimensions of a protein A fragment and an IgG molecule, one protein A·IgG binding complex needs a space of 20 nm diameter minimum (Figure 6.7). In other words, in order to properly bind IgG, the surface density of protein A should be much lower than 3.2×10^{11} molecules/cm^2. As illustrated in Figure 6.6, the surface density of protein A can be controlled by manipulating the composition of EG_3OAc/EG_3OMe silane mixture.

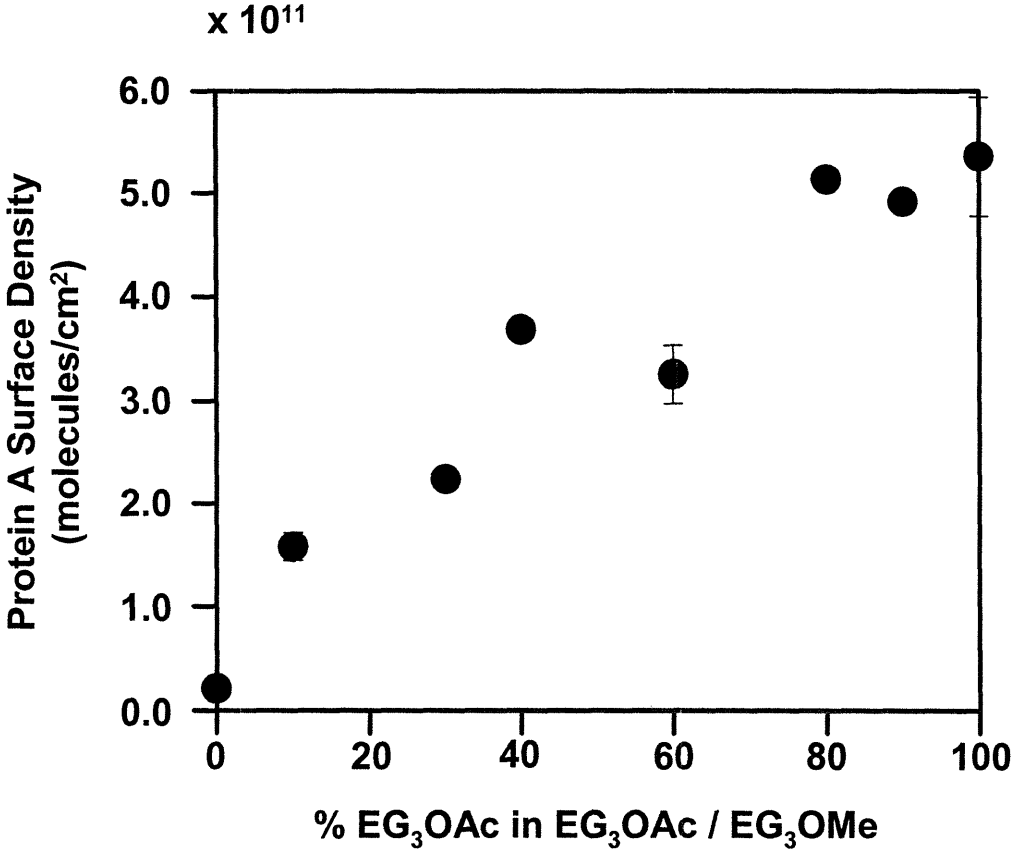

Figure 6.6. Surface density of protein A as a function of the solution composition of EG_3OAc silane in EG_3OAc/EG_3OMe silane solution mixtures.

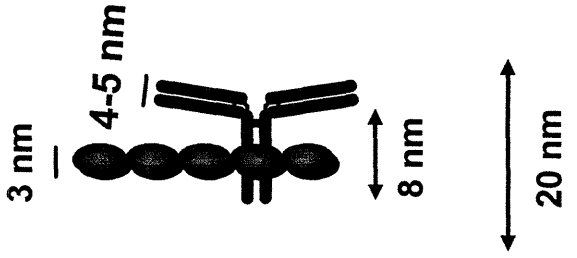

Figure 6.7. Schematic representation of a protein A and IgG Complex.

To assess the IgG binding activity of protein A-immobilized surfaces, we incubated the protein A-coated surfaces into 0.75 mg/mL goat anti-rabbit IgG solution in PBS for 30 min. The molecular weight of IgG is 150,000. Assuming that the average molecular weight of amino acid is 100 and one amino acid molecule contains one nitrogen, the surface density of IgG bound by protein A can be estimated by eq (6.5), an equation similar to eq (6.4).

$$\phi_{\text{Protein A}} = \frac{\text{N(1s) area increased by Protein A}}{\text{N(1s) area for APTES SAM}} \times \left(1.93 \times 10^{14}/\text{cm}^2\right) \times \frac{1}{1500} \qquad (6.5)$$

The amount of IgG immobilized on a protein A-coated surface was plotted as a function of EG_3OAc silane composition in an EG_3OAc/EG_3OMe solution mixture (Figure 6.8). The amount of IgG bound to the protein A films increases with increasing EG_3OAc silane composition of up to 30% by weight, reaches the maximum surface density at intermediate EG_3OAc compositions, and finally decreases at 100% EG_3OAc silane composition. As discussed earlier, the amount of protein A on the surface increases with increasing EG_3OAc silane composition. Hence, at low EG_3OAc silane composition, the surface has a limited amount of protein A and accordingly offers sufficient space for IgG molecules to diffuse into. This available space may increase in the surface density of IgG with increasing EG_3OAc silane composition at these low EG_3OAc compositions. On the surface prepared from 100% EG_3OAc silane, protein A molecules are closely packed and the concomitant spatial

restriction may hinder IgG molecules from binding to surface-immobilized protein A.

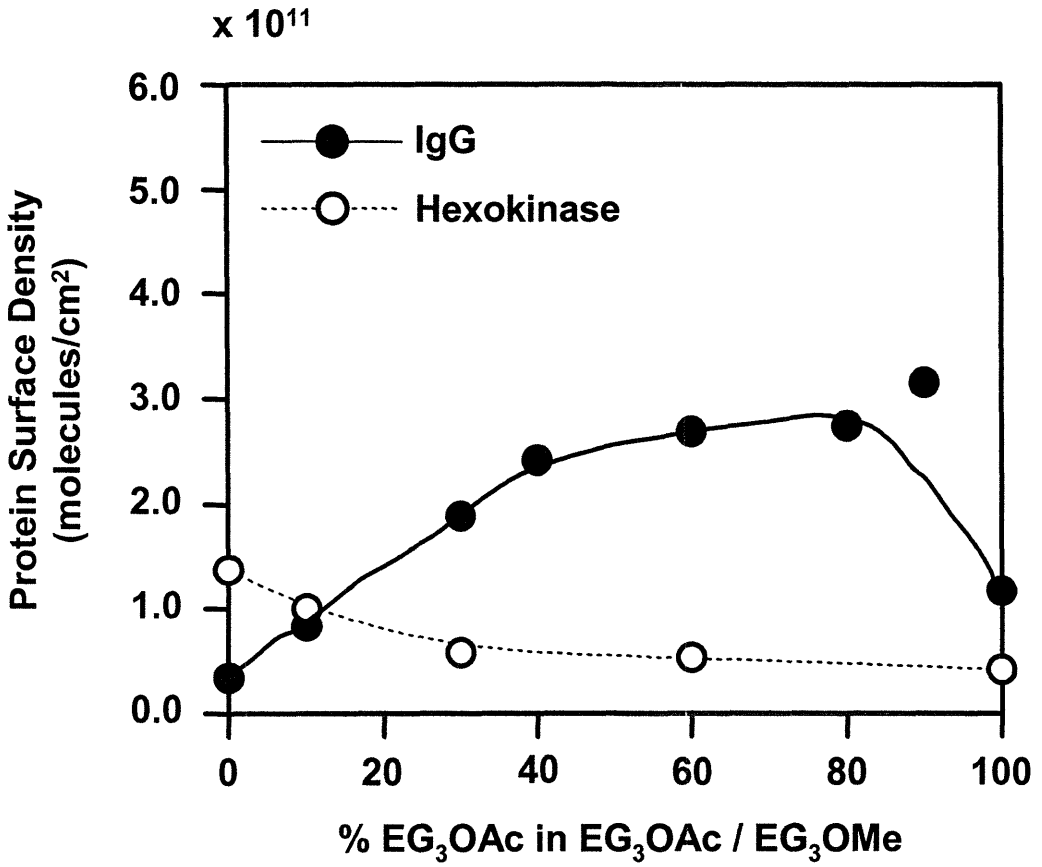

Figure 6.8. Surface densities of immunoglobulin G and hexokinase on protein A array as functions of weight percent of EG_3OAc silane in starting EG_3OAc/EG_3OMe silane mixture. Lines represent guides to the eye.

In addition to achieving maximum IgG binding, it is also important that the surface-immobilized protein A 'selectively' binds IgG. To examine the specificity of the protein A array, the protein A-coated surfaces were incubated in a hexokinase solution at the same condition as in the IgG solution. Hexokinase was chosen as a control system because both goat anti-rabbit IgG and hexokinase had the same molecular weight (Mw) of 150,000 and isoelectric point (pI) of 5.5. Figure 5.4 also illustrates the amount of adsorbed hexokinase as a function of the solution composition of EG_3OAc silane. The surface density of hexokinase

was calculated using eq (6.5). For all compositions of EG_3OAc silane, the amount of nonspecifically adsorbed hexokinase on protein A surfaces were under 1.5×10^{11} molecules/cm^2. At 0% and 10% EG_3OAc solution composition, the surface density of hexokinase is comparable to or higher than that of IgG. In other words, the protein A surfaces prepared from low composition of EG_3OAc silane are not specific towards IgG. Among all the EG_3OAc silane solution compositions examined, surfaces prepared from 30% and 60% EG_3OAc composition show low hexokinase adsorption while maintaining high binding activity to IgG.

Earlier, we discussed that decreasing surface density of protein A leads to higher surface loading of IgG, resulting from the lower spatial restrictions to the incoming IgG molecules. Figure 5.5 is a graphic illustration of this trend. The binding efficiency in Figure 5.5 is determined by dividing the surface density of IgG by the surface density of protein A. Figure 5.3 demonstrated that as the surface reactivity represented by the solution composition of EG_3OAc silane in EG_3OAc/EG_3OMe silane mixture decreased, so did the surface density of protein A available for IgG binding. Accordingly, the binding efficiency of the protein A surface to IgG increased with decreasing surface reactivity.

6.4. Conclusions

This chapter demonstrates that surface reactivity can be manipulated by using mixed monolayers expressing EG_3 caps with 'reactive' hydroxyl termini (EG_3OH) and a diluent expressing 'inert' methoxy termini (EG_3OMe). These mixed monolayers are prepared by forming mixed SAMs of EG_3OAc silane and EG_3OMe silane, and then reducing OAc to OH in EG_3OAc silane. We have noticed that higher surface reactivity leads to higher protein A density on the surface. From the IgG binding studies, we have found that at 100% EG_3OAc

solution composition, *i.e.*, at 100% reactive EG_3 monolayer, the binding activity of protein A coated surface to IgG is not optimum, presumably due to the spatial restriction by closely packed protein A. In addition, the IgG binding activity of protein A was not optimum as well at low EG_3OAc silane solution composition, *e.g.*, up to less than 30%, because of the limited amount of protein A available for IgG binding. The protein A surfaces were specific towards IgG binding when the solution mixture contained more than 30% by weight of EG_3OAc silane. Considering the specificity of the protein A surface towards IgG binding and the amount of IgG loaded to the surface, the optimum composition of EG_3OAc silane in solution was thought to be 60% by weight.

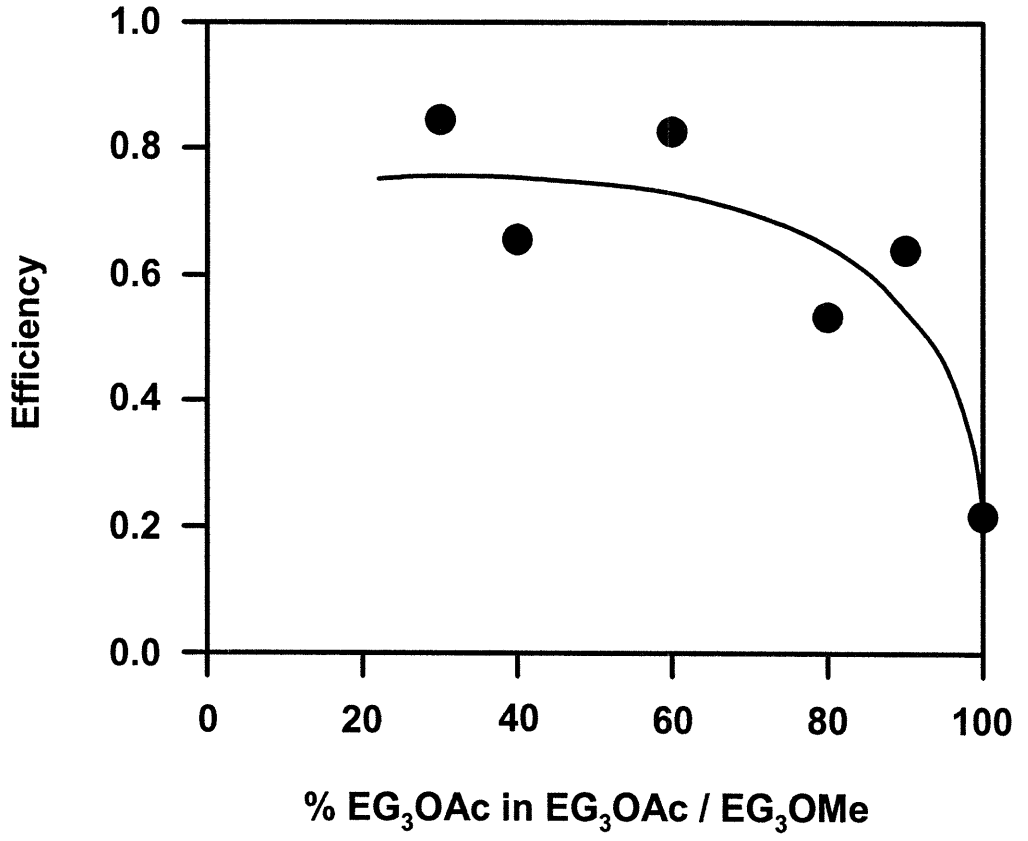

Figure 6.9. IgG binding efficiency of protein A-coated surface as a function of EG_3OAc silane weight percent in EG_3OAc/EG_3OMe silane solution mixtures. The efficiency is defined as the ratio of the amount of IgG to the amount of protein A. The line represents a guide to the eye.

6.5. References for Chapter 6

(1) Templin, M. F.; Stoll, D.; Schrenk, M.; Traub, P. C.; Vohringer, C. F.; Joos, T. O. Protein microarray technology. *Trends Biotechnol.* **2002**, *20*, 160-166.

(2) Wilson, D. S.; Nock, S. Functional protein microarrays. *Curr. Opin. Chem. Biol.* **2002**, *6*, 81-85.

(3) Cahill, D. J. Protein and antibody arrays and their medical applications. *J. Immunol. Methods* **2001**, *250*, 81-91.

(4) Luppa, P. B.; Sokoll, L. J.; Chan, D. W. Immunosensors - principles and applications to clinical chemistry. *Clin. Chim. Acta* **2001**, *314*, 1-26.

(5) Aizawa, M. Immunosensors for clinical analysis. *Adv. Clin. Chem.* **1994**, *31*, 247-275.

(6) Novotny, M. V. Microcolumn liquid chromatography in biochemical analysis. In *High resolution separation and analysis of biological macromolecules, pt a*, **1996**; Vol. 270, pp 101-133.

(7) Novotny, M. V. Capillary biomolecular separations. *J. Chromatogr. B* **1997**, *689*, 55-70.

(8) Davis, D. R.; Padlan, E. A.; Segal, D. M. 3-dimensional structure of immunoglobulins. *Ann. Rev. Biochem.* **1975**, *44*, 639-667.

(9) Gersten, D. M.; Marchalonis, J. J. Rapid, novel method for solid-phase derivatization of igg antibodies for immune-affinity chromatography. *J. Immunol. Methods* **1978**, *24*, 305-309.

(10) Werner, S.; Machleidt, W. Isolation of precursors of cytochrome-oxidase from neurospora-crassa - application of subunit-specific antibodies and protein-a from staphylococcus-aureus. *Eur. J. Biochem.* **1978**, *90*, 99-105.

(11) Dubois, L. H.; Nuzzo, R. G. Synthesis, structure, and properties of model organic surfaces. *Ann. Rev. Phys. Chem.* **1992**, *43*, 437-463.

(12) Ulman, A. *An introduction to ultrathin organic films: From Langmuir-Blodgett to self-assembly*; Academic Press, **1991**.

(13) Bain, C. D.; Whitesides, G. M. Modeling organic surfaces with self-assembled monolayers. *Angew. Chem. Int. Ed.* **1989**, *28*, 506-512.

(14) Offord, D. A.; John, C. M.; Linford, M. R.; Griffin, J. H. Contact angle goniometry, ellipsometry, and time-of-flight secondary ion mass spectrometry of gold supported, mmixed self-assembled monolayers formed from alkyl mercaptans. *Langmuir* **1994**, *10*, 883-889.

(15) Boozer, C.; Yu, Q.; Chen, S.; Lee, C.-Y.; Homola, J.; Yee, S. S.; Jiang, S. Surface functionaliztion for self-referencing surface plasmon resonance (SPR) biosensors by multi-step self-assembly. *Sens. Actuators, B* **2003**, *90*, 22-30.

(16) Hodneland, C. D.; Lee, Y.-S.; Min, D.-H.; Mrksich, M. Selective immobilization of proteins to self-assembled monolayers presenting active site-directed capture ligands. *Proc. Natl. Acad. Sci. U. S. A.* **2002**, *99*, 5048-5052.

(17) Houseman, B. T.; Gawalt, E. S.; Mrksich, M. Maleimide-functionalized self-assembled monolayers for the preparation of peptide and carbohydrate biochips. *Langmuir* **2003**, *19*,

1522-1531.

(18) Nelson, K. E.; Gamble, L.; Jung, L. S.; Boeckl, M. S.; Naeemi, E.; Golledge, S. L.; Sasaki, T.; Castner, D. G.; Campbell, C. T.; Stayton, P. S. Surface characterization of mixed self-assembled monolayers designed for streptavidin immobilization. *Langmuir* **2001**, *17*, 2807-2816.

(19) Elwing, H. Protein adsorption and ellipsometry in biomaterial research. *Biomaterials* **1998**, *19*, 397-406.

(20) Lee, S.-W.; Laibinis, P. E. Protein-resistant coatings for glass and metal oxide surfaces derived from oligo(ethylene glycol)-terminated alkyltrichlorosilanes. *Biomaterials* **1998**, *19*, 1669-1675.

(21) Langone, J. J. Protein-A of *Staphylococcus aureus* and related immunoglobulin receptors produced by streptococci and pneumococci. *Adv. Immunol.* **1982**, *32*, 157-252.

(22) Sjodahl, J. Repetitive sequences in protein-A from *Staphylococcus aureus* - arrangement of 5 regions within protein, 4 being highly homologous and F_c-binding. *Eur. J. Biochem.* **1977**, *73*, 343-351.

(23) Sjodahl, J. Structural studies on 4 repetitive F_c-binding regions in protein-A from *Staphylococcus aureus*. *Eur. J. Biochem.* **1977**, *78*, 471-490.

(24) Deisenhofer, J.; Jones, T. A.; Huber, R.; Sjodahl, J.; Sjoquist, J. Crystallization, crystal-structure analysis and atomic model of complex formed by a human F_c fragment and fragment B of protein A from *Staphylococcus aureus*. *Hoppe-Seyler's Z. Physiol. Chem.* **1978**, *359*, 975-985.

(25) Deisenhofer, J. Crystallographic refinement and atomic models of a human F_c fragment and its complex with fragment B of protein A from *Staphylococcus aureus* at 2.9 Å and 2.8 Å resolution. *Biochemistry* **1981**, *20*, 2361-2370.

(26) Murata, M.; Arakawa, M.; Yoshida, T.; Hato, M. Binding of immunoglobulin molecules to preadsorbed protein A layers as observed by surface forces measurements. *Colloids Surf. B* **1998**, *12*, 35-47.

(27) Cedergren, L.; Andersson, R.; Jansson, B.; Uhlen, M.; Nilsson, B. Mutational analysis of the interaction between Staphylococcal protein A and human IgG(1). *Protein Eng.* **1993**, *6*, 441-448.

(28) Bagchi, P.; Birnbaum, S. M. Effect of ph on the adsorption of immunoglobulin G on anionic poly(vinyltoluene) model latex-particles. *J. Colloid Interface Sci.* **1981**, *83*, 460-478.

(29) Suzawa, T.; Shirahama, H. Adsorption of plasma proteins onto polymer lattices. *Adv. Colloid Interface Sci.* **1991**, *35*, 139-172.

(30) Mathews, C. K.; van Holde, K. E. *Biochemistry*; Benjamin/Cummings Publishing Company: Redwood City, CA, **1990**.

(31) Pale-Grosdemange, C.; Simon, E. S.; Prime, K. L.; Whitesides, G. M. Formation of self-assembled monolayers by chemisorption of derivatives of oligo(ethylene glycol) of structure $HS(CH_2)_{11}(OCH_2CH_2)_mOH$ on gold. *J. Am. Chem. Soc.* **1991**, *113*, 12-20.

Chapter 7. Summary and Future Directions

7.1. Summary

This thesis addressed the development of ultrathin films of poly(ethylene glycol) (PEG) on SiO_2-based surfaces that 1) resist non-specific adsorption of proteins and cells (*"bioinert surfaces"*) and 2) provide specific immobilization of biomolecules (*"bioactive surfaces"*). Chapter 2 and 3 discussed the immobilization of PEG through multivalent attachment of a PEG-grafted polymer backbone. Chapter 2 showed that PEG-containing films could be formed by electrostatic interaction between the poly(acrylic acid) (PAA) backbone and the underlying amine-modified surface. Grafting of the random copolymer of PEG and poly(propylene glycol) (PPG), *i.e.*, PEG-*r*-PPG, provided an inexpensive alternative to the use of homogeneous PEG chains, where the work in Chapter 2 demonstrates the effectiveness of this more readily available and thermally stable industrial material. The polymer films on Si/SiO_2 wafers and PDMS substrates were stable in various harsh conditions, and exhibited good resistance against protein adsorption and bacterial adhesion.

Chapter 3 reported the synthesis of a PEG-grafted surface-reactive copolymer and its self assembled structure on the substrates. The copolymer was poly(TMSMA-*r*-PEGMA), a random copolymer of trimethoxysilylproply methacrylate (TMSMA) and PEG methyl ether methacrylate (PEGMA). It consisted of an "anchor part" (trimethoxysilane) and a "function part" (PEG). The polymer film showed good protein- and cell-resistance, and especially, showed superior resistance against fibrinogen. Compared with the PAA-*g*-(PEG-*r*-PPG) system described in Chapter 2, the current system of poly(TMSMA-*r*-PEGMA) has advantages in that the PEG film is formed by "covalent" bond formation, which may impart better stability, and PEG can be directly attached to SiO_2-based surfaces without prior

modification of surfaces with amine.

Chapter 4 discussed direct patterning of proteins and cells by a soft lithographic technique called capillary force lithography (CFL). By introducing PEG dimethacrylate (PEGDMA) as the patterned polymer, spatially well-resolved images of selective protein and cell attachment were obtained on a large area. In this system, PEG microstructures confined proteins and cells not only by the inert nature of PEG but also by acting as a physical barrier. The number of cells in a given PEG barrier could be manipulated by varying the feature sizes. The ability to control the cell positioning and number of cells in a given pattern demonstrates the potential of CFL in the fabrication of protein- and cell-based chips.

Chapter 5 described the generation of densely-packed, hydroxyl-terminated tri(ethylene glycol) (EG_3)-expressing surfaces from the self-assembly of $Cl_3Si(CH_2)_{11}(OCH_2CH_2)_3OC(=O)CH_3$. The molecule produced an acetate-terminated EG_3 (EG_3OAc) surface that is subsequently reduced to hydroxyl-terminated EG_3 expressing (EG_3OH) film. The resulting EG_3OH surface provided a non-biofouling surface which simultaneously allows subsequent immobilization of biomolecules. The attachment of Protein A onto this surface and its binding to an immunoglobin G (IgG) demonstrated this ability.

Chapter 6 demonstrated that surface reactivity needs to be controlled to construct a biofunctional surface with optimum activity, and can be controlled by using mixed monolayers expressing EG_3 caps with "reactive" hydroxyl termini (EG_3OH) and a diluent expressing "inert" methoxy termini (EG_3OMe). Higher surface reactivity led to higher protein A density on the surface. The binding activity of the surface protein A, however, showed an optimum at the intermediate composition of EG_3OH. The loss of activity at 100% EG_3OH surface was proposed as a result of the spatial restriction by closely packed protein A.

7.2. Future Directions

The work described in this thesis can be further explored to various directions. The graft copolymer series of PAA-g-(PEG-r-PPG) are known to stabilize magnetic iron oxide nanoparticles.[1] This thesis demonstrated the protein- and cell-resistance of this system. Thus, this graft copolymer system may be applied to bioinert coating of magnetic nanoparticles, which can be useful in the contrast agents in magnetic resonance imaging (MRI). The multiple covalent attachment groups in poly(TMSMA-*r*-PEGMA) may allow the preparation of various structures (*e.g.*, micro- and nanoparticles, and crosslinked networks) from one system. In the project of biofunctional surfaces, the importance of steric hindrance on the binding activity of protein A surface can be further pursued by morphological studies and the studies of interactions between the target IgG and the protein A surface.

7.3. References for Chapter 7

(1) Moeser, G. D.; Roach, K. A.; Green, W. H.; Laibinis, P. E.; Hatton, T. A. Water-based magnetic fluids as extractants for synthetic organic compounds. *Ind. Eng. Chem. Res.* **2002**, *41*, 4739-4749.